

Generic Model-Based Tailor-Made Design and Analysis of Biphasic Reaction Systems

Anantpinijwatna, Amata; Gani, Rafiqul; Woodley, John

Publication date:
2016

Document Version
Publisher's PDF, also known as Version of record

[Link back to DTU Orbit](#)

Citation (APA):

Anantpinijwatna, A., Gani, R., & Woodley, J. (2016). Generic Model-Based Tailor-Made Design and Analysis of Biphasic Reaction Systems. Kgs. Lyngby: Technical University of Denmark (DTU).

DTU Library

Technical Information Center of Denmark

General rights

Copyright and moral rights for the publications made accessible in the public portal are retained by the authors and/or other copyright owners and it is a condition of accessing publications that users recognise and abide by the legal requirements associated with these rights.

- Users may download and print one copy of any publication from the public portal for the purpose of private study or research.
- You may not further distribute the material or use it for any profit-making activity or commercial gain
- You may freely distribute the URL identifying the publication in the public portal

If you believe that this document breaches copyright please contact us providing details, and we will remove access to the work immediately and investigate your claim.

Generic Model-Based Tailor-Made Design and Analysis of Biphasic Reaction Systems

Amata Anantpinijwatna

PhD Thesis

July 2016

**Generic Model-Based Tailor-Made
Design and Analysis of Biphasic Reaction Systems**

**PhD Thesis
Amata Anantpinijwatna**

July 2016

**Department of Chemical and Biochemical Engineering
Technical University of Denmark**

PREFACE

This thesis is submitted as partial fulfilment of the requirements for the degree of Doctor of Philosophy (PhD) in chemical engineering at the Technical University of Denmark (DTU).

The work has been carried out under the supervision of Professor Rafiqul Gani at the Department of Chemical and Biochemical Engineering from August 2013 to August 2016. The project included external research periods at University of Virginia, USA; Syngenta Ltd, UK; and Universidad Autónoma Metropolitana (Cuajimalpa Campus), Mexico.

The project has been financed by the Royal Thai Government Scholarship Program offered by The Office of the Civil Service Commission (OCSC), Thailand.

Amata Anantpinijwatna

อมตะ อนันต์พิณีจวัฒนา

July 2016, Kgs. Lyngby

ACKNOWLEDGEMENT

I'd like to dedicate the first line of acknowledgement to thank the Thai government and OCSC for granting me the scholarship. I'd also like to thank the Royal Thai Embassy for taking care of me during my time in Denmark.

I have the pleasure to acknowledge numerous persons who have contributed directly and indirectly to the development of this project:

I'd like to start by expressing my special gratitude to my main supervisor Rafiqul Gani for his support, inspiring ideas, and enthusiasm for my project and for providing me with so many opportunities to meet with interesting people related to my field of study.

I wish to thank my co-supervisor John Woodley his useful suggestions throughout the period of my work.

I'd like to express my gratitude to my collaborators throughout the project. Special thanks to Professor Felipe Lopez-Isunza, Professor John O'Connell, and Professor Mauricio Sales-Cruz for always giving invaluable recommendations and taking care of me during the research stays. My gratitude to Doctor Steve Girt and Syngenta Ltd (UK) for giving me an opportunity to experience the real industrial situation.

I'd like to thank Ms. Jitikan for her hospitality since the first time we've met until today. I'd also like to thank Carlos Eduardo Ramirez Castellan, Clémentine Henri, and Kaesinee Petchkaewkul for making my time in Denmark very special and pleasant. Moreover, I'd like to thank all my colleagues at CAPEC and SPEED the quality time, academically, we have spent together.

Lastly and most importantly, I would like to express my heartfelt gratitude to my parents and sisters for the encouragement and support.

Amata Anantpinijwatna

อมตะ อนันต์พินิจวัฒนา

July 2016, Kgs. Lyngby

ABSTRACT

Biphasic reaction systems are composed of immiscible aqueous and organic liquid phases where reactants, products, and catalysts are partitioned. These biphasic conditions point to novel synthesis paths, higher yields, and faster reactions, as well as facilitate product separation. The biphasic systems have a broad range of application, such as the manufacture of petroleum-based chemicals, pharmaceuticals, and agro-bio products. Major considerations in the design and analysis of biphasic reaction systems are physical and chemical equilibria, kinetic mechanisms, and reaction rates.

The primary contribution of this thesis is the development of a systematic modelling framework for the biphasic reaction system. The developed framework consists of three modules describing phase equilibria, reactions and mass transfer, and material balances of such processes. Correlative and predictive thermodynamic models, including newly developed group-contribution electrolyte model (e-KT-UNIFAC), have been implemented to predict the partitioning and equilibria of electrolyte and non-electrolyte species for a wide variety of reacting substances. Reaction kinetics and mass transfer are described by non-elementary reaction rate laws. Extents of reaction are used to calculate the species material balances.

The resulting mathematical model contains temperature dependent reaction rate parameters, equilibrium constants, and partition coefficients; where only the reaction rates are to be regressed to a minimum of time-dependent data. The application of the framework is made to five distinct cases in order to highlight the performance of the model for correlating the data and predicting the overall rates, the ultimate amounts of product formation, the ultimate impurities amount, and the optimum operating condition using different organic solvents leading to an improved and innovative design of the system.

DANISH ABSTRACT

Reaktive to-fase systemer består af ikke-blandbare vandige og organiske faser, hvor reaktanter, produkter og katalysatorer er fordelt. Disse to-fase betingelser kan lede mod nye synteseveje, højere udbytte og hurtigere reaktioner, ligesom de kan lette separationen af produkter. To-fase systemer har en bred anvendelse i, for eksempel, fremstilling af petroleumsbaserede kemikalier, lægemidler og landbrugsrelaterede biologiske produkter. Nogle af de vigtigste fænomener i design og analyse af reaktive to-fase systemer er fysiske og kemiske ligevægtsbetingelser, kinetiske mekanismer, samt reaktionshastigheder.

Det primære bidrag fra denne afhandling er udviklingen af en systematisk fremgangsmetode til modellering af reaktive to-fase systemer. Fremgangsmetoden består af tre moduler til beskrivelse af fase-ligevægte, reaktioner og stofovergang, samt stofbalancer for disse processer. Korrelative og prædiktive termodynamiske modeller, inklusiv den nyudviklede elektrolytiske gruppebidragsmetode (e-KT-UNIFAC), er blevet anvendt til at forudsige fasefordelingen og ligevægten af elektrolytiske og ikke-elektrolytiske forbindelser for en lang række reaktive systemer. Reaktionskinetik og stofovergang er beskrevet med ikke-elementære reaktionshastighedsudtryk. Reaktionernes omdannelsesgrad benyttes til at beregne forbindelsernes stofbalancer.

Den resulterende matematiske model har temperaturafhængige parametre for reaktionshastigheder, ligevægtskonstanter og fordelingskoefficienter, hvor kun reaktionshastighederne skal tilpasses til en lille mængde tidsafhængig data. Fremgangsmetoden anvendes på fem forskellige cases for at illustrere modellens evne til at korrelere data og forudsige overordnede hastigheder, slutmængden af produkt dannelse og slutmængden urenheder, såvel som optimale driftsbetingelser med forskellige organiske opløsningsmidler, hvilket leder frem til et forbedret og innovativt design af systemerne.

CONTENTS

Preface.....	I
Acknowledgement.....	III
Abstract.....	V
Danish Abstract.....	VI
Contents.....	VII
List of Figures.....	IX
List of Tables.....	XII
1 Introduction and Overview.....	1
1.1 Introduction.....	2
1.2 Objectives.....	3
1.3 Thesis Structure.....	3
2 Literature Review.....	5
2.1 Modelling Methodology.....	6
2.2 Review of the Application.....	9
2.3 Review of the Available Models.....	23
3 The Modelling Framework.....	29
3.1 Biphasic Reaction System Modelling Framework.....	30
3.2 Constitutive Thermodynamic Models.....	37
4 Implementation of the Framework and Thermodynamic Models.....	49
4.1 Implementation of Thermodynamic Models.....	50
4.2 Reactor Models.....	57
4.3 Computational Algorithm.....	78
5 Model-Aided Design and Analysis.....	81
5.1 PTC I, Benzoin Condensation.....	82
5.2 PTC II, Chlorination of Organobromine.....	84
5.3 Epoxidation of Unsaturated Long Chain Fatty Acid.....	93
5.4 Production of Furan Derivatives from Biomass.....	100
5.5 Production of Alpha-Aminobutyric Acid.....	111
6 Conclusion.....	115

6.1 Achievements.....	116
6.2 Remaining Challenges	118
References	121
Nomenclature	131
Appendix	133

LIST OF FIGURES

Figure 2-1: A conceptual modelling system perspective.....	6
Figure 2-2: Generic model development framework	7
Figure 2-3: Molecular structure of phase transfer catalysts (PTC)	9
Figure 2-4: Reaction mechanism of a generic PTC system.....	10
Figure 2-5: Makosza's replacement reactions [17]: (A) acyl cyanide production; (B) cyanohydrin production.....	12
Figure 2-6: Makosza's alkylations reactions [17]	13
Figure 2-7: De Zani's alkylation reaction [20].....	14
Figure 2-8: Vanden Eynde's alkylation reactions [21].....	14
Figure 2-9: Hydrolysis of 4-methoxyphenylacetic acid butyl ester [24].....	15
Figure 2-10: Dicarboxylic acid production from cyclo-olefin [40].....	16
Figure 2-11: Nowothnick's hydroformylation [43]; (a) utilised surfactant; (b) reaction scheme.....	17
Figure 2-12: Obrecht's hydroformylation; (a) pH controlled; (b) temperature controlled [44]	18
Figure 2-13: Biphasic reactive absorption [45]	18
Figure 2-14: Productions of furfural and levulinic acid from hemicellulose [48].....	19
Figure 2-15: Lozano's transesterification in IL-SCCO ₂ [52]	20
Figure 2-16: Thermomorphic biphasic production of biodiesel [53]	20
Figure 2-17: Atom transfer radical polymerisation [54]	21
Figure 2-18: Biphasic production of active pharmaceutical ingredients [56]	22
Figure 3-1: Framework for modelling of biphasic reaction systems.....	31
Figure 3-2: Detail steps of module 1 in the framework.....	32
Figure 3-3: Detail steps of module 2 in the framework.....	33
Figure 3-4: Detail steps of module 3 in the framework.....	35
Figure 4-1: Activity coefficients of tetraalkylammonium bromide and chloride PTC, comparison between eNRTL-SAC model calculation and measured data.....	51
Figure 4-2: Activity coefficients of tetraalkylammonium PTC, comparison between eNRTL-SAC model calculation and measured data	51

Figure 4-3: Solubilities of tetraalkylammonium PTC, comparison between NRTL-SAC model calculation and measured data.....	53
Figure 4-4: Activity coefficients of tetraalkylammonium PTC, comparison between e-KT-UNIFAC model calculation and measured data.....	56
Figure 4-5: Solubilities of tetraalkylammonium PTC, comparison between e-KT-UNIFAC model calculation and measured data.....	56
Figure 4-6: Benzoin condensation process mechanism.....	58
Figure 4-7: Chlorination of organobromine reaction mechanism.....	61
Figure 4-8: Epoxidation process reaction mechanism.....	65
Figure 4-9: Production of furan derivatives reaction mechanism.....	70
Figure 4-10: Production of α -aminobutyric acid in biphasic systems.....	75
Figure 4-11: Algorithm for solving the models of the biphasic reaction systems.....	80
Figure 5-1: Conversion of benzaldehyde to benzoin, comparison between the measured data and the calculated value from the model.....	83
Figure 5-2: Conversion rate of benzaldehyde to benzoin at various initial conditions, comparison between the model prediction and the measured data.....	83
Figure 5-3: Maximum possible conversion of the reaction system with tetrabutylammonium PTC in different solvents.....	86
Figure 5-4: Impurities amount in organic phase at different conversion with two PTCs and two solvents.....	87
Figure 5-5: Relation between activity coefficient of active PTC organic phase (γ_{Ocl}^{β}) and the reaction half-life ($t_{1/2}$) and equilibrium time (t_E) calculated from the kinetic model.....	88
Figure 5-6: Relation between activity coefficient of active PTC organic phase (γ_{Ocl}^{β}) and apparent rate of reaction (k_{App}).....	88
Figure 5-7: Relationship between amounts of PTC fed and the distribution of its into each form in both phases calculated by the kinetic model.....	89
Figure 5-8: Maximum, minimum, and average conversion achieved from the reaction system by different configuration of tetraalkylammonium PTCs.....	91
Figure 5-9: Maximum, minimum, and average conversion achieved from the reaction system using different solvents.....	91
Figure 5-10: Production of epoxide compound, the comparison between measured data [58] and model prediction, a reaction catalysed by formic acid.....	94
Figure 5-11: Production of epoxide compound, the comparison between measured data [58]	

and model prediction, a reaction catalysed by acetic acid.....	94
Figure 5-12: Solubility of water and partitions of acid and peracid.....	97
Figure 5-13: Production of epoxide at 80 °C catalysed by formic acid	97
Figure 5-14: Production of epoxide at 80 °C catalysed by acetic acid.....	98
Figure 5-15: Apparent rate of reaction in different solvent.....	99
Figure 5-16: The rate of raw material conversion in 4 different reaction scenarios, the comparison between measured data [49] and model prediction.....	101
Figure 5-17: The rate of furan production in 4 different reaction scenarios, the comparison between measured data [49] and model prediction	101
Figure 5-18a: LLE predictions between solvents (1), (2), (3) and water	105
Figure 5-19: Partition of products (HMF and furfural) and waste (cyclopentanone).....	107
Figure 5-20: Rate of the overall products generation.	108
Figure 5-21: Rate of the products partitioned into the organic phase.....	108
Figure 5-22: Rate of products and waste generation in different solvents	109
Figure 5-23: Maximum amount of products and waste generation during the reaction period	110
Figure 5-24: Comparison between model prediction biphasic and single phase production of α -aminobutyric acid and experimental data [55].....	111
Figure 5-25: The partition coefficients of the involved species in hydrocarbon solvents.....	112

LIST OF TABLES

Table 3-1: Overview of the constitutive thermodynamic models for predicting behaviours of chemical species in different subsystems	37
Table 3-2: NRTL binary interaction for conceptual segment of NRTL-SAC model.....	40
Table 3-3: NRTL binary interaction for the new conceptual segment of eNRTL-SAC model.....	42
Table 4-1: Segments numbers for subsystem <i>B</i> of the PTC ions	52
Table 4-2: Segments numbers for subsystem <i>C</i> of the PTC species	54
Table 4-3: e-KT-UNIFAC model parameters for PTC systems.....	55
Table 4-4: Classification of the involved chemical species in the benzoin condensation process.....	59
Table 4-5: Classification of the involved reactions in the benzoin condensation process	59
Table 4-6: Physico-chemical properties of the involved species in the benzoin condensation process.....	59
Table 4-7: Classification of the involved chemical species in the chlorination process	62
Table 4-8: Physico-chemical properties of the involved species in the chlorination process	62
Table 4-9: Palm oil compositions and their respective molecular weight and reactive status	66
Table 4-10: Classification of the involved chemical species in the epoxidation process.....	66
Table 4-11: Classification of the involved reactions in the epoxidation process	66
Table 4-12: Physico-chemical properties of the involved species in the epoxidation process	67
Table 4-13: Epoxidation model analysis	69
Table 4-14: Classification of the involved reactions in the furan derivatives production process.....	71
Table 4-15: Classification of the involved chemical species in the furan derivatives production process.....	71
Table 4-16: Physico-chemical properties of the involved species in the furan derivatives production process.....	71
Table 4-17: Production of furan derivative model analysis	74
Table 4-18: Physico-chemical properties of the involved species in the AABA production process.....	75
Table 4-19: Production of α -aminobutyric acid model analysis	77
Table 5-1: Initial condition of organobromine chlorination process	84

Table 5-2: The PTC systems with available parameters	85
Table 5-3: Comparison of conversions calculated with the SAC and e-KT-UNIFAC models	92
Table 5-4: Regressed reaction parameters from experimental data [58].....	93
Table 5-5: Result of epoxide process solvent screening.....	95
Table 5-6: Selected solvent for detail calculation based on water solubility	96
Table 5-7: Regressed reaction parameters for furan derivative production process from experimental data [49].....	100
Table 5-8: Hansen solubility parameters of the analysed chemical species.....	102
Table 5-9: Sets of criteria for solvents selection for production of furan derivative process	103
Table 5-10: Result of solvent screening for furan derivatives production process	103
Table 5-11: Selected solvent for the furan derivatives production detailed calculation.....	104
Table 5-12: Partition coefficient of the involved species in the long chain hydrocarbon solvents.....	112
Table 5-13: Predicted reaction information carried out in different solvents.....	113
Table S - I: Comparison between measured rate of conversion and model calculation of benzoin condensation process	133
Table S - II: Apparent rate of reaction, reaction half-life, equilibrium time, and activity coefficients of PTC from kinetic model	135
Table S - III: Configuration of PTC, between C4 to C16.....	136
Table S - IV: Conversion of organobromine with different PTC, in different solvents.....	138

INTRODUCTION AND OVERVIEW

**"Essentially, all models are wrong,
...but some are useful"**

George E.P. Box [1]

1.1 INTRODUCTION

Biphasic reaction systems have a broad range of application, such as the manufacture of petroleum-based chemicals, pharmaceuticals, agricultural and biochemical products. In these systems, two liquid phases are established by immiscibility between co-existing solvent pairs such as aqueous/organic, ammonium/organic, supercritical-CO₂/ionic liquid, or separated by a permeable membrane. The reactants, catalysts (including also biocatalysts and enzymes), and inert species partition differently in the liquid phases, allowing novel synthesis routes with higher conversion, selectivity, and yield of desired products; as well as, lower amounts of an unwanted side products. Additionally, the reactants, catalysts, and products can often be found in different phases, making downstream separation processes easier.

Mathematical modelling can be valuable tool for efficiently analysing and designing these complex systems. For example, solution and reaction properties of many chemicals involved (reactants, solvents, products, co-products, and catalysts) need to be described; the extent of miscibility (totally, partially, or fully immiscible) must be established; the phases where reactions occur need to be identified; and the reaction and mass transfer mechanisms must be established. Also, the effects of inert species on partitioning and of mixture composition on reaction rates must be characterised.

Issues concerning the formulation of the model involve:

1. The purposes of the model
2. The properties of the involved chemicals
3. The reactor configurations
4. The reaction related issues:
 - a. The location of the reaction
 - b. The type of the reaction (kinetic or equilibrium controlled)
 - c. The rates of main and side reactions
5. The distributions (partitions) of the involved chemicals
 - a. The distribution during the reaction
 - b. The post-reaction distributions
6. The lack of experimental data

1.2 OBJECTIVES

To overcome the above challenges and to demonstrate the practicality of this project, three consecutive objectives are defined:

1. To develop a systematic framework for modelling of the biphasic reaction system;
2. To apply the developed framework for constructing models of the specific case;
3. To implement the developed model for the process design, optimisation, and analysis.

Whereas, the developed framework should provide an efficient and systematic procedure for developing the model of biphasic reacting systems that also requiring the minimum effort on the experiment. The selected cases should underline broad range of applications of the framework. And, lastly, the models are implemented for the improved and innovative design(s) of the systems.

1.3 THESIS STRUCTURE

This chapter gives a brief introduction to the biphasic systems, the issues concerning modelling of the system, and the objectives of this project. Chapter 2 covers the previous work done on modelling and applications of the system. The modelling methodology which is used as a guideline for developing the framework is described. Various applications of the system and their importance are presented. The previous attempts to model the systems are also displayed. Chapter 3 elaborates on the developed framework together with the corresponding generic model; as well as, implemented the constitutive models. The framework is then implemented for modelling of the selected processes in chapter 4. The constructed models are then employed for design and analysing of their relevant processes in chapter 5. Lastly, chapter 6 summarises the contribution of this project and presents the intriguing aspects that are not yet solved by this work for future consideration.

“Since all models are wrong the scientist must be alert to what is importantly wrong. It is inappropriate to be concerned about mice when there are tigers abroad”

George E.P. Box [2]

LITERATURE REVIEW

This chapter starts with the review of the generic modelling methodology, in section 2.1. This methodology has been used as a guideline for developing the framework for modelling of the biphasic reaction systems in chapter 3.

Section 2.2 presents applications of biphasic reaction systems including, but not limiting to, phase transfer catalyst involved systems, epoxidation, hydroformylation, and amino acid production. Five of the most interesting cases are selected for modelling and analysis in chapters 4 and 5.

Section 2.3 collects and displays the attempts to model biphasic reaction systems in an open literature. Although these models contain some limitations, they can be used as a good starting point for examining biphasic reaction systems in detail.

Although this chapter does not contain any novel contribution of this work, it gives an overview of what has been done before; in order to appreciate the accomplishment of this project.

2.1 MODELLING METHODOLOGY

The main objective of this section is to review the generic modelling methodology suitable to apply for biphasic reaction systems.

The modelling fundamentals, modelling methodologies, and generic model structure are taken from the *Product and Process Modelling: A Case Study Approach* by Cameron and Gani [3]. Figure 2-1 shows a conceptual perspective of the modelling system.

- In a general system (S), the system boundary is shown as the box, providing the limit of the model consideration
- The states variables (x) indicate the state of the system at a point in time and space
- The parameters (p) are the variables associated with geometric, physical, and chemical properties of the system
- The inputs (u) are the properties variables that can be chosen to affect the behaviour of the system, they are usually known or controllable variable
- The outputs (y) are the internal properties variables that are usually linked to the states
- The disturbances (d) are the properties variables that those effects are uncontrollable but sometimes measurable

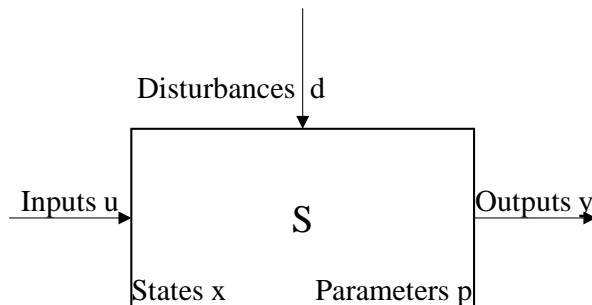


Figure 2-1: A conceptual modelling system perspective

The model development process, as shown in Figure 2-2, is an iterative procedure of eight major tasks, as followed:

- Problem and model definition, specifying the necessity and the goal of the model.
- Model conceptualisation, defining clear boundaries and crucial state of the model.
- Model data requirement, identifying the data needed for model construction and validation.
- Model construction, translating the verbal conceptualisation of the model into the mathematical description.
- Model solution, generating a solution of the model using appropriate numerical method(s). In this task, several issues relating to model construction task need to be resolved prior to solution generation.

- Model verification, checking the model implementation against the conceptual description and debugging the error of coding.
- Model validation, checking if the model is a reasonable representation of the actual system. If the validation is poor, conceptualisation and collected data need to be reviewed. The principle is to start with the simplest “fir-for-purpose” model.
- Model deployment and maintenance, applying and documenting the model without losing the information leading to significant rework.

The specific modelling framework, in chapter 3, is developed based on this generic framework with the focus on biphasic reaction systems.

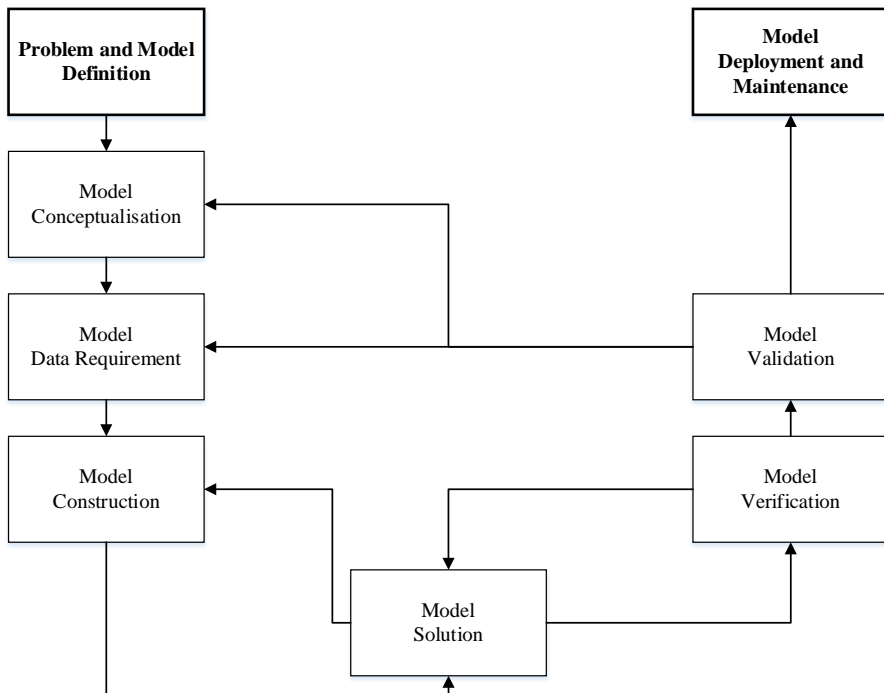


Figure 2-2: Generic model development framework

The generic model structure for chemical and biochemical applications consists of:

1. Balance equations
2. Constitutive equations
3. Conditional equations

The balance equations are established within the system boundary, they are based on the law of conservation, taken from the following forms:

$$0 = f(x, u, d) \quad 2-1$$

$$\frac{dx}{dt} = f(x, u, d, t) \quad 2-2$$

In the above equations, equation 2-1 represents a set of algebraic equations (AEs) and steady-state model behaviour; equation 2-2 represents a set of ordinary differential equations (ODEs) and lumped-dynamic model behaviour. x represents a vector of state variables, u represents a vector of specified variables, d and t represent independent variables. The two-dimensional PDE system is not considered in this work since the systems under interested have been described by lumped-ODE models.

The constitutive equations are algebraic equations in a form:

$$0 = \theta - g(T, P, n, \beta) \quad 2-3$$

where, θ is a constitutive variable, which may be a function of temperature (T), pressure (P), composition (n), and properties model parameters (β). Thermodynamic models are the most important part of constitutive equations in biphasic reaction systems models.

The conditional equations (or connection equations) are usually a set of algebraic equations, represented as:

$$0 = x - h(x, y, u, d, t) \quad 2-4$$

which can be either implicit or explicit depended on if they are functions of x or not.

These generic models are modified and extended for the modelling of biphasic reaction systems in the next chapter. The balance, constitutive reaction kinetic, and conditional equations are presented in section 3.1.2. Section 3.2 discusses and displayed constitutive thermodynamic models options suitable for biphasic reaction systems.

2.2 REVIEW OF THE APPLICATION

This section presents a review of applications of biphasic reaction systems. Section 2.2.1 presents a review of phase transfer catalyst (PTC) based systems while section 2.2.2 presents a review of other systems which utilise the concept of the biphasic reaction system.

2.2.1 PTC-Based Systems

Phase transfer catalysis is a synthetic organic method and manufacturing process technology that brings two substances located in different phases of a mixture by the use of small quantities of an agent which transfers one reactant across the interface into the other phase [4,5]. The first known commercial use of a PTC system was reported by Rueggeberg et al. [6], for the production of benzyl benzoate from benzyl chloride and sodium benzoate catalysed with diethyl- and triethylamines as PTC. Since then, the approach has been applied to various types of organic synthesis opening novel reaction routes and allowing selection of faster and/or cheaper catalysts. The focus of this work is the system that uses quaternary ammonium cations as the transfer agent. The quaternary ammonium cation has the structure of R_4N^+ , as shown in Figure 2-3, where four short chain alkyl or aryl groups attach to the nitrogen atom which makes it permanently charged. The electrolytic nature of the charged cation allows it to exist in the aqueous phase, while the hydrocarbon part helps it penetrating into the organic phase.

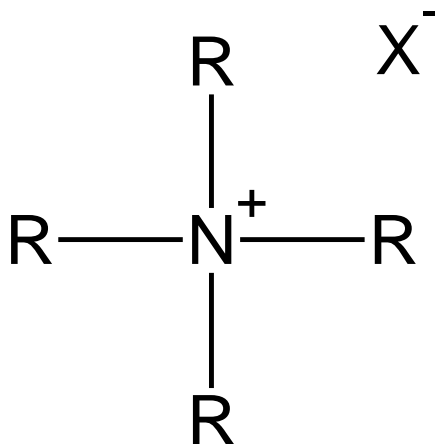


Figure 2-3: Molecular structure of phase transfer catalysts (PTC)

The generic PTC reaction mechanism is shown in Figure 2-4, the biphasic PTC system contains two completely immiscible liquid phases created by water and an organic compound. The PTC transfers as an active species from one phase to the other in order to convert the reactant to the desired product and then transferring as an inactive species back to be regenerated in the aqueous phase. The desired reaction is to form the product RY from the reactant RX. The PTC is identified as Q, which in the aqueous phase is a positively charged cation (Q^+), coexisting with anions (X^- and Y^-). In the organic phase, the PTC is in a neutral form (active QY and inactive QX). The reaction occurs in the organic phase with RX going to the desired RY while

QY goes to QX. Then the inactive PTC (QX) transfers to the aqueous phase and ionises. The added salt (M^+Y^-) reforms the inactive PTC (Q^+X^-) to transfer back to the organic phase, forming a spent salt product (M^+X^-). The applications of PTC system are presented in subsections below.

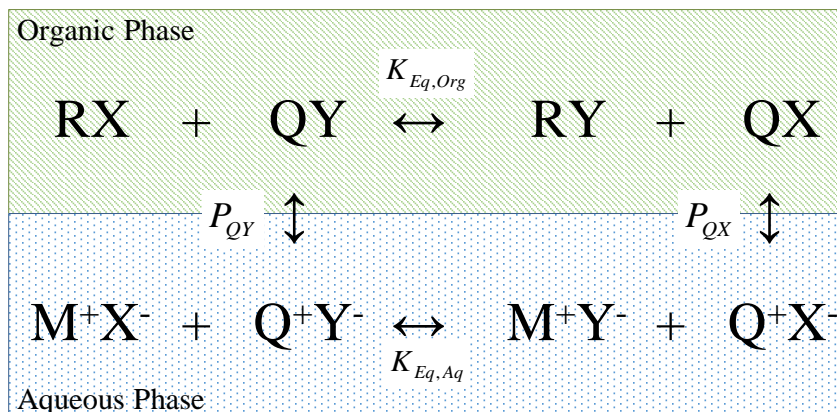


Figure 2-4: Reaction mechanism of a generic PTC system

2.2.1.1 Active Ion Transfer Systems

The biggest application area of the PTC system is the transferring of the active ions across the interface for substitution reactions. Some important examples include halogenations and cyanation, which are shown below. The models of the biphasic halogenation reaction, *chlorination of organobromine*, are constructed in chapter 4, section 4.2.2; while the model-based analysis and design of the processes are presented in chapter 5, section 5.2.

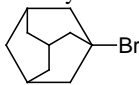
1. Halogenation

The halogenation reaction is the addition of one or more halogens to an organic compound. The halogenated products are used in pharmaceutical, chemical, and agricultural industries. PTC-induced halogenations in biphasic systems have been reported in several publications.

- Starks [4] uses methyltrioctylammonium ($CH_3(C_8H_{17})_3N^+$) to catalyse the reaction of chlorooctane to bromooctane and iodoctane. The organic phase is formed by the haloctane itself, the product yield reaches 95% after 1 hour.
- Dillow et al. [7] present the production of benzyl bromide (C_7H_7Br) from the reaction between benzyl-chloride (C_7H_7Cl) and potassium bromide (KBr) catalysed by tetraheptylammonium ($(C_7H_{15})_4N^+$) PTC. The reaction is carried out in a two-phase mixture of supercritical carbon dioxide ($SCCO_2$) and acetone at 50 and 75 °C and 200 bars. The reactions reach 50% conversion in 20-60 hours, with maximum conversion around 65% in 100 hours.
- Landini et al. [8,9] report using tetraalkylammonium and phosphonium (R_4N^+ and R_4P^+) PTCs, which contain 12-16 carbon atoms, to catalyse the reaction of n-octyl methanesulphonate ($C_8H_{17}OSO_2ME$) with potassium chloride, bromide, and iodide

(*KCl*, *KBr*, and *KI*) in water-chlorobenzene two-phase mixture.

- Vander Zwan and Hartner [10] employ methyltrioctylammonium ($CH_3(C_8H_{17})_3N^+$) for catalysing the reaction of benzyl-chloride (C_7H_7Cl) with potassium fluoride (*KF*) in the water-acetonitrile two-phase mixture. The reaction half-life is 42 hours, with maximum conversion greater than 95% and yield above 90%.
- Royer and Husson [11] use tetrabutylammonium ($(C_4H_9)_4N^+$) and crown ether to catalyse the reaction of chloro-ketal (2-butyl-2-(2-chloroethyl)-1,3-dioxolane, $C_9H_{17}ClO_2$) with potassium iodide in the water-toluene mixture. They achieve 74% yield of the product (2-butyl-2-(2-iodoethyl)-1,3-dioxolane, $C_9H_{17}IO_2$), which is an intermediate for the production of *Gephyrotoxin* compound.
- Schreiner et al. [12] obtain 11-92% yields of complex halogenated products such as



Bromoadamantane ($C_{10}H_{15}Br$,) using tetrabutylammonium ($(C_4H_9)_4N^+$) as a catalyst in the water-fluorobenzene mixture.

- Yufit and Zinovyev [13] also employ methyltrioctylammonium ($CH_3(C_8H_{17})_3N^+$) to catalyse the reactions of bromohexane ($C_6H_{13}Br$) with potassium chloride and n-octyl methanesulphonate ($C_8H_{17}OSO_2ME$) with potassium chloride, bromide, iodide, and fluoride in the water-toluene biphasic mixture. They've observed first order behaviour of the overall reaction rates, where iodide has the highest rate and fluoride is not reactive.

2. Cyanide displacement

Cyanide displacement or cyanation process is the attachment or substitution of a cyanide group (*CN*) on various substrates to produce nitrile compounds (a.k.a. cyano compounds). Nitriles are mainly used in pharmaceutical industry, as more than 30 nitrile-containing medicines are currently prescribed for a diverse variety of medicinal indications in 2010 [14]. Moreover, some organic nitriles such as adiponitrile, an important precursor to the nylon polymer, are produced on a large scale. PTC-induced cyanation processes in biphasic systems have been reported in several publications.

- Aside from halogenation, Starks and co-worker [4,15] also employ methyltrioctylammonium ($CH_3(C_8H_{17})_3N^+$) to catalyse the production of nitriles from secondary and tertiary alkyl halides, cyclohexyl, n-octylmethanesulfonate, and haloctanes. The reactions give 85-90% yield of cyanide products, with 95% conversion reached within 4 hours.
- Landini et al. [9] use tetraalkylammonium catalyse the reaction of n-octyl methanesulfonate ($C_8H_{17}OSO_2ME$), in the water-chlorobenzene mixture. The reaction follows first order kinetic with higher reaction rate compared to halogenations processes.
- Vander Zwan and Hartner [10] use methyltrioctylammonium ($CH_3(C_8H_{17})_3N^+$) for catalysing the reaction of benzyl-chloride (C_7H_7Cl) and bromohexane ($C_6H_{13}Br$) with potassium cyanide (*KCN*) in the water-acetonitrile mixture. The reactions half-lives are 2.20 and 0.98 hours. for benzyl-chloride and bromohexane reactions respectively.
- Chandler et al. [16] employ tetraheptylammonium ($(C_7H_{15})_4N^+$) PTC to catalyse the

reaction of benzyl chloride with potassium cyanide in two phases that created from SCCO_2 and the reactant itself. The reaction reaches 100% conversion after 10 hours, with first order kinetic behaviour.

- Mąkosza and Fedoryński [17] report using triethylbenzylammonium (TEBA, $\text{C}_6\text{H}_5\text{CH}_2(\text{C}_2\text{H}_5)_3\text{N}^+$) catalyse the acyl cyanide and cyanohydrin derivative, as shown in Figure 2-5, in water-dichloromethane mixture with 74% and 92% conversion respectively.

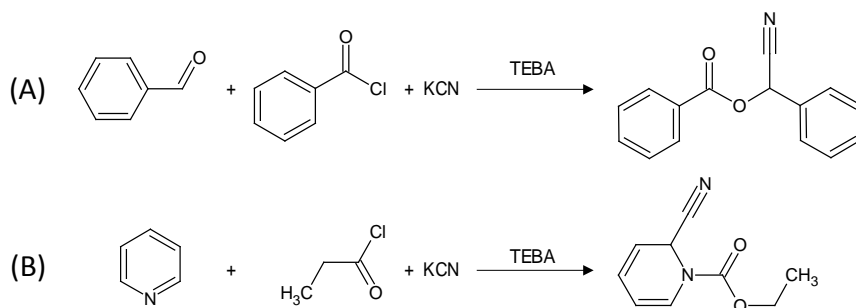


Figure 2-5: Makosza's replacement reactions [17]:
(A) acyl cyanide production; (B) cyanohydrin production

3. Other displacements

Besides halogens and cyanide, PTC can also be used for displacements of other active ions or groups such as nitrite (NO_2^-), cyanate (NCO^-), hydroxide (OH^-) [4]; thiocyanate (SCN^-), azide (N_3^-) [9]; acetate (OAc^-) [10]; and sulphide (S^{2-}) [18].

2.2.1.2 Catalysed-ion Transfer Systems

Phase transfer catalyst can also be used to transfer the catalysed-ion across the liquid-liquid interface from the aqueous phase to initialise the oxidation reaction in the organic phase. In these reactions scenarios, the active PTCs are not spent; but constantly catalysing the reaction between the organic compounds. Some important examples include benzoin condensation, alkylations, and hydrolysis are reported below.

1. Benzoin condensation

Yadav and Kadam [19] propose using tetramethyl- and tetrabutylammonium ($(\text{CH}_3)_4\text{N}^+$ and $(\text{C}_4\text{H}_9)_4\text{N}^+$) PTCs as catalyst for the benzaldehyde condensation reaction to create benzoin. The detailed reaction mechanism and the constructed reaction model are presented in chapter 4, section 4.2.1. The model implementation is shown in chapter 5, section 5.1.

2. Alkylations

The alkylation is the reaction that combines two alkyl compounds. Conventionally, these reactions require organic alkylating agents such as organometallics or carbenes.

The use of PTC systems for the alkylation reactions has been reported in several publications. The PTC-induced alkylation help eliminating the use of expensive or highly unstable alkylating

agents by transferring hydroxide ion (OH^-) from the aqueous phase to initiate the alkylation in the organic phase.

- Mąkosza and Fedoryński [17] present the alkylations and dialkylations of benzyl cyanide with primary alkyl halides, secondary alkyl halides, and dihaloalkanes catalysed by tetraalkylammonium PTCs in a biphasic mixture of water-benzene. The reactions, employed PTCs, and achieved conversion are shown in Figure 2-6.

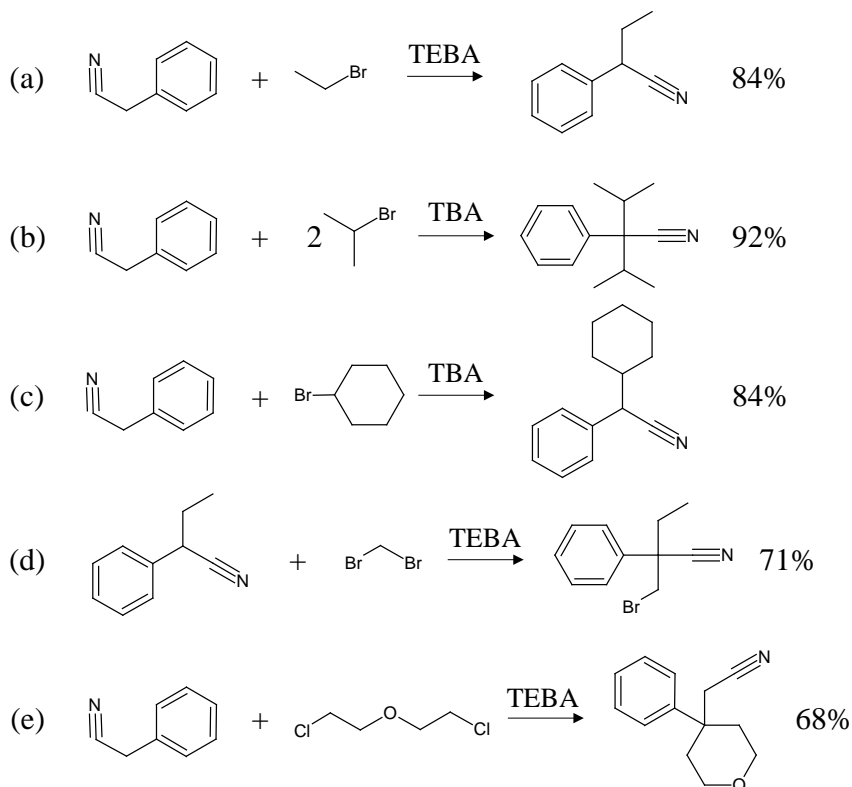


Figure 2-6: Makosza's alkylations reactions [17]

- (a) Alkylation of benzyl cyanide with primary alkylhalide
- (b) Dialkylation of benzyl cyanide with secondary alkylhalide
- (c) Alkylation of benzyl cyanide with cycloalkylhalide
- (d) Alkylation of 2-phenylbutanenitrile with dihaloalkane
- (e) Alkylation of benzyl cyanide with dihaloalkane

TBA: tetrabutylammonium ($(C_4H_9)_4N^+$)

TEBA: triethylbenzylammonium ($(C_6H_5)CH_2(C_2H_5)_3N^+$)

- De Zani and Colombo [20] employ tetrabutylammonium ($(C_4H_9)_4N^+$) PTC to catalyse the reaction between 4-*tert*-butyl phenol ($HOC_6H_4C(CH_3)_3$) and benzyl-bromide ($C_6H_5CH_2Br$) in a continuous plug-flow reactor containing water-dichloromethane mixture as shown in Figure 2-7. They achieve 100% conversion with 1.25 mL·min⁻¹ flow rate of raw material and resident time 4 minutes.

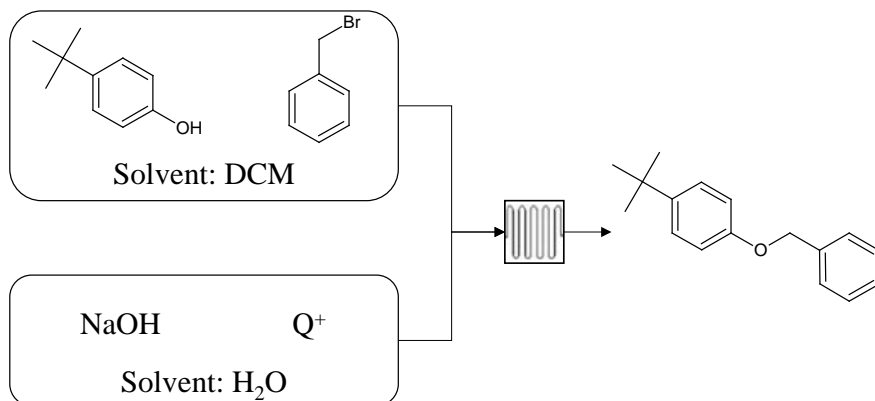


Figure 2-7: De Zani's alkylation reaction [20]

- Vanden Eynde and Maillieux [21] present the PTC-induced productions of aryl ethers. The most notable results are shown in Figure 2-8, consist of (a) the production of 1,2-dimethoxybenzene ($C_6H_4(OCH_3)_2$) from the reaction between 1,2-benzenediol ($C_6H_4(OH)_2$) and methyl-iodide (CH_3I); (b) the production of 4-nitroanisole ($O_2NC_6H_4OCH_3$) from the reaction between 4-nitrophenol ($O_2NC_6H_4OH$) and iodomethane; and (c) the production of (hexyloxy)benzene ($C_6H_5OC_6H_{13}$) from the reaction between phenol and 1-bromopentane, which have 90%, 90%, and 95% conversion respectively. The employed PTC is tetrabutylammonium ($(C_4H_9)_4N^+$), the two liquid phases are created by immiscibility between water and the reactant itself.

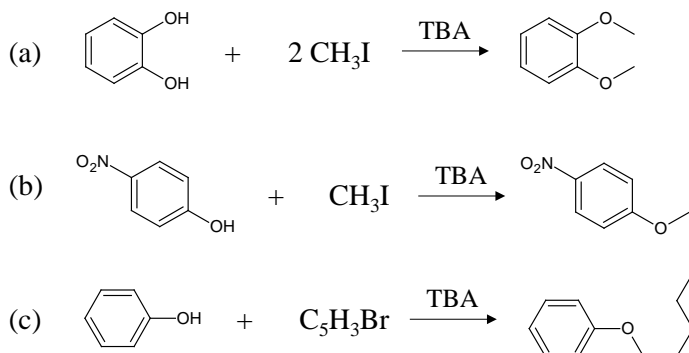


Figure 2-8: Vanden Eynde's alkylation reactions [21]

- Meanwhile, Lygo and Andrews [22] use quaternary ammonium salts to catalyse the production of imines compounds and Cassani et al. [23] also employ the quaternary ammonium salt to catalyse the Mannich reaction.

3. Hydrolysis

Aside from condensation and alkylations, PTC is also used to transfer the nucleus-seeking agents for hydrolysis reaction across the interface.

- Starks [4] report the use of quaternary ammonium salts for catalysing the hydrolysis of long-chain esters to carboxylic acids in mixed esters-water systems and sulphonyl chlorides to antibacterial sulphonamides drugs in the water-dodecane mixed biphasic system.
- Wang et al. [24] use tetrabutylammonium ($(C_4H_9)_4N^+$) and benzyltributylammonium ($C_6H_5CH_2(C_4H_9)_3N^+$) to initialise the hydrolysis of 4-methoxyphenylacetic acid butyl ester ($CH_3OC_6H_4COOC_4H_9$), in the mixtures of water and 3 organic solvents (chlorobenzene, n-hexane, and dibutyl ether), as shown in Figure 2-9. They achieve maximum conversion around 99% in hexane, with tetrabutylammonium gives the fastest overall reaction rate.

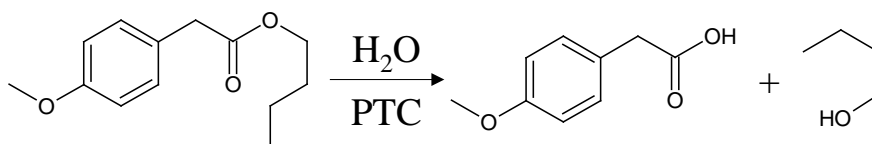


Figure 2-9: Hydrolysis of 4-methoxyphenylacetic acid butyl ester [24]

2.2.1.3 Free-Radical Transfer Systems

Other than transferring the active- and catalysing ions, PTC can also be used to initiate free radical reactions of long chain organic compounds.

- Starks [4] present the use of quaternary ammonium salts to initialise the oxidations of 1-octene and 1-decene in benzene or toluene solvents and water mixtures. The oxidising agent is potassium permanganate ($KMnO_4$), the reaction is highly exothermic and auto-catalytic after the initialisation. The reaction completes within 0.5 hours, with 91% yield of the carboxylic acids products.
- Kaur et al. [25] use tetrabutylammonium ($(C_4H_9)_4N^+$) to initialise the polymerisation of styrene, methyl methacrylate, and acrylonitrile in the water-benzene biphasic mixture. Potassium persulfate (KPS) is used as an initiator; yields of homopolymers products of polystyrene (PS), poly-methyl-methacrylate (PMMA), and poly-acrylonitrile (PAN) are 23%, 8.5%, and 62% respectively.

2.2.2 Other Biphasic Reaction Systems

In addition to PTC-based reaction systems, chemicals, pharmaceuticals, and agro-bio products have also been synthesised by biphasic reaction systems. Similar to the PTC systems, the reactants and catalysts (including also biocatalysts and enzymes) will partition differently in the liquid phases, allowing novel synthesis routes as well as higher selectivity, conversion, and yield of desired products with lower amounts of side reactions. In addition, following reaction, the reactants, catalyst, and products can often be found in different phases, making for easier separation. However, without the involvement of the quaternary ammonium species.

Subsections 2.2.2.1 to 2.2.2.3 present some applications of the biphasic reaction system in chemical, biochemical, and pharmaceutical industries; most notable examples are epoxidation of unsaturated fatty acid by hydrogen peroxide, production of furan derivatives from biomass, and enhancement of the α -aminobutyric acid (AABA) production; which are selected for modelling and analysing in chapters 4 and 5.

2.2.2.1 Chemical Industry

1. Epoxidations of unsaturated fatty acids

The production of epoxide compounds from unsaturated fatty acids is accomplished by employing heterogeneous species to oxygen atom from oxygen donors (such as hydrogen peroxide) in the aqueous phase to react with the unsaturated acids in the organic phase.

- Antonelli et al. [26], Khlebnikova et al. [27,28], and Santacesaria et al. [29] employ tungsten-based complex catalysts to transfer the oxygen atom. Although the reactions are carried out in mild condition (below 100 °C and 1 atm), the overall reaction rates are slow and the epoxide products yields are dissatisfied. Moreover, the complex catalysts are hardly predictable by any thermodynamic model, the opportunity for the improved design of this reaction scenario relies purely on the experiment.
- Recently, Köckritz and Martin [30], Campanella et al. [31,32], Dinda et al. [33], Santacesaria [34,35], and Sinadinovic-Fiser [36] propose an alternative scenario for the epoxidation of fatty acid, including long-chain fatty acid, using carboxylic acids to transfer the oxygen atom in peracid forms. This reaction scenario provides faster, or equivalent, overall reaction rate and higher product yields at the same reaction condition. Moreover, the modelling parameters are generally available. Therefore, it is selected for modelling in section 4.2.3; the analysis and novel-optimal design based on the constructed model are presented in section 5.3.

2. Production of carboxylic acids

Adipic, suberic, and benzoic acids are desirable products for large-scale industry [37–39]. The production of these acids through direct oxidation is either resulted in moderate yield or generate toxic by-products. Pai et al. [40] proposed the production of mono- and dicarboxylic acids from cycloolefins and hydrogen peroxide, as shown in Figure 2-10. The product yield is higher than the corresponded direct oxidation scenario; as well as, the reaction rate is faster; moreover, the reaction does not generate undesirable toxic by-products.

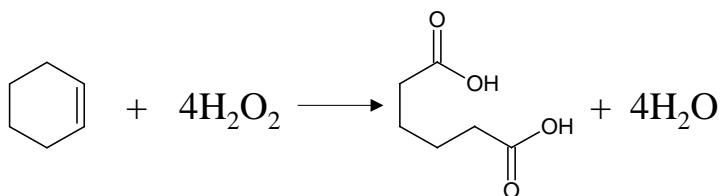


Figure 2-10: Dicarboxylic acid production from cyclo-olefin [40]

3. Hydroformylation of higher olefins

The hydroformylation reaction is a reaction of 1-alkenes with carbon monoxide and hydrogen in the presence of a catalyst [41]. Generally, the rhodium complex is employed to catalyse the hydroformylation of short-chain olefins. However, due to the problems related to the separation of the product from the catalyst, the hydroformylation of long-chain (> 6 carbon atoms) olefins is not yet successfully commercialised [42,43]. To overcome the separation limitation, various researches on novel solvents systems, novel complex catalysts, and novel operation procedures were conducted.

- Sellin et al. [42] apply a biphasic mixture of ionic liquid (IL), 1-butyl-3-methylimidazolium hexafluorophosphate ($[BMIM]PF_6$), and $SCCO_2$ for hydroformylation of 1-hexene (C_6H_{12}). Although the conversion is lower than the reaction in conventional toluene solvent (40% to 99%), with a similar selectivity of aldehyde (83-84%); the loss of the complex rhodium catalyst is less than 1 ppm (less than 0.6% of fed catalyst).
- Nowothnick et al. [43] successfully apply nonionic surfactants, Marlophen NP 9 (see Figure 2-11a), into biphasic hydroformylation of 1-octene and 1-dodecene. As shown in Figure 2-11b, at first, the catalyst and raw material are soluble in the organic phase at high temperature; then the temperature is lowered, the third phase is created, mixing water, catalyst, and raw material together, and the reaction is taking place; after the reaction time, the mixture is cooled to room temperature to give a two-phase system where the catalyst ends up in the aqueous phase, separating from the product.

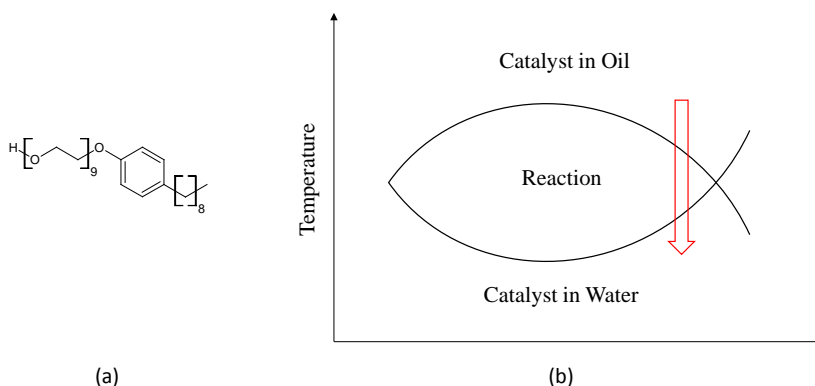


Figure 2-11: Nowothnick's hydroformylation [43];
(a) utilised surfactant; (b) reaction scheme

- Obrecht et al. [44] also present similar hydroformylation operation where the catalysts solubilities are controlled by pH and temperature. Figure 2-12 shows the operation procedures and employed catalysts for (a) pH controlled hydroformylation and (b) temperature controlled hydroformylation. In scenario (a), the catalyst is soluble in the aqueous phase in acidic condition; the reaction is carried out in a neutral condition, then the process is acidified to separate the catalyst from the product. In scenario (b), the operation is similar to Nowothnick's.

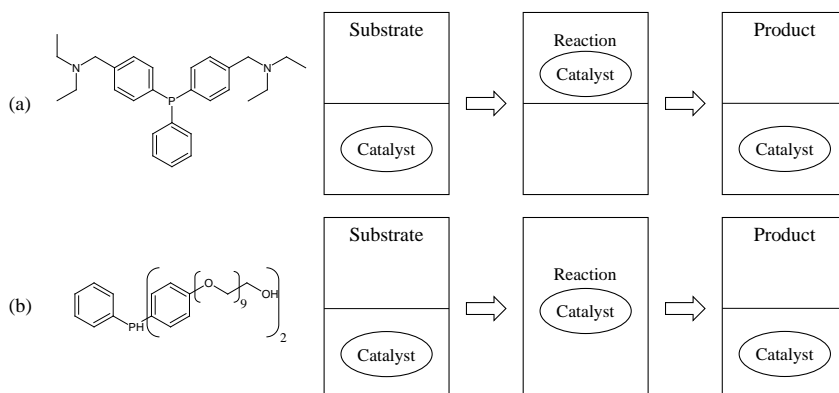


Figure 2-12: Obrecht's hydroformylation; (a) pH controlled; (b) temperature controlled [44]

4. Carbon dioxide absorption

Besides chemical synthesis, the biphasic reaction system is also applied to the absorption of carbon dioxide. As global warming becomes an important issue, carbon capture is one of the solutions for decreasing greenhouse gases emissions. Initially, the post-combustion carbon capture process requires high energy consumption for the regeneration of the amine solvent. Xu et al. [45] proposed the use of two phase reactive absorption. The mechanism of this process is shown in Figure 2-13, at first, the CO_2 is absorbed into the mixture of butanediamine (BDA) and water by reaction 2-5; and then diethylethanolamine (DEEA) is added into the system, forming the upper phase where CO_2 is partitioned into; the lower phase, consist of BDA and water, is then recycled for another absorption cycle.

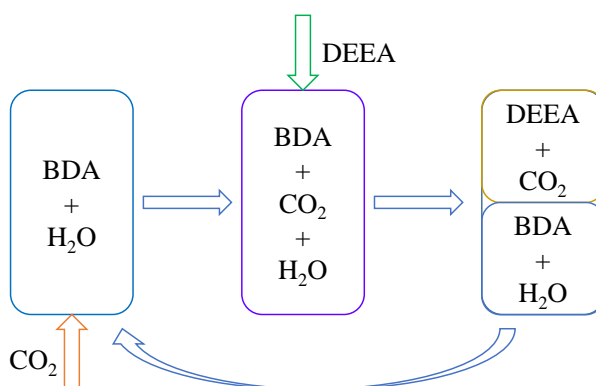
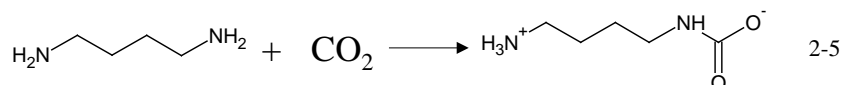


Figure 2-13: Biphasic reactive absorption [45]

2.2.2.2 Biochemical Industry

1. Furan derivatives production

The biphasic reaction system is employed to enhance the production yield and reduce reaction time of the furan derivatives production process. Generally, the production is limited by the unfavourable chemical equilibrium and the formation of undesired side-product; the addition of solvents help to overcome these issues by extracting the desired product into the organic phase. This process is selected for further studying, the detail description and constructed model can be found in chapter 4, section 4.2.4; the model-based design and analysis is presented in chapter 5, section 5.4.

- Amiri et al. [46] present the production of 5-Hydroxymethylfurfural (HMF) and furfural from rice straw using 2-propanol, 1-butanol, methyl isobutyl ketone (MIBK), and acetone as extraction solvents. The reactions are carried out at 180 °C for 3 hours; the achieved maximum conversion is 76% in acetone; production yields of HMF and furfural are 60% and 80% respectively.
- Gallo et al. [47] employ bio-based solvents (γ -valerolactone (GVL), γ -hexalactone (GHL), γ -octalactone (GOL), and γ -undecalactone (GUL)) for the production of HMF from monosaccharide sugars (glucose and fructose). They achieved 94% highest conversion and 84% HMF highest selectivity of fructose with GVL organic solvent.
- Gurbuz et al. [48] present the production of furfural and levulinic acid from corn stover hemicellulose in biphasic reactors with alkylphenol solvents, the production scheme is highlighted in Figure 2-14. The furfural production (on the left reactor) has 98% conversion of xylose and furfural selectivity of 80%; while the levulinic acid production (on the right reactor) can reach complete conversion with 70% selectivity.
- Ordonsky et al. [49,50] design a biphasic rotating foam reactor for the production of HMF in 1-butanol, 2-methyltetrahydrofuran (MTHF), and cyclohexane. However, the outputs from their zeolite-based catalyst are not satisfying with furfural yield between 40-60% only.

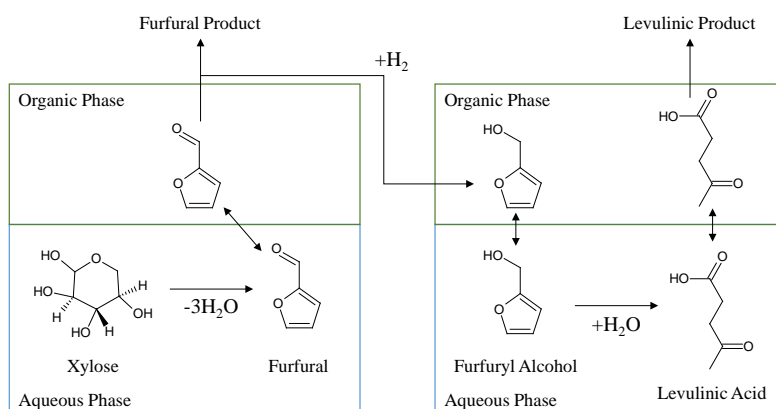


Figure 2-14: Productions of furfural and levulinic acid from hemicellulose [48]

2. Biodiesel

Transesterification of vegetable oils to fatty acid methyl esters (FAME) has been carried out in biphasic systems. These systems offer higher production yield, higher purity product, faster reaction, as well as prevent biocatalyst from deactivating.

- Dube et al. [51] use a two-phase membrane reactor for the production of FAME from canola oil and methanol. The help removing unreacted canola oil from the FAME and shifting the reaction equilibrium to the product side resulting in higher conversion and faster reaction rate.
- Lozano et al. [52] employ the IL-SCCO₂ system for the production of biodiesel with enzymatic catalyst biphasic reaction. Generally, the catalytic efficiency of the enzyme is lowered because of its direct contact with methanol, as shown in Figure 2-15. This approach is not only preventing the deactivation of the biocatalyst, but also enhancing mass transfer of the reactive species toward the catalyst and reducing the separation step after the reaction. They've achieved 79% product yield with 1-octadecyl-3-methylimidazolium bis((trifluoromethyl)sulfonyl)imide ([C18mim][NTf2]) IL.

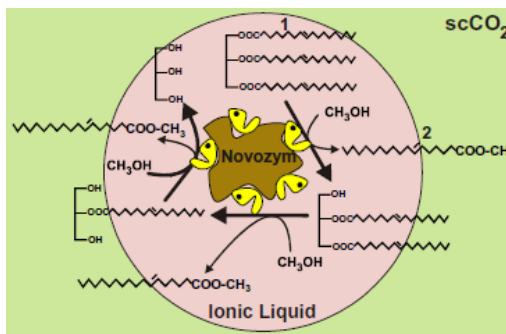


Figure 2-15: Lozano's transesterification in IL-SCCO₂ [52]

- Hongfa et al. [53] proposed a thermomorphic biphasic system of heptane and methanol for the production of biodiesel, the reaction scheme is shown in Figure 2-16. This reaction system gives 95-97% product yield and leaves virtually no undetectable level of glycerol and free fatty acid.

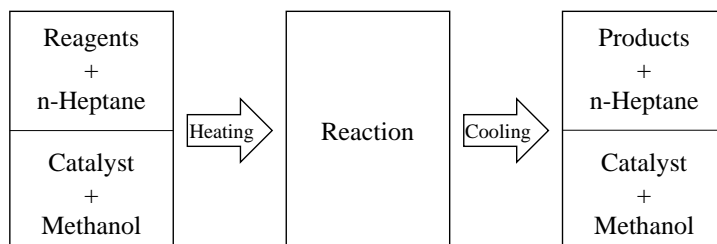


Figure 2-16: Thermomorphic biphasic production of biodiesel [53]

2.3 REVIEW OF THE AVAILABLE MODELS

As presented in the previous section, biphasic reaction system has been applied to a broad range of production systems. Undoubtedly, there is a great demand for the mathematical modelling of these systems. This section presents models of the biphasic reaction systems reported in publications, especially for those system discussed in the previous section. Herein, section 2.3.1 presents reaction models of the system and section 2.3.2 presents phase equilibrium models of the related chemical species.

2.3.1 Reaction Models

2.3.1.1 PTC-Related Reactions Models

Landini et al [9] use simple first order reaction rate law, as shown in equation 2-6, for describing the halogenations and active ions (including cyanide) displacements reactions in the biphasic water-chlorobenzene mixture. Vander Zwan and Hartner [10] also assume first order reaction rate law for the calculations of processes half-lives of halogenations and acetate displacement processes. Later Dillow et al. [7] modify Landini's equation for their halogenations in SCCO₂-acetone by adding the reversible term, as shown in equation 2-7.

$$r_j = k_j [S][QX] \quad 2-6$$

$$r_j = k_j [QX]([S] - [S]^E) \quad 2-7$$

where, r_j is the reaction rate of reaction j , k_j is the first order rate constant of reaction j , $[QX]$ is the concentration of PTC, and $[S]$ and $[S]^E$ are the concentration of the substrate at any given time and equilibrium concentration of the substrate respectively.

Whereas, Yufit and Zinovyev [13] adopt the enzyme-promoted reaction rate, equation 2-8, for calculating the amount of the halogenated products at any given time.

$$[P] = \frac{k_2 k_3 [E]_0 t}{k_2 + k_3} + \frac{k_2^2 [E]_0 \{1 - \exp[-(k_2 + k_3)t]\}}{(k_2 + k_3)^2} \quad 2-8$$

where, $[P]$ is the product concentration, $[E]_0$ is the initial concentration of raw material, and k_2 and k_3 are the adjustable rate constants.

Starks and Owens [15] use the lumped-phase kinetic-equilibrium equation for the cyanation of simple halide molecules. Their equation is a simplified pseudo-first order reaction equation as shown in equation 2-9.

$$\ln \left[\frac{P}{P_0} \right] = - \left[\frac{kK}{r + K} \right] Q_0 t \quad 2-9$$

where, k is the first order rate constant, K is the equilibrium constant, Q_0 is the initial amount

of PTC, r is the ratio between active and inactive ions, and P and P_0 are the amount of product and the initial amount of product respectively.

Yadav and Kadam [19] have made a detailed analysis of benzoin condensation process with the assumption that it is controlled by only one rate-determining step; therefore, the model eventually turns out to be first order, as shown in equation 2-10.

$$\frac{X}{1-X} = kP_0N_0t \quad 2-10$$

where, X is the conversion and N_0 is the amount of PTC.

Similarly, Wang et al. [24] also describe the hydrolysis of 4-methoxyphenylacetic acid butyl ester (see Figure 2-9) by pseudo-first order reaction rate equation, as shown in equation

$$-\ln(1-X) = kt \quad 2-11$$

Those reactions equations of the PTC-based systems have simple first order, or modified-first order reaction rate equations. Although the model could match the measured data fairly well, they have limited application toward the prediction and design of these complex PTC systems. Moreover, none of the above-mentioned models is included predictive, or even correlative, thermodynamic models into consideration.

Ng and co-workers [57] propose a design procedure for liquid-liquid phase transfer catalysis (LLPTC) systems from the process system engineering perspective. The mathematical model is developed for the stirred cell reactor while assuming ideal behaviour of the PTC phase equilibriums, first order reaction rate, and well-mixed of the organic phase. The model analysis is done through Damkohler number and ideal partition coefficients. The guidelines for flowsheet selection, comparison of PTC, and solvent selection recommendation are presented. Although this model is still far from widely applicable with PTC systems, it gives more information on the effect of the solvent and PTC to the conversion, partition, and overall reaction rate.

2.3.1.2 Other Biphasic reaction systems

1. Epoxidation

For the epoxidation process model, Gan et al. [58] assume one rate determining step and use simple first order reaction rate equation to describe the production of epoxides from palm oil. Similarly, Dinda et al. [33] also reduce the model to pseudo-first order equation, as shown in equation 2-12.

$$\ln\left(\frac{[H_2O_2]_0 - [EP]}{[H_2O_2]_0}\right) = -k[RCOOH]_0t + \ln[H_2O_2]_0 \quad 2-12$$

where, $[]$ stand for the concentration and subscript 0 denotes the initial concentration.

On the other hand, Rangarajan et al. [59], Campanella et al. [31,32], and Sinadinovic-Fiser et al. [36] use seven differential equations to describe the reactive species within the process. While Santacesaria et al. [34] describe the system with four reaction kinetic equations and six mass transfers equations for the heterogeneous species.

Campanella and co-workers apply UNIFAC thermodynamic model for calculating the partitions of acid and peracid but does not further apply their model for the novel design of the system. On the other hand, Santacesaria group uses simple correlation for partitions of the heterogeneous compounds.

2. Furan derivatives production

For the production of furan derivatives, only Weingarten et al. [60] present a simple first order kinetic model for the production of furfural from xylose by microwave heating in single phase (equations 2-13 and 2-14) and biphasic systems (equations 2-13, 2-15, and 2-16).

$$\frac{d[X]}{dt} = k_1[X][H^+] - k_2[X][F][H^+] \quad 2-13$$

$$\frac{d[F]}{dt} = k_1[X][H^+] - k_2[X][F][H^+] - k_3[F][H^+] \quad 2-14$$

$$\frac{d[F]_{Aq}}{dt} = k_1[X][H^+] - k_2[X][F]_{Aq}[H^+] - k_3[F]_{Aq}[H^+] - k_4[F]_{Aq} + k_5[F]_{Org} \quad 2-15$$

$$\frac{d[F]_{Org}}{dt} = k_4[F]_{Aq} - k_5[F]_{Org} \quad 2-16$$

where, $[X]$ is the xylose concentration, $[F]$ is the furfural concentration, $[H^+]$ is the acid concentration, and subscripts *Aq* and *Org* denote the aqueous and organic phases respectively.

The model does not include any prediction of the heterogeneous species partition, but assumes fixed value between the two transfer coefficients $\frac{k_4}{k_5} = 7.1$.

2.3.2 Phase Equilibrium Models

The calculation of partition coefficient (P_i) is one of the most important features for further application of the constructed model. The partition coefficient is defined as the ratio of the concentrations of a chemical species in the two phases at equilibrium. The equation for calculating partition coefficient is taken from the work of Piccolo et al. [61], as displayed in equation 2-17.

$$P_i = \frac{\gamma_i^\alpha}{\gamma_i^\beta} \quad 2-17$$

where, P_i is the partition coefficient of the species i , γ_i^α and γ_i^β are the activity coefficients of the species i in the respective phases α and β .

Unfortunately most biphasic reaction systems models do not include the partition coefficient into consideration, or omits the calculation by assuming constant coefficient. As discussed in the previous section, only Ng and co-workers [57] include the partition coefficient into consideration. However, they have also assumed ideal behaviour, in order to avoid dealing with complex activity coefficient model. Moreover, concerning the PTC system, there is virtually no predictive model for the activity coefficient calculation available in an open literature.

This section collects and presents attempts to model the activity or partition coefficients of the quaternary ammonium PTC. As well as, presents the model that can potentially be useful for the prediction of the activity and partition coefficients of the PTC system.

2.3.2.1 Activity Coefficient Model of PTC system

Belveze et al. [62] use electrolyte extension of the non-random two liquid (eNRTL) for correlating the activity coefficients of tetramethyl-, tetraethyl-, and tetrapropyl ammonium PTCs. The model equations are the same as the model presented in chapter 3, section 3.2. They achieve unacceptably high absolute average deviation at 6.2% for a PTC ion.

Fukumoto et al. [63] apply electrolyte extension of the variable range – statistical associating fluid theory with (SAFT-VRE) model [64]. Although the result looks optically well fitted in the figure, there is no quantitative report on the different between experimental and predictive values.

Papaiconomou et al. [65] and Simonin et al. [66] succeed employing mean spherical approximation model (MSA) for calculating the activity and osmotic coefficients of tetramethyl-, tetraethyl-, and tetrapropyl (C_1N to C_3N) ammonium PTCs. The absolute average deviations are between 0.1% and 0.5%. However, they omitted the calculation of tetrabutylammonium (C_4N) PTC, which has most complex behaviour, from their publications.

2.3.2.2 Potential Activity Coefficient Models

Although isn't applied directly to the system involved with PTC, the UNIFAC model has successfully implemented for calculating the activity coefficient and equilibrium of the system

containing ionic liquids, under the name of UNIFAC-IL. However, the model has been approached differently from different research groups.

Originally, Lei and co-workers [67] consider every ionic liquid molecules as a group, each of them needs structural parameters (R_i and Q_i) which are estimated roughly from equations 2-18 and 2-19.

$$R_i = 0.02928V_m \quad 2-18$$

$$Q_i = \frac{(z-2)R_i}{z} + \frac{2(1-L_i)}{z} \quad 2-19$$

where, V_m is the molar volume, z is the coordination number, and L_i is the bulk factor.

Moreover, they also need interaction parameter (a_{ij}) between the new ionic liquid groups and the original UNIFAC groups. This approach leads to the inefficient application of the group contribution concept of the UNFAC model. Furthermore, their model also neglects the effect of long range interaction between ions.

On the other hand, Santiago et al. [68] also apply UNIFAC for predicting liquid-liquid equilibrium of ionic liquid in ternary systems. Although they also use original UNIFAC with neglecting long range interactions, they considered cation and anion embodied in the ionic liquid as separated groups. With this approach, there are more parameters required; however, a wider range of applications is also feasible.

THE MODELLING FRAMEWORK

When modelling the biphasic reaction systems, the objective of the constructed model is diverse. For example, the model can be used for analysing the behaviour of chemical species within one phase, determining the partition of heterogeneous species between two phases, or predicting the effect of solvent to the partition of chemical species or reaction rate.

In order to efficiently and systematically set up a tailor-made model for various applications, a flexible and reliable framework for modelling of the biphasic reaction system is needed. Likewise, in order to determine the physico-chemical behaviour of involved chemical species and solvents, the predictive and partially predictive thermodynamic models or the combinations of several thermodynamic models are also required.

Section 3.1 describes the developed biphasic reaction systems modelling framework and the generic equations. And section 3.2 presents the implemented and developed constitutive thermodynamic models.

The output from this chapter is the biphasic reaction system modelling framework and the options of constitutive thermodynamic models for constructing the combined rate-equilibrium tailor-made model of the biphasic reaction systems. The framework and thermodynamic models are implemented to specific systems in chapter 4.

3.1 BIPHASIC REACTION SYSTEM MODELLING FRAMEWORK

In this section, the step-by-step framework for the modelling of the biphasic reaction system is presented. Section 3.1.1 show the framework scaffold and section 3.1.2 presents the detail decision-making step for each module in the framework and the corresponding generic equations.

3.1.1 The Framework

The systematic biphasic modelling framework is developed based on model generation method of Cameron and Gani [3]. The process modelling starts with defining the modelling objectives, followed by model construction, model analysis and model solution according to a derived numerical solution strategy. The model equations are classified in terms of balance equations, constitutive equations and conditional equations.

Prior to biphasic model construction, information on the reactive system is collected. The involved chemical species are classified into homogeneous species (they stay in only one phase); and heterogeneous species (they distribute-partition into the two phases). Next, the chemical species present are classified in terms of solvent, reactive (reactant and product) and inert species. The dissociations of chemical species into ions are considered only for the aqueous phase. Physico-chemical properties, such as, vapour pressure, density, viscosity, Gibbs free energy of formation, heat of formation, standard melting and boiling temperature are retrieved from a database or estimated by an appropriate group contribution method such as Constantinou and Gani method [69].

Reactions are classified into those that are kinetic-controlled, those that are equilibrium-controlled, and those that are mixed. The reaction location is also needed to be specified. If the transfers of the heterogeneous chemical species between the phases are not spontaneous, mass transfer effects are also considered. The balance equations are generated based on the reaction system information and the reactor type (CSTR, batch, or fed-batch).

In this work, the constitutive and conditional equations are combined into modules for different systems and/or modelling objectives. After a model consisting of equations from the three modules has been generated, it is validated for compatibility with the available data before further use in design and analysis of the biphasic reaction system. If the model fails the validation test, the collected data is used to fine-tune the model parameters.

The final result is a problem-specific model generated through different combinations of the equation from the three modules, as shown in Figure 3-1.

For each module, there are various decision-making steps for equation selection and model generation which is described together with generic equations in the next section.

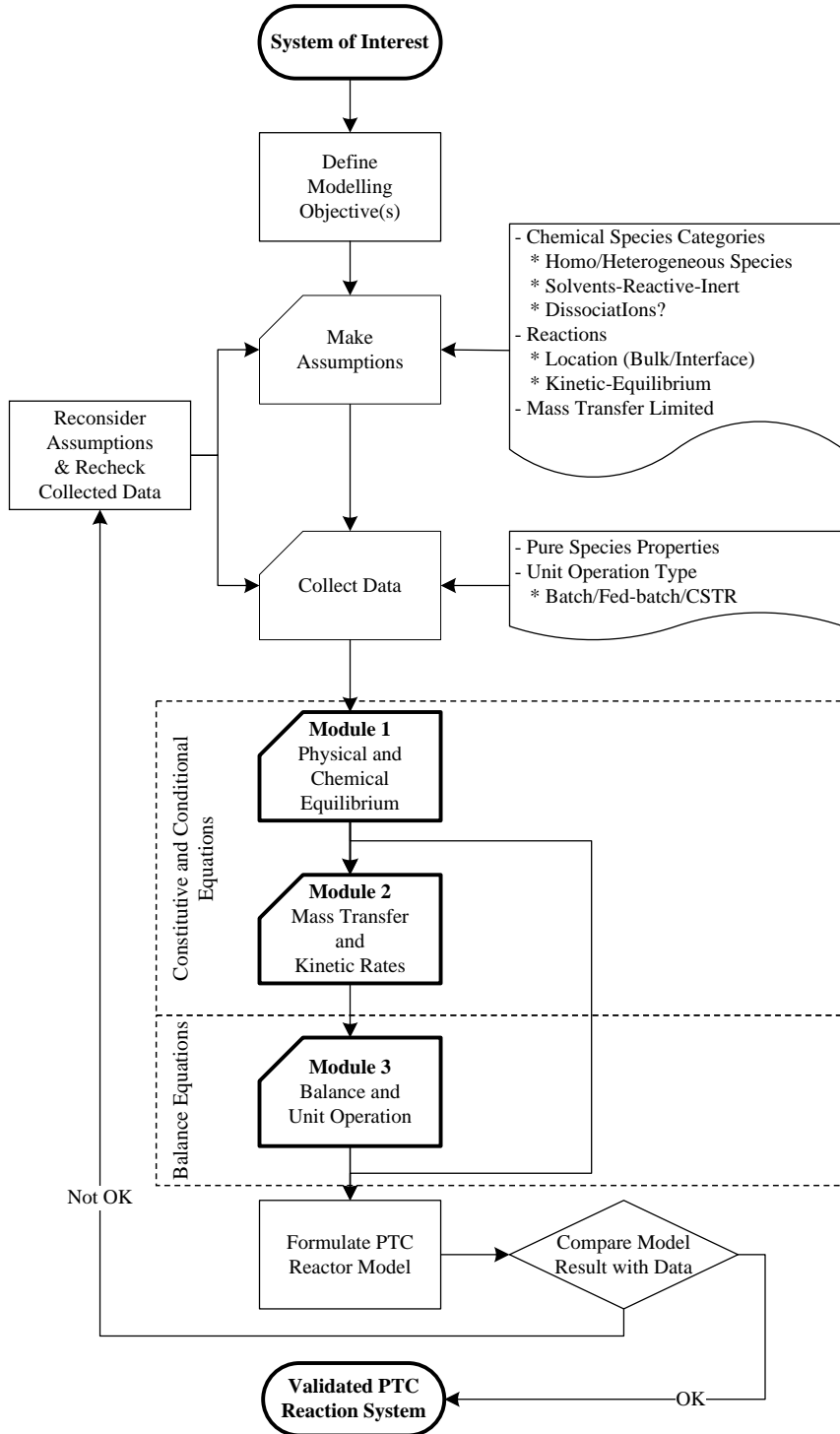


Figure 3-1: Framework for modelling of biphasic reaction systems

3.1.2 Generic Equations

For each module, the decision-making steps for selecting generic equations are derived and displayed in this section. The intention is to develop a generic model that can be used for entire biphasic reaction systems problems.

3.1.2.1 Module 1: physical equilibrium

Module 1 describes physical equilibrium and partition of heterogeneous chemical species between two co-existing phases. The detailed step of this module is shown in Figure 3-2.

1. The solvents and heterogeneous species are decomposed into pairs of subsystems.
2. A proper thermodynamic model is selected for each subsystem.
3. The corresponding model parameters are needed for calculating activity coefficient of the chemical species in the solvent.

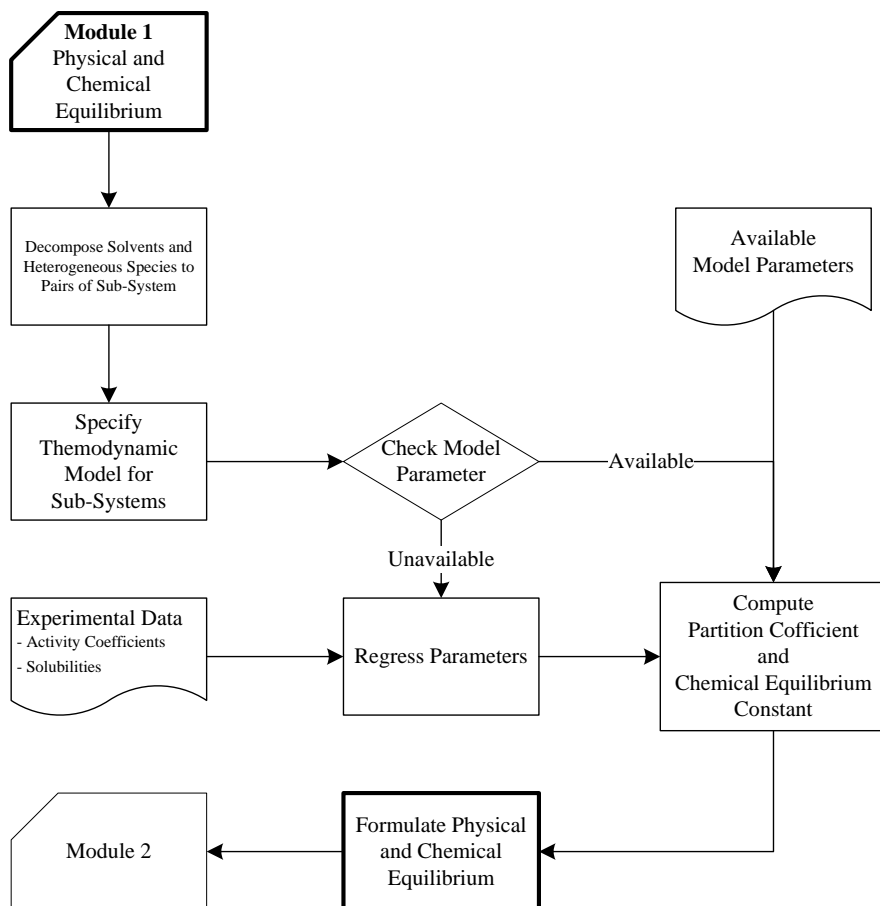


Figure 3-2: Detail steps of module 1 in the framework

- a. When parameters have not been established, experimental data (for example activity coefficient and solubilities) need to be measured for parameter regression. The intention is to develop a model with parameters that can be used for other systems.
4. Physical equilibrium model can then be formulated. In particular, the partition coefficient as a function of activity coefficients is defined as the distribution of each heterogeneous species between the two co-existing phases, as given by equation 3-1.

$$P_i \equiv \frac{x_i^\beta}{x_i^\alpha} = \frac{\gamma_i^\alpha}{\gamma_i^\beta} \tag{3-1}$$

where, P_i is partition coefficient of species i ; γ_i^α and γ_i^β are activity coefficients of species i in respective phases α and β .

5. If the modelling objective is to analyse equilibrium or partition of heterogeneous species only, there is no need for other two modules.

3.1.2.2 Module 2: reaction and transfer rate

Module 2 describes reaction rates of the reactive species and transfer rates of the heterogeneous species. The detailed step of module 2 is shown in Figure 3-3.

1. Location of the reaction is considered whether the reaction occurs at the interface or in the bulk phase.
2. The arbitrary third phase is established if the reaction occurs at the interface.
3. The reaction type is specified for the formation of rate model.
4. Experimental data, such as the measured amount or the concentration of the reactive

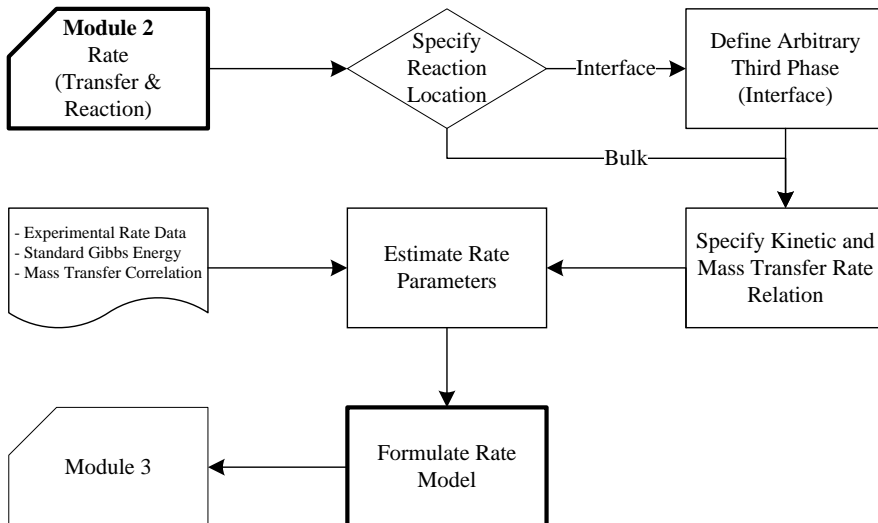


Figure 3-3: Detail steps of module 2 in the framework

species during reaction time is needed for kinetic parameters regression, while standard Gibbs of formation is needed for equilibrium parameters. Mass transfer coefficients, if need, can be estimated from the experimental data or the correlation between Sherwood, Schmidt, and Reynold numbers (for example, the correlations reported by reported by Kumar and Hartland [70]).

5. The generic reaction model is formulated based on the non-elementary reaction rate law, as given by equation 3-2.

$$R_j = k_j S \left(\prod_i (C_i \gamma_i)^{\varepsilon_{ij}^>} - \frac{\prod_i (C_i \gamma_i)^{\varepsilon_{ij}^<}}{K_{Eq,j}} \right) \quad 3-2$$

where, R_j is the rate of reaction j ; S is the effective area per volume for mass transfer; C_i is the concentration of species i ; γ_i is the activity coefficient of species i ; k_j is the forward rate coefficient of reaction j ; $K_{Eq,j}$ is the equilibrium constant of reaction j ; and $\varepsilon_{ij}^>$ and $\varepsilon_{ij}^<$ are order of reaction of species i in reaction j for forward and backward reaction respectively.

- a. In the case of reaction rate (not transfer rate), S is equal to 1.
- b. In the case of purely kinetic driven forward reactions, the equilibrium-

reversible term $\left(\frac{\prod_i (C_i \gamma_i)^{\varepsilon_{ij}^<}}{K_{Eq,j}} \right)$ is omitted. The equation is transformed into equation 3-2a.

$$R_j = k_j \prod_i (C_i \gamma_i)^{\varepsilon_{ij}^>} \quad 3-2a$$

- c. In the case of fast equilibrium, or pseudo-equilibrium, controlled reactions, the rate of reaction (R_j) is set to zero, which transforming to equation 3-2b.

$$0 = \prod_i (C_i \gamma_i)^{\varepsilon_{ij}^>} - \frac{\prod_i (C_i \gamma_i)^{\varepsilon_{ij}^<}}{K_{Eq,j}} \quad 3-2b$$

- d. For the mass transfer of the heterogeneous species across phases, or to the interface, mass transfer coefficient (k_L) and partition coefficient (P_i) from the module 1 are used as the forward rate of reaction and reaction equilibrium respectively. Mole fractions (x_i^α) are used instead of the concentration (C_i^α) as shown in equation 3-2c.

$$R_j = k_L S \left(x_i^\alpha - \frac{x_i^\beta}{P_i} \right) \quad 3-2c$$

- e. If the mass transfer limited is neglected, the transfer rate is set to 0. Equation 3-2c is truncated into equation 3-2d.

$$0 = x_i^\alpha - \frac{x_i^\beta}{P_i} \quad 3-2d$$

The chemical equilibrium constant ($K_{Eq,j}$) is related to the standard Gibbs energy of formation by equation 3-3.

$$K_{Eq,j} = \exp \left(-\frac{\Delta G_j}{RT} \right) \quad 3-3$$

where ΔG_j is the standard Gibbs free energy change for the reaction j , R and T are the universal gas constant and temperature respectively.

The equations in this module are linked with the balance module through the extent of reaction concept.

3.1.2.3 Module 3: balance and unit operation

Module 3 describes the mass balance of the reactive species and unit operation. The detailed step of module 3 is shown in Figure 3-4.

1. The generic balance equations are to connect with rate equations by the extent of reaction concept, as shown in equation 3-4.

$$\frac{d\xi_j}{dt} = R_j V_j \quad 3-4$$

where, ξ_j is the extent of reaction j as a function of time and rate of reaction, and V_j is the volume of the phase at which the reaction occurred.

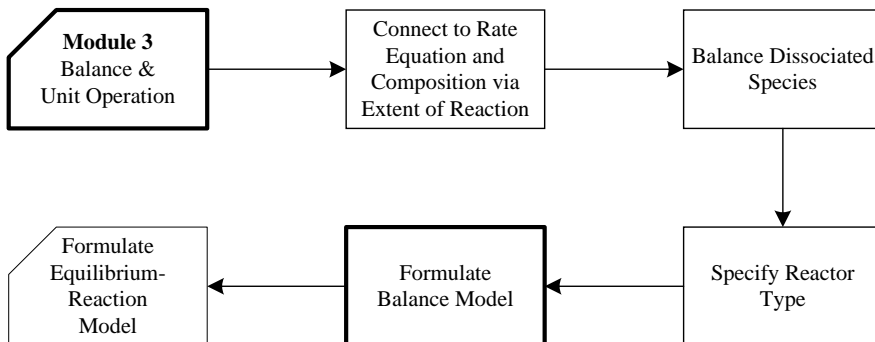


Figure 3-4: Detail steps of module 3 in the framework

2. If dissociated species presented, equations 3-5 and 3-6 are used to initialise cation and anion species.

$$N_{i^+}^0 = \sum_k N_{ik}^0 \quad 3-5$$

$$N_{i^-}^0 = \sum_k N_{ki}^0 \quad 3-6$$

where, N_{ik}^0 is an initial molar amount of dissociable species with cation i and anion k ; $N_{i^+}^0$ and $N_{i^-}^0$ are dissociated cationic and anionic species, respectively.

3. The reactor type (batch, fed-batch, or CSTR) is specified.
 4. The generic balance equation is formulated from equation 3-7.

$$N_i^\alpha = N_i^0 + \sum_j V_{ij} \xi_j + F_i^0 t - F_i t - N_i^\beta \quad 3-7$$

where, N_i^α is the molar amount of species i in α phase; N_i^0 is the initial amount of i ; N_i^β is the amount of species i in the β phase; V_{ij} is the stoichiometric number of the species i in reaction j ; F_i^0 and F_i are the inlet and outlet flow of the species i respectively.

- a. For a batch reactor, both F_i and F_i^0 are equal to 0.
- b. For a fed-batch reactor, F_i is 0 while F_i^0 can be continuous or pulse function.

3.2 CONSTITUTIVE THERMODYNAMIC MODELS

The key information for the improved and innovative design of a biphasic reaction process are the partitions of heterogeneous species between the two co-existing phases (or to the interface), as well as, the equilibrium of reaction in both phases, which require a reliable thermodynamic model capable of describing the phase behaviours of all the species present in the system.

Equation-of-state (EOS) and activity coefficient (γ) models are most commonly used to describe equilibria behaviour such as phase compositions and partition coefficients [71–74]. In this work, the models are constructed for the systems containing mainly liquid phases, the activity coefficient models are more suitable for describing the systems. The non-random two liquid (NRTL), its electrolyte extension (eNRTL) and the segment-based activity coefficient (SAC) models are implemented for correlating and predicting the behaviours of the involved species. Additionally, electrolyte extension of group contribution-based KT-UNIFAC model is developed and initially applied to the alkali halide electrolyte solution [75], where some representative alkali halide salts appear in the studied systems as a donor or receptor of the active or inactive ions. Therefore, the e-KT-UNIFAC model is also extended to various systems involving electrolyte and non-electrolyte chemical species.

Generally, biphasic reaction systems consist of 2 liquid phases, aqueous and organic. The aqueous phase is commonly an electrolyte solution that contains ionised species. While, the organic phase is a nonelectrolyte phase, with no dissociate species. Therefore, the biphasic reaction system is decomposed into 3 subsystems (*A* – *C*):

Subsystem A (co-existing solvents): describes the mutual solubilities between two co-existing solvents using NRTL, NRTL-SAC, UNIQUAC, or KT-UNIFAC models

Subsystem B (electrolyte solutions): describes the behaviour of dissociated chemical species in electrolyte solution using e-NRTL, e-NRTL-SAC, or e-KT-UNIFAC models

Subsystem C (nonelectrolyte solutions): describes the behaviour of species in non-aqueous solvent using NRTL, NRTL-SAC, or e-KT-UNIFAC models

Thermodynamic descriptions of subsystem *A* are well-established with existing models, whereas subsystems *B* and *C* lack of the model parameters or the accuracy model or both. Combinations of different appropriate thermodynamic models for subsystems *B* and *C* are applied to calculate the partitions of heterogeneous species between aqueous – organic phases. The behaviours of dissociated species in the aqueous phase of subsystem *B* are predicted using the eNRTL, eNRTL-SAC, and e-KT-UNIFAC models with the newly fitted parameters reported in section 4.1, while, the solubilities of the non-electrolyte species in various organic solvents are determined using the NRTL, NRTL-SAC, and e-KT-UNIFAC models with the newly fitted parameters as well. An overview of the models for the subsystem is given in Table 3-1 and sections 3.2.1-3.2.3 below present the implemented and developed constitutive thermodynamic models and their equations.

Table 3-1: Overview of the constitutive thermodynamic models for predicting behaviours of

chemical species in different subsystems

Subsystem	Model	Model Type
A	NRTL	Correlative
	NRTL-SAC	Partially Predictive
	UNIQUAC	Partially Predictive
	KT-UNIFAC/e-KT-UNIFAC	Predictive
B	eNRTL	Correlative
	eNRTL-SAC	Partially Predictive
	e-KT-UNIFAC	Predictive
C	NRTL	Correlative
	NRTL-SAC	Partially Predictive
	e-KT-UNIFAC	Predictive

3.2.1 NRTL Model and Its Electrolyte Extension

3.2.1.1 NRTL

Non-random two liquid model (NRTL) is a local composition based activity coefficient model developed by Renon and Prausnitz in 1968 [76]. The model is widely used for behaviour and equilibria calculation of binary and multicomponent systems. The NRTL model activity coefficient expression is shown in equation 3-8.

$$\ln \gamma_I = \frac{\sum_J x_J G_{JI} \tau_{JI}}{\sum_J x_J G_{JI}} + \sum_J \frac{x_J G_{IJ}}{\sum_K x_K G_{KJ}} \left(\tau_{IJ} - \frac{\sum_K x_J G_{KJ} \tau_{KJ}}{\sum_K x_K G_{KJ}} \right) \quad 3-8$$

where x_I is the mole fraction of the chemical species I ; τ_{IJ} and G_{IJ} are expressed as following equations 3-9 to 3-11, with R and T are the universal gas constant and the temperature respectively.

$$\tau_{IJ} = \frac{\alpha_{JI}}{RT} \quad 3-9$$

$$G_{JI} = \exp(-\alpha_{JI} \tau_{JI}) \quad 3-10$$

$$\alpha_{JI} = \alpha_{IJ} \quad 3-11$$

For any binary pairs, the NRTL model has 3 adjustable parameters: the nonrandomness factor (α_{JI}) and two interaction parameters (α_{IJ} and α_{JI}).

3.2.1.2 eNRTL

Chen and his co-workers [77–80] extend NRTL model for describing electrolyte system behaviour by accounting local interactions between species with NRTL expression and long-range interactions with Pitzer–Debye–Hückel (PDH) formula [81], as shown in equation 3-12.

$$\ln \gamma_i^* = \ln \gamma_i^{*,lc} + \ln \gamma_i^{*,PDH} + \Delta \ln \gamma_i^{Born} \quad 3-12$$

where the notation “*” denotes the unsymmetric convention, $\gamma_i^{*,lc}$ is the contribution of activity coefficient from the local composition interactions, $\gamma_i^{*,PDH}$ is the contribution of activity coefficient from the long-range interactions, and the Born term ($\Delta \ln \gamma_i^{Born}$) is the correction term for the change of the reference state from the mixed-solvent to the aqueous solution.

The local composition unsymmetric convention activity coefficient is calculated as shown in equation 3-13.

$$\ln \gamma_i^{*,lc} = \ln \gamma_i^{lc} - \ln \gamma_i^{\infty,lc} \quad 3-13$$

where, $\gamma_i^{\infty,lc}$ is the infinite-dilution activity coefficient of the ionic species I , calculated at $x_i \rightarrow 0$ by equation 3-8.

The expressions for PDH and Born correction terms are shown in equations 3-14 and 3-15.

$$\ln \gamma_i^{*,PDH} = - \left(\frac{1000}{M_S} \right)^{1/2} A_\varphi \left[\left(\frac{2z_i^2}{\rho} \right) \ln \left(1 + \rho I_x^{1/2} \right) + \frac{z_i^2 I_x^{1/2} - 2I_x^{1/2}}{1 + \rho I_x^{1/2}} \right] \quad 3-14$$

$$\Delta \ln \gamma_i^{Born} = \frac{Q_e^2}{2k_B T} \left(\frac{1}{\varepsilon_S} - \frac{1}{\varepsilon_W} \right) \frac{z_i^2}{r_i} 10^{-2} \quad 3-15$$

A_φ and I_x are calculated from equations 3-16 and 3-17.

$$A_\varphi = \frac{1}{3} \left(\frac{2\pi N_A d_S}{1000} \right)^{1/2} \left(\frac{Q_e^2}{\varepsilon_S k_B T} \right)^{3/2} \quad 3-16$$

$$I_x = \frac{1}{2} \sum_I x_i z_i^2 \quad 3-17$$

where, A_φ is the Debye–Hückel parameter; I_x is the ionic strength; z_i is the charge number of species I ; M_S is the molecular weight of solvent S ; ρ is the closest approach parameter; Q_e is the electron charge; ε_S is the dielectric constant of the solvent S ; k_B is the Boltzmann constant; ε_W is the dielectric constant of water; r_i is the Born radius of species I ; N_A is Avogadro’s number; and d_S is the density of the solvent S .

Piccolo et al. [61] had used a combination of NRTL and eNRTL models for subsystems B and C for calculating partition coefficient of heterogeneous species between co-existing aqueous-

organic phases. The applicability of this combination is limited by the need of experimental data for each pair of heterogeneous species-solvents. Although it is less useful in term of predictability, the uncertainty of this combination is lower than other combinations, due to the specific interaction parameter of each system.

The NRTL and the eNRTL combination are applied in the PTC case study I, benzoin condensation in section 4.2.1, the model is a correlative model with limited prediction capability for the design of the process.

3.2.2 Segment Activity Coefficient (SAC) Models

3.2.2.1 NRTL-SAC

The segment based NRTL model was originally developed for polymer solutions [82]. The model adopts Flory-Huggins equation [83] to represent the configurational entropy of mixing as a combinatorial term (γ_i^{FH}) and modifies NRTL expression for local composition contribution as a residual term (γ_i^{lc}) . The model has been applied for predicting the behaviour and equilibrium of the non-ideal complex mixture systems containing pharmaceutical compounds, aroma compounds, polymers, and ionic liquids [84–88].

The NRTL-SAC model decomposes molecules into three conceptual segments based on molecular interactions in solutions. For each chemical species, their interactions are described in term of the pairwise segment-segment interactions among hydrophobic segment (X), polar segment (Y), and hydrophilic segment (Z). The interaction between hydrophilic and polar segment can be positive and negative, therefore, the polar segment is divided into two types (Y- and Y+). Binary interactions between segments are displayed in Table 3-2.

Table 3-2: NRTL binary interaction for conceptual segment of NRTL-SAC model

Segment 1	X	X	Y-	Y+
Segment 2	Y+/Y-	Z	Z	Z
τ_{12}	1.643	6.547	-2.000	2.000
τ_{21}	1.834	10.949	1.787	1.787
$a_{12} = a_{21}$	0.2	0.2	0.3	0.3

where, the interaction between Y- and Y+ polar segments is 0.

The NRTL-SAC activity coefficient equations are expressed as equation 3-18.

$$\ln \gamma_i = \ln \gamma_i^{lc} + \ln \gamma_i^{FH} \quad 3-18$$

The local composition part is calculated from the sum of segments interactions as displayed in equation 3-19.

$$\ln \gamma_i^{lc} = \sum_m r_{m,i} \left[\ln \Gamma_m^{lc} - \ln \Gamma_m^{lc,i} \right] \quad 3-19$$

The segment activity coefficients $(\Gamma_m^{lc}$ and $\Gamma_m^{lc,i})$ are calculated from equations 3-20 to 3-24.

$$\ln \Gamma_m^{lc} = \frac{\sum_j x_j G_{jm} \tau_{jm}}{\sum_k x_k G_{km}} + \sum_{m'} \frac{x_{m'} G_{mm'}}{\sum_k x_k G_{km'}} \left(\tau_{mm'} - \frac{\sum_j x_j G_{jm'} \tau_{jm'}}{\sum_k x_k G_{km'}} \right) \quad 3-20$$

$$\ln \Gamma_m^{lc,I} = \frac{\sum_j x_{j,I} G_{jm} \tau_{jm}}{\sum_k x_{k,I} G_{km}} + \sum_{m'} \frac{x_{m',I} G_{mm'}}{\sum_k x_{k,I} G_{km'}} \left(\tau_{mm'} - \frac{\sum_j x_{j,I} G_{jm'} \tau_{jm'}}{\sum_k x_{k,I} G_{km'}} \right) \quad 3-21$$

$$x_j = \frac{\sum_I x_{j,I} r_{j,I}}{\sum_I \sum_i x_{i,I} r_{i,I}} \quad 3-22$$

$$x_{j,I} = \frac{r_{j,I}}{\sum_i r_{i,I}} \quad 3-23$$

$$G_{ij} = \exp(-a_{ij} \tau_{ij}) \quad 3-24$$

where, the i, j, k, m , and m' denote the segment based species; I and J denote the molecular species; x_j is the segment based mole fraction of segment j ; x_i is the mole fraction of the molecule J ; $r_{j,I}$ is the number of the segment j contained in molecule J ; a_{ij} and τ_{ij} are taken from Table 3-2.

The combinatorial (Flory-Huggins) part is calculated from equations 3-25 to 3-27.

$$\ln \gamma_I^{FH} = \ln \frac{\phi_I}{x_I} + 1 - r_I \sum_j \frac{\phi_j}{r_j} \quad 3-25$$

$$r_I = \sum_i r_{i,I} \quad 3-26$$

$$\phi_I = \frac{r_I x_I}{\sum_j r_j x_j} \quad 3-27$$

where, r_i is the total segment number of molecule I and ϕ_i is the segment mole fraction of molecule I .

3.2.2.2 eNRTL-SAC

The NRTL-SAC model has been extended for describing electrolyte system based on the generalised eNRTL model [89]. A new conceptual segment E , which would completely dissociate to cationic segment (c) and anionic segment (a), is introduced. The binary segment interactions for NRTL segments are taken from Table 3-2, while the new segment binary interactions to the other are reported in Table 3-3.

Table 3-3: NRTL binary interaction for the new conceptual segment of eNRTL-SAC model

Segment 1	X	Y+/Y-	Z
Segment 2	E	E	E
τ_{12}	15	12	8.885
τ_{21}	5	-3	-4.549
$a_{12} = a_{21}$	0.2	0.2	0.2

Following general eNRTL model, the eNRTL-SAC model equations are expressed as following equations 3-28.

$$\ln \gamma_i^* = \ln \gamma_i^{*,lc} + \ln \gamma_i^{*,PDH} + \ln \gamma_i^{*,FH} + \Delta \ln \gamma_i^{*,Born} \quad 3-28$$

The local composition term ($\ln \gamma_i^{*,lc}$) is computed as the sum of individual segment contributions as equation 3-29.

$$\ln \gamma_i^{*,lc} = \sum_m r_{m,I} \ln \Gamma_m^{*,lc} + r_{c,I} \ln \Gamma_c^{*,lc} + r_{a,I} \ln \Gamma_a^{*,lc} \quad 3-29$$

With the unsymmetric local composition segment activity coefficients ($\Gamma_m^{*,lc}$, $\Gamma_c^{*,lc}$, and $\Gamma_a^{*,lc}$) express as follow.

$$\ln \Gamma_m^{*,lc} = \ln \Gamma_m^{lc} - \ln \Gamma_m^{\infty,lc} \quad 3-30$$

$$\ln \Gamma_c^{*,lc} = \ln \Gamma_c^{lc} - \ln \Gamma_c^{\infty,lc} \quad 3-31$$

$$\ln \Gamma_a^{*,lc} = \ln \Gamma_a^{lc} - \ln \Gamma_a^{\infty,lc} \quad 3-32$$

The notation “ ∞ ” denotes infinite dilution. The local composition segment activity coefficients (Γ_m^{lc} , Γ_c^{lc} , and Γ_a^{lc}) are calculated by the following equations 3-33 to 3-35.

$$\begin{aligned} \Gamma_m^{lc} = & \frac{\sum_j x_j G_{jm} \tau_{jm}}{\sum_k x_k G_{km}} + \sum_{m'} \frac{x_m G_{mm'}}{\sum_k x_k G_{km'}} \left(\tau_{mm'} - \frac{\sum_j x_j G_{jm'} \tau_{jm'}}{\sum_k x_k G_{km'}} \right) \\ & + \frac{x_c G_{mc}}{\sum_k x_k G_{kc}} \left(\tau_{mc} - \frac{\sum_j x_j G_{jc} \tau_{jc}}{\sum_k x_k G_{kc}} \right) + \frac{x_a G_{ma}}{\sum_k x_k G_{ka}} \left(\tau_{ma} - \frac{\sum_j x_j G_{ja} \tau_{ja}}{\sum_k x_k G_{ka}} \right) \end{aligned} \quad 3-33$$

$$\Gamma_c^{lc} = \frac{\sum_j x_j G_{jc} \tau_{jc}}{\sum_k x_k G_{kc}} + \sum_m \frac{x_m G_{cm}}{\sum_k x_k G_{km}} \left(\tau_{cm} - \frac{\sum_j x_j G_{jm} \tau_{jm}}{\sum_k x_k G_{km}} \right) - \frac{x_a}{\sum_k x_k G_{ka}} \left(\frac{\sum_j x_j G_{ja} \tau_{ja}}{\sum_k x_k G_{ka}} \right) \quad 3-34$$

$$\Gamma_a^{-lc} = \frac{\sum_j x_j G_{ja} \tau_{ja}}{\sum_k x_k G_{ka}} + \sum_m \frac{x_m G_{am}}{\sum_k x_k G_{km}} \left(\tau_{am} - \frac{\sum_j x_j G_{jm} \tau_{jm}}{\sum_k x_k G_{km}} \right) - \frac{x_c}{\sum_k x_k G_{ka}} \left(\frac{\sum_j x_j G_{jc} \tau_{jc}}{\sum_k x_k G_{kc}} \right) \quad 3-35$$

The infinite dilution local composition segment activity coefficients ($\Gamma_m^{\infty,lc}$, $\Gamma_c^{\infty,lc}$, and $\Gamma_a^{\infty,lc}$) are calculated by equations 3-33 to 3-35 with a mole fraction of water equal to 1.

While the long-range interaction contribution term ($\ln \gamma_l^{*,PDH}$) is also computed from the sum of its segment contributions by the following equation 3-36.

$$\ln \gamma_l^{*,PDH} = \sum_m r_{m,l} \ln \Gamma_m^{*,PDH} + r_{c,l} \ln \Gamma_c^{*,PDH} + r_{a,l} \ln \Gamma_a^{*,PDH} \quad 3-36$$

where, the unsymmetric long-range segment activity coefficients ($\Gamma_m^{*,PDH}$, $\Gamma_c^{*,PDH}$, and $\Gamma_a^{*,PDH}$) are calculated from unsymmetric Pitzer–Debye–Hückel (PDH) formula on the segment basis, as displayed in equations 3-37 and 3-38.

$$\ln \Gamma_m^{*,PDH} = 2 \left(\frac{1000}{M_s} \right)^{1/2} \frac{A_\phi I_x^{3/2}}{1 + \rho I_x^{1/2}} \quad 3-37$$

$$\ln \Gamma_c^{*,PDH} = \ln \Gamma_a^{*,PDH} = - \left(\frac{1000}{M_s} \right)^{1/2} A_\phi \left[\frac{2}{\rho} \ln(1 + \rho I_x^{1/2}) + \frac{I_x^{1/2} - 2I_x^{3/2}}{1 + \rho I_x^{1/2}} \right] \quad 3-38$$

The combinatorial ($\ln \gamma_l^{*,FH}$) term is calculated from equations 3-39.

$$\ln \gamma_l^{*,FH} = r_l - \ln \left(\sum_j x_j r_j \right) - \frac{r_l}{\sum_j x_j r_j} \quad 3-39$$

The Born correction term ($\Delta \ln \gamma_l^{Born}$) is calculated from the sum of segment contributions by equation 3-40.

$$\Delta \ln \gamma_l^{Born} = r_{c,l} \Delta \ln \Gamma_c^{Born} + r_{a,l} \Delta \ln \Gamma_a^{Born} \quad 3-40$$

where

$$\Delta \ln \Gamma_c^{Born} = \frac{Q_e^2}{2k_B T} \left(\frac{1}{\epsilon_s} - \frac{1}{\epsilon_w} \right) \frac{1}{r_c} 10^{-2} \quad 3-41$$

$$\Delta \ln \Gamma_a^{Born} = \frac{Q_e^2}{2k_B T} \left(\frac{1}{\epsilon_s} - \frac{1}{\epsilon_w} \right) \frac{1}{r_a} 10^{-2} \quad 3-42$$

where, the definitions of A_ϕ , I_x , M_s , ρ , Q_e , ϵ_s , ϵ_w , k_B , and r_i are the same as the definitions

from the general eNRTL model in the previous section.

The implementation of SAC models for PTC systems is discussed in chapter 4, section 4.1.1. The applications of SAC model for design and analysis of PTC system are demonstrated in chapter 5, section 5.2 for the chlorination of organobromine process.

3.2.3 Electrolyte Extension of the KT-UNIFAC Model

e-KT-UNIFAC is a newly developed group contribution based thermodynamic model for the correlation and prediction of thermodynamic properties of electrolyte and nonelectrolyte solutions [75]. The model combines the predictive local composition models of the KT-UNIFAC model [90] for the short range interactions between molecules; the second virial coefficient type equation [91] for the special “middle range” interactions between ions pair for describing highly non-ideal systems; and the Debye–Hückel theory [92] for the long range electrostatic interactions between charged ions.

The activity coefficient of species I is obtained from the sum of the three different contributions and the Born correction term.

$$\ln \gamma_I = \ln \gamma_I^{UNIFAC} + \ln \gamma_I^{Vir} + \ln \gamma_I^{DH} + \Delta \ln \gamma_I^{Born} \quad 3-43$$

3.2.3.1 The short range term

The activity coefficient of the short range term of the species I ($\ln \gamma_I^{UNIFAC}$) is taken from the KT-UNIFAC model as a combination of combinatorial (γ_I^C) and residual (γ_I^R) terms.

$$\ln \gamma_I^{UNIFAC} = \ln \gamma_I^C + \ln \gamma_I^R \quad 3-44$$

The combinatorial and residual terms are expressed as shown in equations 3-45 and 3-46.

$$\ln \gamma_I^C = 1 - J_I + \ln J_I - 5q_I \left(1 - \frac{J_I}{L_I} + \ln \frac{J_I}{L_I} \right) \quad 3-45$$

$$\ln \gamma_I^R = q_I (1 - \ln L_I) - \sum_j \left(\frac{s_{jI} \theta_j}{\eta_j} - G_{jI} \ln \frac{s_{jI}}{\eta_j} \right) \quad 3-46$$

The quantities (J_I , L_I , G_{jI} , θ_j , s_{jI} , and η_j) in these equations are defined in equations 3-47 to 3-52.

$$J_I = \frac{r_I}{\sum_j x_j r_j} \quad 3-47$$

$$L_I = \frac{q_I}{\sum_j x_j q_j} \quad 3-48$$

$$G_{jl} = \sum_{m \in j} v_{ml} Q_m \quad 3-49$$

$$\theta_j = \sum_I x_I G_{jl} \quad 3-50$$

$$s_{jl} = \sum_m G_{ml} \tau_{mj} \quad 3-51$$

$$\eta_j = \sum_I x_I s_{jl} \quad 3-52$$

And the pure component parameters r_I and q_I are calculated from the sum of the group structural parameters (R_k and Q_k).

$$r_I = \sum_k v_{kl} R_k \quad 3-53$$

$$q_I = \sum_k v_{kl} Q_k \quad 3-54$$

where, v_{kl} is the number of the group k in chemical species I . The τ_{mj} is calculated from adjustable interaction parameters (a_{mj}) in KT-UNIFAC format, which is expressed by first-order linear temperature dependent.

$$\tau_{mj} = \exp\left(-\frac{a_{mj}}{T}\right) \quad 3-55$$

$$a_{mj} = a_{mj,1} + a_{mj,2}(T - T_0) \quad 3-56$$

3.2.3.2 The middle range term

The middle range second virial coefficient term ($\ln \gamma_I^{vir}$), which accounts for only the binary interaction between ions groups, is calculated by equations 3-57 and 3-58 for the original KT-UNIFAC groups (m) and the ions groups (k) receptively.

$$\begin{aligned} \ln \gamma_m^{vir} = & \sum_j m_j B_{mj} - \frac{M_m \sum_m \sum_l v_{ln} x_n'}{M_s} \sum_l \sum_j x_l' m_j \left(B_{lj} + I \frac{\partial B_{lj}}{\partial I} \right) \\ & - M_m \sum_c \sum_a m_c m_a \left(B_{ca} + I \frac{\partial B_{ca}}{\partial I} \right) \end{aligned} \quad 3-57$$

$$\ln \gamma_k^{Vir} = \frac{1}{M_S} \sum_l x_l B_{lk} + \frac{z_k^2}{2M_S} \sum_l \sum_j x_l m_j \frac{\partial B_{lj}}{\partial I} + \sum_j m_j B_{jk} + \frac{z_k^2}{2} \sum_c \sum_a m_c m_a \frac{\partial B_{ca}}{\partial I} - \frac{1}{M_S} \sum_l x_l (b_{lk} + c_{lk}) \quad 3-58$$

where

$$B_{jk} = b_{jk} + c_{jk} \exp(-\sqrt{I} + 0.125I) \quad 3-59$$

$$\frac{\partial B_{jk}}{\partial I} = \left(-\frac{1}{2\sqrt{I}} + 0.125 \right) c_{jk} \exp(-\sqrt{I} + 0.125I) \quad 3-60$$

The middle range binary interaction parameters (b_{jk} and c_{jk}) are expressed as first order temperature dependent parameters.

$$b_{ik} = b_{ik,1} + b_{ik,2}(T - T_0) \quad 3-61$$

$$c_{ik} = c_{ik,1} + c_{ik,2}(T - T_0) \quad 3-62$$

The activity coefficient of the chemical species I is described by a summation of the groups' activity coefficients included in the species.

$$\ln \gamma_I^{Vir} = \sum_j v_{ji} \ln \gamma_j^{Vir} \quad 3-63$$

3.2.3.3 The long range term

The corresponding long range activity coefficient equations for the original KT-UNIFAC groups (m) and the ions groups (k) are expressed as follow.

$$\ln \gamma_m^{DH} = \frac{2A_\phi M_S d_S}{b^3 d_m} \left[1 + b\sqrt{I_x} - \frac{1}{1 + b\sqrt{I_x}} - 2 \ln(1 + b\sqrt{I_x}) \right] \quad 3-64$$

$$\ln \gamma_k^{DH} = -\frac{A_\phi z_k^2 \sqrt{I}}{1 + b\sqrt{I}} \quad 3-65$$

where, the Debye-Hückel parameters (A_ϕ and b) are calculated by equations 3-66 and 3-67.

$$A_\phi = 1.327757 \times 10^5 \frac{\sqrt{d_s}}{(\epsilon_s T)^{3/2}} \quad 3-66$$

$$b = 6.359696 \frac{\sqrt{d_s}}{(\epsilon_s T)^{1/2}} \quad 3-67$$

where, d_s is the density of solvent, calculated with equations 3-68.

$$d_s = \frac{M_s}{\sum_m \frac{x_m M_m}{d_m}} \quad 3-68$$

The long range term ($\ln \gamma_i^{DH}$) of chemical species I is calculated from the summation of the groups' activity coefficients included in the species.

$$\ln \gamma_i^{DH} = \sum_j v_{ji} \ln \gamma_j^{DH} \quad 3-69$$

3.2.3.4 The Born correction term

The Born correction term ($\Delta \ln \gamma_i^{Born}$) is expressed in the same manner as eNRTL and eNRTL-SAC models for the ions groups (k).

$$\Delta \ln \gamma_k^{Born} = \frac{Q_e^2}{2k_B T} \left(\frac{1}{\epsilon_s} - \frac{1}{\epsilon_w} \right) \frac{1}{r_k} 10^{-2} \quad 3-70$$

$$\Delta \ln \gamma_i^{Born} = \sum_j v_{ji} \Delta \ln \gamma_j^{Born} \quad 3-71$$

The implementation of the e-KT-UNIFAC models for PTC systems is discussed in chapter 4, section 4.1.2. The applications of the e-KT-UNIFAC model for design and analysis of PTC system (the chlorination of organobromine process), epoxidation process, and furan production process are demonstrated in chapter 5.

IMPLEMENTATION OF THE FRAMEWORK AND THERMODYNAMIC MODELS

In this chapter, the biphasic reaction modelling framework and the thermodynamic models are implemented for constructing tailor-made models for specific case studies.

The implementation of thermodynamic models for the system with the unavailable parameters is shown in section 4.1. In section 4.2, the application of the developed framework has been illustrated through 5 examples. The benzoin condensation process model in section 4.2.1 is an early developed reactor model for the applied PTC systems, it combines with the correlative thermodynamic models NRTL/eNRTL for correlating with measured data. The model for chlorination of organobromine process in section 4.2.2 is another reactor model for PTC systems, this model is combined with the partially predictive SAC models and the predictive e-KT-UNIFAC model for design and analysis of the process. The epoxidation, furan derivatives production, and α -amino acid production processes models in section 4.2.3 to 4.2.5 show the capability of the framework to handle a wide range of systems and design targets. In section 4.3 the computational algorithm for solving mathematical models that contain both differential and implicit algebraic equations is presented.

The output of this chapter is the mathematical models describing biphasic reaction systems. The models are validated and applied to the design and analysis of the reaction system for the optimal design and/or operation in the next chapter.

4.1 IMPLEMENTATION OF THERMODYNAMIC MODELS

While, the thermodynamic description of subsystem *A* is well established and doesn't need extra work; subsystems *B* and *C* lack a proper predictive thermodynamic model, model parameters, as well as, measured data for fitting the model parameter especially for complex cationic electrolytic systems, such as PTC systems.

Piccolo et al. [61] succeeded applying NRTL and eNRTL models for PTC systems; however, the models are only correlative, thus having a limited range of application for the design and analysis of the systems. In this section, the attempt to implement the constitutive thermodynamic models for subsystems *B* and *C* are presented. The segment number parameters of the semi-predictive SAC models and the interaction parameters of the predictive e-KT-UNIFAC model are fitted to the measured data from the literature. The aim is to provide the key information for calculating the partitions and the activities of the involved heterogeneous species, particularly the PTC species, between the two co-existing phases.

4.1.1 Implementation of the SAC Models

The NRTL-SAC model has been successfully applied for calculation of solubilities of complex molecules in organic solvents [84–88], while the eNRTL-SAC model has been applied for activity coefficient calculations of various electrolytes [89,93,94]. As presented in the previous chapter, the model describes a chemical species by conceptual segments, which have specific interactions between themselves, and thus, it does not require interaction between a pair of species, given the capability to predict the systems with replaceable known solvents and known chemical species. However, it does still require experimental data to estimate the number of the segment for each chemical species, after segments numbers of each species established, it can be employed to any known solvents systems.

4.1.1.1 eNRTL-SAC with PTC in aqueous phase

In this work, the eNRTL-SAC model is applied for subsystem *B*. For simple cations and anion species, the segment parameters are well established [89]; while there is no parameter available complex PTC ions. In order to apply the eNRTL-SAC models for prediction, design and/or analysis of the PTC systems, segment numbers of each PTC ions are needed. The measured activity coefficients data by Lindenbaum, Boyd, and co-workers [95–97] and Wen et al. [98] of tetraalkylammonium PTC that contain 4 to 12 carbon atoms are used for the segment numbers parameters regression.

In total, there are 470 experimental data points, from 24 binary systems. The graphical comparisons between model calculation and measured data of tetraalkylammonium bromide and chloride are presented in Figure 4-1 and the comparison between model calculation and measured data of all available data points is shown in Figure 4-2.

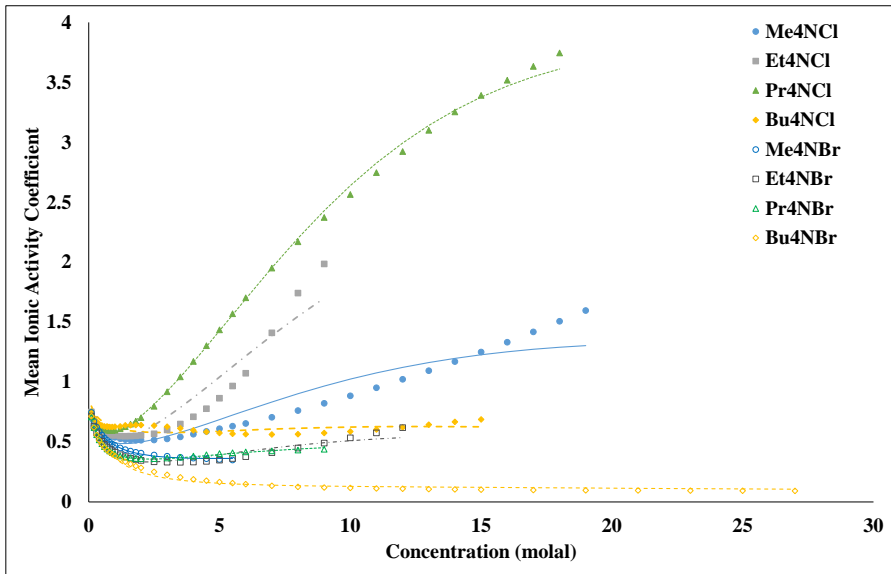


Figure 4-1: Activity coefficients of tetraalkylammonium bromide and chloride PTC, comparison between eNRTL-SAC model calculation and measured data

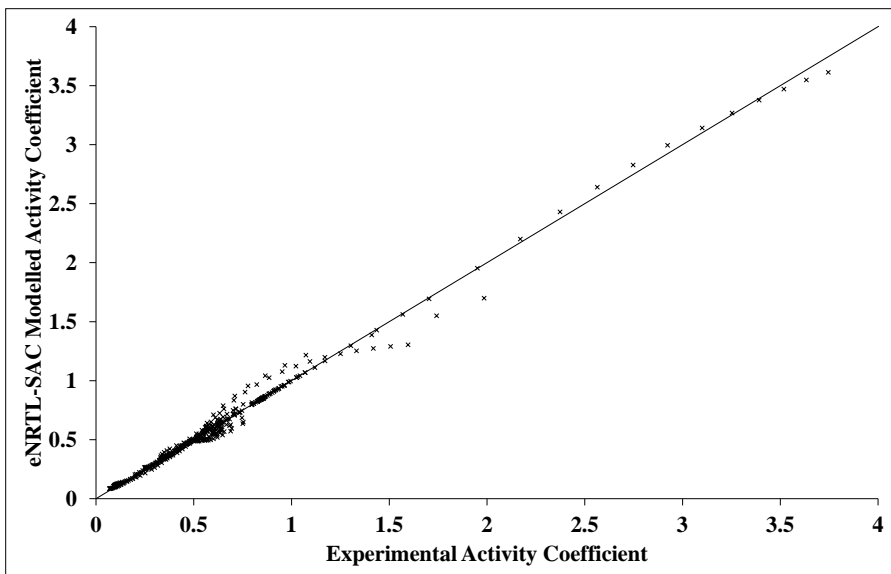


Figure 4-2: Activity coefficients of tetraalkylammonium PTC, comparison between eNRTL-SAC model calculation and measured data

The regressed segment numbers parameters of tetraalkylammonium PTC is shown in Table 4-1, with the average absolute deviations (σ) for each PTC systems as calculated by equation 4-1.

$$\sigma = 100 \left(\sum_{i=1}^N \left| \frac{x_i^{Cal} - x_i^{Mea}}{x_i^{Mea}} \right| \right) / N \quad 4-1$$

where, N is the number of the measured points, x_i^{Cal} and x_i^{Mea} are the calculated value and the measured value respectively.

Both the graphical and the numerical comparisons show good agreement between measured data and model calculations. The average absolute deviation of all system is only 0.53%, with the maximum deviation among the PTC data is only 1.04%.

Table 4-1: Segments numbers for subsystem B of the PTC ions

PTC		Segment Numbers					σ
Cation	Anion	X	Y-	Y+	Z	E	
Me ₄ N	Br	0	0	1.144	1.301	0.986	1.03E-02
	Cl	0	4.242	4.267	0	0.220	0.58
	I	0	0	1.519	0.018	1.049	2.14E-03
	OH	0.099	3.391	1.831	0.018	1.015	6.34E-06
	Ac	0.171	2.390	0.937	2.142	1.029	3.82E-05
Et ₄ N	Br	0	2.067	3.545	0	0.730	0.26
	Cl	0.626	3.744	0	0	0.162	1.04
	I	0.166	0.131	1.549	0.018	1.091	5.00E-03
	OH	0.422	3.260	0	0.018	0.963	3.52E-04
	Ac	0	1.545	0.503	0.018	1.076	6.02E-04
Pr ₄ N	Br	0.462	0.486	0.414	3.216	1.048	6.17E-03
	Cl	0	0.015	0	0	1.502	0.16
	I	0	0	2.773	0	1.137	4.10E-04
	OH	0	1.366	0	3.896	1.108	1.57E-03
	Ac	0.063	2.332	1.581	0.144	1.025	8.11E-06
Bu ₄ N	Br	0.077	0	1.770	0.529	0.794	0.72
	Cl	0	0	0.433	1.426	0.868	0.18
C ₁₁ H ₁₇ NO	Br	0.107	0	2.066	0.077	0.883	0.39
	Cl	0	0	1.680	0.294	0.938	2.19E-02
C ₅ H ₁₄ NO	Br	0	0	1.232	0.921	1.020	2.44E-02
	Cl	0	0	0.699	0.480	1.088	9.09E-04
BzMe ₃ N	Br	0.015	0	2.228	0	0.919	0.19
	Cl	0	0	1.390	0	1.010	7.80E-03
C ₈ H ₂₁ NO ₅	Br	0	0	1.431	0.662	0.985	3.77E-02

4.1.1.2 NRTL-SAC with PTC in organic phase

In this work, the NRTL-SAC model is applied for subsystem *C*. The system under concerned is also the PTC systems. The experimental data used for parameter regression are measured solubilities of PTC collected from the works of Yu and Friedman [99], Frank and Clarke [100], Abraham and co-workers [101–106], Talukdar and Kundu [107], and Lee and Huang [108].

In total, 63 binary systems, with 65 experimental points are collected. The graphical comparison between model calculation and measured data highlighted in Figure 4-3, and the regressed segment numbers for tetraalkylammonium PTC are given in Table 4-2.

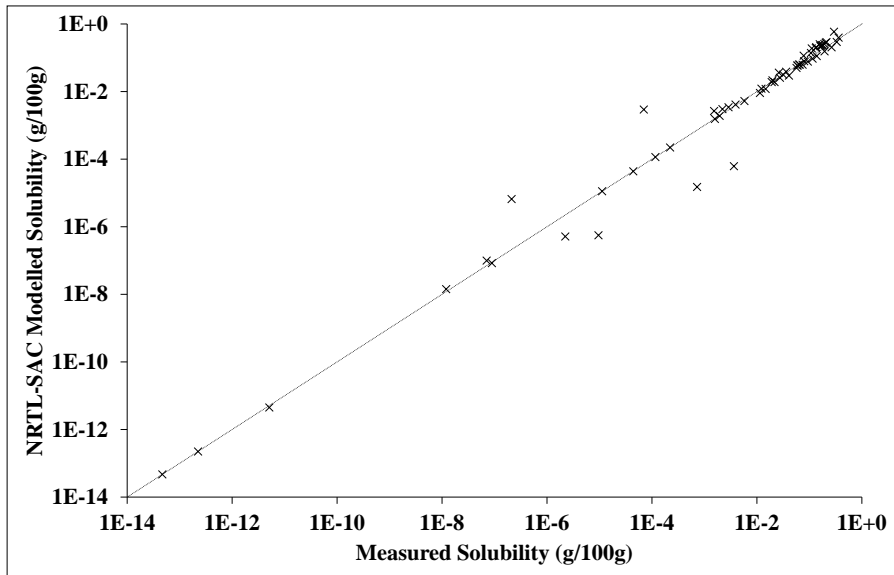


Figure 4-3: Solubilities of tetraalkylammonium PTC, comparison between NRTL-SAC model calculation and measured data

The parameters fitting results show some moderate deviations of iodide and bromide PTCs. Though, the average absolute deviation is 5.21%, the maximum deviation of the tetraethylammonium bromide PTC case elevates up to 8%.

Both of the SAC thermodynamic models are used for determining partition coefficients of PTCs in the chlorination process case study for different design targets. The results are shown in chapter 5, section 5.2.

Table 4-2: Segments numbers for subsystem *C* of the PTC species

PTC	Segment Number				σ
	X	Y-	Y+	Z	
Me ₄ NBr	0.074	0.003	0.106	0.057	0.31
Me ₄ NCl	2.908	3.863	0	2.787	0.38
Me ₄ NI	0	0	0	2.506	6.61
Et ₄ NBr	0.924	1.344	0	1.17	0.81
Et ₄ NCl	1.113	0.039	0	0.189	0.03
Et ₄ NI	0	1.287	1.862	2.101	8.03
Pr ₄ NBr	0.028	2.07	0	0.01	0.03
Pr ₄ NI	0.496	2.088	0	0.513	5.71
Bu ₄ NBr	2.346	0	0	0.981	3.92
Bu ₄ NCl	0.046	2.915	0	0.547	4.07
Bu ₄ NI	0.074	0.003	0.106	0.057	0.12

4.1.2 Implementation of the e-KT-UNIFAC Model

In this work, the e-KT-UNIFAC model is adopted for subsystems *B* and *C*. The model is adopted for calculating the partition of heterogeneous species in the chlorination (with involved PTC systems), epoxidation, and furan production processes. Whereas, the volume (R_k), surface area (Q_k), and interaction ($a_{mj,1}$, $a_{mj,2}$, $b_{mj,1}$, $b_{mj,2}$, $c_{mj,1}$, and $c_{mj,2}$) parameters, if available, are obtained from the original KT-UNIFAC model [90] and the published parameter [75]. Within the involved systems, parameters are lacking for only the PTC systems.

To implement the model for PTC systems, the cations part of PTC are considered as chains of UNIFAC groups attached to a central ion group (N^+), as already shown in Figure 2-3, chapter 2. The UNIFAC chain groups have well-established parameters from the KT-UNIFAC model, while the anions parameters are reported in the published paper. The only group that needs new parameters is the N^+ group. The structural parameters (R_k and Q_k) of the N^+ group can be calculated by using ionic radii (r_{wk}) report by Marcus [109], and the same standard segment radius as other cations ($r_{ws} = 1.0 \text{ \AA}$), with equations 4-2 to 4-5.

$$V_{w_j} = \frac{4}{3} \pi r_{w_j}^3 \quad 4-2$$

$$A_{w_j} = 4\pi r_{w_j}^2 \quad 4-3$$

$$R_k = \frac{V_{w_k}}{V_{w_s}} \quad 4-4$$

$$Q_k = \frac{A_{wk}}{A_{ws}} \quad 4-5$$

where, V_{wj} and A_{wj} are the van der Waals volume and surface area of the group respectively.

The same set of experimental data which use for regressing SAC models parameters in section 4.1.1 together with new data for asymmetric and isomer PTC reported by Blanco, G, and co-worker [110–113] are used for regressing the interaction parameters between the N^+ group and the others. In total, 763 data points altogether are used.

Due to the lack of measured data at various temperature, the parameters are fitted to the data at 25 °C only. All new calculated structural parameters and regressed interaction parameters are reported in Table 4-3.

Table 4-3: e-KT-UNIFAC model parameters for PTC systems

Group		R_k	Q_k		
N^+		0.2854	0.0920		
m	j	Interaction Parameters			
		$a_{mj,1}$	$a_{mj,2}$	$b_{mj,1}$	$c_{mj,1}$
CH_2	N^+	13274.342	-3782.346	-	-
CH_2	F^-	542.4272	8589.996	-	-
CH_2	Cl^-	-2079.152	-6336.760	-	-
CH_2	Br^-	-671.308	-6435.327	-	-
CH_2	I^-	62650.253	-6870.798	-	-
H_2O	N^+	123.054	1698.363	-	-
N^+	F^-	11619.598	5815.511	1.393	-15.927
N^+	Cl^-	876.403	12505.214	1.138	-3.692
N^+	Br^-	2701.832	641.027	-0.517	12.739
N^+	I^-	-3906.310	-9249.773	-15.500	153.687

Figure 4-4 shows a comparison between model calculation and measured activity coefficient of all available data points, average deviation is 1.07%. While Figure 4-5 shows a comparison between model calculation and measured solubilities, average deviation is 1.48%.

Although, e-KT-UNIFAC gives a bit more deviation for activity coefficients prediction in the aqueous phase (subsystem B) compare to the SAC models; it gives better solubilities predictions of PTC in the organic phase (subsystems C). Moreover, because of the group contribution approach used by e-KT-UNIFAC, it gives the possibility to generate new PTC cations, by reconstructing the groups to other structure having similar properties.

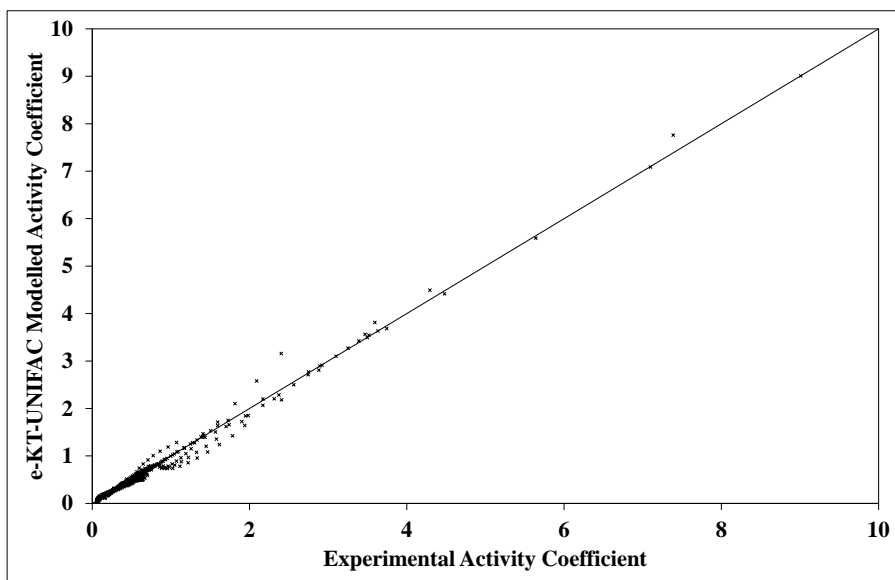


Figure 4-4: Activity coefficients of tetraalkylammonium PTC, comparison between e-KT-UNIFAC model calculation and measured data

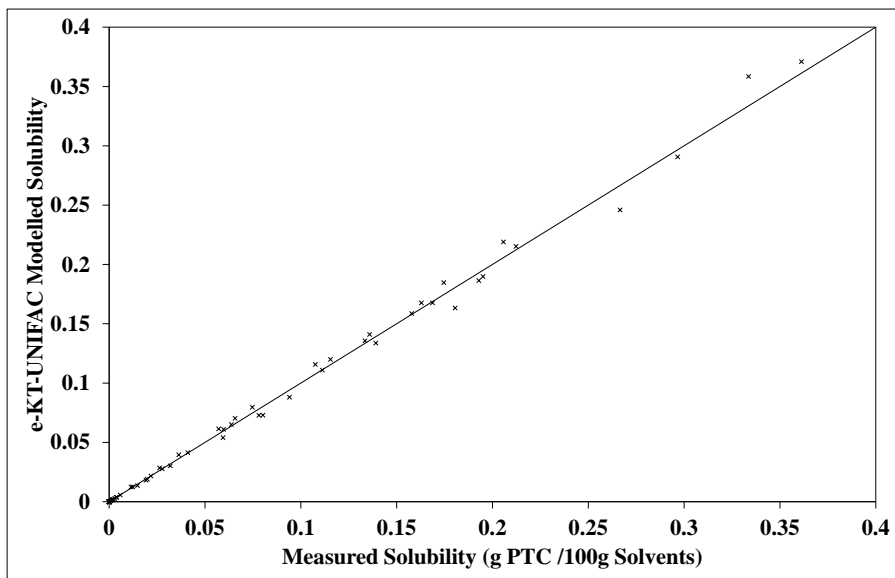


Figure 4-5: Solubilities of tetraalkylammonium PTC, comparison between e-KT-UNIFAC model calculation and measured data

4.2 REACTOR MODELS

This section presents some versions of biphasic reaction models are constructed via the modelling framework given in chapter 3. Process models are combined with thermodynamic models (see section 3.2) to obtain the final system model capable of estimating the process design-performance variable (product yield, amount of impurities, acceleration of reactions, etc.).

Example cases of the problem-specific models of the biphasic reaction systems under different reaction conditions and design targets are employed to illustrate that the assembled models have wide range of predictive capability in terms of matching data from the measured systems and extrapolations, particularly in the studies involving search of solvents and design of the catalyst for better product yields, faster reaction rate, and easier separation. The cases include pseudo-PTC and PTC system, epoxidation, furan production, and amino acid production.

4.2.1 PTC I, Benzoin Condensation

4.2.1.1 Process Introduction

Benzoin (2-hydroxy-1,2-diphenylethanone, $C_6H_5CH(OH)C(O)C_6H_5$) is a hydroxyl ketone used as a synthon for polymeric and pharmaceutical materials. Benzoin is produced by a condensation reaction of benzaldehyde (C_6H_5CHO) with a cyanide ion catalyst. In a PTC system, the benzaldehyde is principally in the organic phase with sodium cyanide (Na^+CN^-) in the aqueous phase. The PTC is tetrabutylammonium bromide (TBAB) [19] with the reaction mechanism given in Figure 4-6.

The reactor is of the batch type and the reactor operation starts in the aqueous phase with TBAB and sodium cyanide reacting (1) to form tetrabutylammonium cyanide (TBACN, TBA^+CN^-) and the spent salt sodium bromide. The TBACN is transferred from the aqueous phase to the organic phase (2) to react with benzaldehyde (3), generating a cyanohydrin intermediate, which rearranges to nucleophilic cabanion. Another benzaldehyde molecule is then undergone a nucleophilic addition reaction (4) with the cabanion species. Then the cyanide group is eliminated (5), resulting in the benzoin product and a TBA^+CN^- compound which transfers to the aqueous phase for another cycle. This system may be considered as pseudo phase transfer catalyst, since both the active and inactive PTC forms are not consumed during the reaction. Thus, the aqueous Na^+CN^- and PTC are treated as inert species at constant concentration.

Due to the lack of available measured data and parameters of the predictive thermodynamic model, the target of this case is to build a correlative combined partition-rate model for determining the effect of changing the initial concentration of the involved compounds.

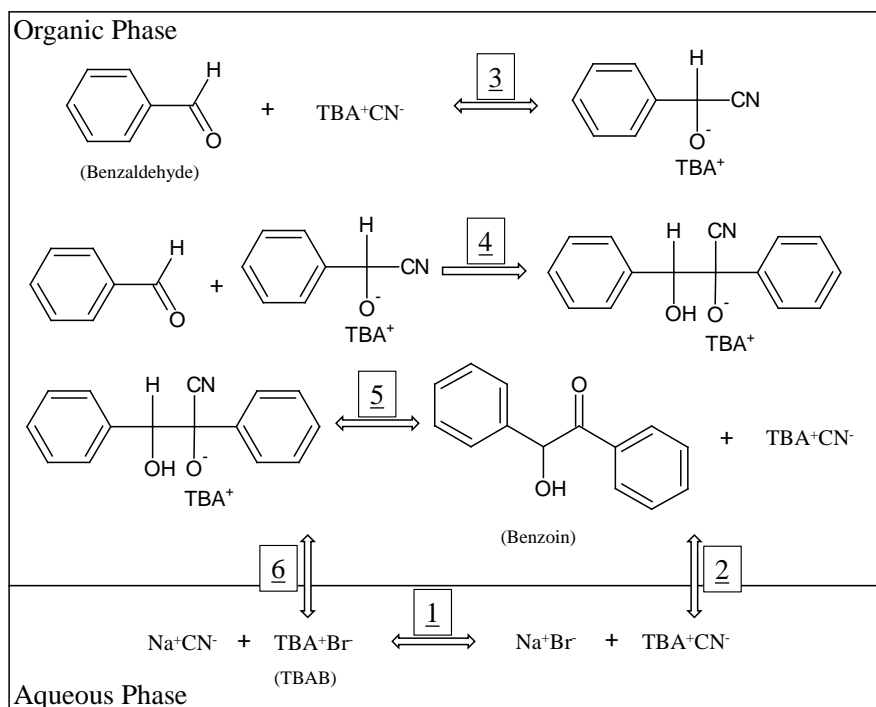


Figure 4-6: Benzoin condensation process mechanism

4.2.1.2 Model Construction

The first step of the framework is gathering the system information. The classifications of involved chemical species and reaction types are shown in Tables 4-4 and 4-5 respectively. The essential physico-chemical properties are collected in Table 4-6. The reactor is a batch reactor and it is also assumed that all reactions follow elementary rate law, with no mass transfer limit, and concentration of *TBAB* and *TBACN* are constant throughout the reaction period.

The model is constructed based on the assumption and information gathered.

Table 4-4: Classification of the involved chemical species in the benzoin condensation process

Chemical Species	Heterogeneous	Reactive	Solvent	Dissociation
Water	N (A)	N	Y	N
Toluene	N (O)	N	Y	N
TBAB	Y	N	N	Y (A)
TBACN	Y	N	N	Y (A)
Na^+CN^-	N (A)	N	N	Y
Na^+Br^-	N (A)	N	N	Y
Benzaldehyde	N (O)	Y	N	N
Intermediates	N (O)	Y	N	N
Benzoin	N (O)	Y	N	N

*N (A), homogeneous species, stay in aqueous phase

N (O), homogeneous species, stay in organic phase

Y (A), dissociated species, only in aqueous phase

Table 4-5: Classification of the involved reactions in the benzoin condensation process

Reactions*	Kinetic-Controlled	Equilibrium-Controlled	Mass Transfer
1		A	
2			I
3		O	
4	O		
5		O	
6			I

*Reaction numbers are as shown in Figure 4-6

*A: Aqueous phase, O: Organic phase, I: Instantaneous, L: Limited (mass transfer)

Table 4-6: Physico-chemical properties of the involved species in the benzoin condensation process

Chemical Species	Molecular Weight ($g \cdot mol^{-1}$)	Density at 25 °C ($kmol \cdot m^{-3}$)	Gibbs of Formation ($kJ \cdot mol^{-1}$)	Heat of Formation ($kJ \cdot mol^{-1}$)
Water	18.01	55.34	-237.21	-285.83
Toluene	92.14	9.38	113.80	12.01
TBAB	322.37		202.67*	-293.55*
TBACN	268.48		325.94*	-176.77*
Na^+CN^-	49.01		-76.4	-91.00
Na^+Br^-	102.89		-349.30	-361.41
Benzaldehyde	106.12	9.81	6.53	-86.82
Benzoin	212.25	5.70*	27.92*	-101.31*

*Estimated from group contribution method by Marrero and Gani [114]

In module 1, the distributions between the aqueous (α) and the organic (β) phases of *TBAB* and *TBACN* are defined as functions of the activity coefficients, as given below.

$$P_{TBAB} = \frac{\gamma_{TBA}^{\alpha} \gamma_{Br^-}^{\alpha}}{\gamma_{TBAB}^{\beta}} \quad 4-6$$

$$P_{TBACN} = \frac{\gamma_{TBA}^{\alpha} \gamma_{CN^-}^{\alpha}}{\gamma_{TBACN}^{\beta}} \quad 4-7$$

From module 2, the reaction in the aqueous phase is considered as an equilibrium-controlled reaction.

$$0 = C_{NaCN}^{\alpha} \gamma_{NaCN}^{\alpha} C_{TBAB}^{\alpha} \gamma_{TBAB}^{\alpha} - \frac{C_{NaBr}^{\alpha} \gamma_{NaBr}^{\alpha} C_{TBACN}^{\alpha} \gamma_{TBACN}^{\alpha}}{K_{Eq,1}} \quad 4-8$$

In the organic phase, the nucleophilic addition is the kinetic-controlled reaction; while the other two reactions are the equilibrium-controlled reactions.

$$0 = C_B \gamma_B C_{TBACN}^{\beta} \gamma_{TBACN}^{\beta} - \frac{C_{Cab} \gamma_{Cab}}{K_{Eq,3}} \quad 4-9$$

$$R_4 = k_4 C_B C_{Cab} \quad 4-10$$

$$0 = C_I \gamma_I - \frac{C_P \gamma_P C_{TBACN}^{\beta} \gamma_{TBACN}^{\beta}}{K_{Eq,5}} \quad 4-11$$

where, subscripts *B*, *Cab*, *I*, and *P* denote benzaldehyde, benzaldehyde-intermediate, benzoin-intermediate, and benzoin respectively.

There are two immediate mass transfers across the phases of the PTC species.

$$0 = x_{TBAB}^{\beta} - P_{TBAB} x_{TBA}^{\alpha} x_{Br^-}^{\alpha} \quad 4-12$$

$$0 = x_{TBACN}^{\beta} - P_{TBACN} x_{TBA}^{\alpha} x_{CN^-}^{\alpha} \quad 4-13$$

From the balance module, the batch reactor model does not have flow-in or flow-out terms. The reaction only directly affects the amount of raw material (benzaldehyde) and product (benzoin), therefore, the balance equations of affected species are derived as given in equations 4-14 to 4-16, while the amounts of other species are implicitly calculated by the equilibrium equations.

$$\frac{d\xi_4}{dt} = R_4 V \quad 4-14$$

$$N_B = N_B^0 - \xi_4 \quad 4-15$$

$$N_p = N_p^0 + \xi_4 \quad 4-16$$

The NRTL and eNRTL models are combined with the above process model for the benzoin condensation process. Measured data are needed for regression of the kinetic parameter k_3 . The interaction parameters were taken from Piccolo et al. [61]. The results of the full model calculations are given in section 5.1.

4.2.2 PTC II, Chlorination of Organobromine

4.2.2.1 Process Introduction

Organochloride is used as synthetic rubber in chemical industries [115,116], insecticide and its intermediate in the agricultural industry [116,117], and intermediate for antibacterial in the pharmaceutical industry [118]. It has been synthesised by the chlorination reaction between the organobromine compound and sodium chloride catalysed by tetraalkylammonium PTC.

Figure 4-7 shows the PTC reaction mechanism of organobromine chlorination. The process starts in the aqueous phase with the reaction between tetraalkylammonium bromide (Q^+Br^-) and sodium chloride to generate the active PTC, tetraalkylammonium chloride (Q^+Cl^-), that transfers from the aqueous to the organic phase. This active PTC reacts with organobromine to create organochloride and an inactive PTC that transfers back to aqueous phase for further reaction.

There are multiple design targets based on the applications of the model. Therefore, multiple types of models are constructed for accommodating different targets in the next section.

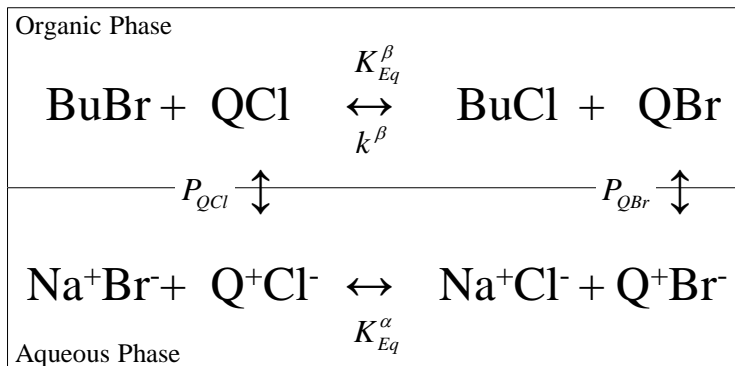


Figure 4-7: Chlorination of organobromine reaction mechanism

4.2.2.2 Model Construction

Prior to model construction, the system information is gathered. The classifications of involved chemical species are shown in Table 4-7. The reaction in the aqueous phase is an equilibrium-controlled reaction, while the reaction in the organic phase is modelled based on different design targets. The essential physico-chemical properties are collected in Table 4-8.

Table 4-7: Classification of the involved chemical species in the chlorination process

Chemical Species	Heterogeneous	Reactive	Solvent	Dissociation
Water	N (A)	N	Y	N
Solvents	N (O)	N	Y	N
<i>QBr</i>	Y	Y	N	Y (A)
<i>QCl</i>	Y	Y	N	Y (A)
<i>Na⁺Br⁻</i>	N (A)	Y	N	Y
<i>Na⁺Cl⁻</i>	N (A)	Y	N	Y
<i>BuBr</i>	N (O)	Y	N	N
<i>BuCl</i>	N (O)	Y	N	N

*See bottom 4-4 for the explanations

Table 4-8: Physico-chemical properties of the involved species in the chlorination process

Chemical Species	Molecular Weight (g·mol ⁻¹)	Density at 25 °C (kmol·m ⁻³)	Gibbs of Formation (kJ·mol ⁻¹)	Heat of Formation (kJ·mol ⁻¹)
Water	18.01	55.34	-237.21	-285.83
<i>Na⁺Br⁻</i>	102.89		-349.30	-361.41
<i>Na⁺Cl⁻</i>	58.44		-384.1	-411.12
<i>BuBr</i>	137.02	9.26	-17.40	-143.80
<i>BuCl</i>	92.57	9.52	-51.47	-189.30

Here, there are 2 heterogeneous chemical species, tetraalkylammonium bromide and tetraalkylammonium chloride. Water and an organic compound are treated as solvents; in this case 13 immiscible organic substances are studied to examine their differences in effectiveness (toluene, benzene, dichloromethane, methyl tert-butyl ether, dichloroethane, bromobenzene, chlorobenzene, chloroform, ethylacetate, methylcyclohexane, ethyl ether, cyclohexane, and hexane). The reactive species are organobromine, the PTC, and the sodium salts, and complete dissociation of sodium salts and tetrabutylammonium species is assumed in the aqueous phase.

Again, the process is a batch reactor without any mass transfer limit. The reaction in the organic phase has been formulated with both kinetic control and equilibrium control, depending on the design targets.

In module 1, the distribution between aqueous (α) and organic (β) phases of active and inactive forms of PTC (*QBr* and *QCl*) are derived as functions of activity coefficients.

$$P_{QBr} = \frac{\gamma_Q^\alpha \gamma_{Br^-}^\alpha}{\gamma_{QBr}^\beta} \quad 4-17$$

$$P_{QCl} = \frac{\gamma_Q^\alpha \gamma_{Cl^-}^\alpha}{\gamma_{QCl}^\beta} \quad 4-18$$

From module 2, there are two instantaneous mass transfers across the phases of the

heterogeneous species.

$$0 = x_{QBr}^{\beta} - P_{QBr} x_{Q^+}^{\alpha} x_{Br^-}^{\alpha} \quad 4-19$$

$$0 = x_{QCl}^{\beta} - P_{QCl} x_{Q^+}^{\alpha} x_{Cl^-}^{\alpha} \quad 4-20$$

The reaction in the aqueous phase is the equilibrium-controlled reaction.

$$0 = x_{Br^-}^{\alpha} \gamma_{Br^-}^{\alpha} x_{QCl}^{\alpha} \gamma_{QCl}^{\alpha} - K_{Eq}^{\alpha} x_{Cl^-}^{\alpha} \gamma_{Cl^-}^{\alpha} x_{QBr}^{\alpha} \gamma_{QBr}^{\alpha} \quad 4-21$$

The reaction in the organic phase is derived for describing the PTC system under different operational scenarios, with three different assumptions that depend on specified process design targets. The three sets of the model are equilibrium model, conversion model, and kinetic model.

1. Equilibrium model

This model set is constructed to estimate the final amount of each species in both aqueous and organic phases, with the assumption that the organic phase reaction reaches the equilibrium state. It needs one equation (4-22a) and one parameter, the equilibrium constant (K_{Eq}^{β}) for the organic phase reaction. In this model set, the extent of reaction in the organic phase (ζ^{β}) is and unknown variable, which is implicitly calculated.

$$0 = x_{Bu-Br} \gamma_{Bu-Br} x_{QCl}^{\beta} \gamma_{QCl}^{\beta} - K_{Eq}^{\beta} x_{Bu-Cl} \gamma_{Bu-Cl} x_{QBr}^{\beta} \gamma_{QBr}^{\beta} \quad 4-22a$$

2. Conversion model

This model is used when the conversion of limiting reactant is known. It is used to estimate the amounts of each species partitioned within both phases at a given conversion. Similar to equilibrium model, conversion model also requires one equation (4-22b) and one parameter, the conversion (C^{β}). In this model set, the extent of reaction (ζ^{β}) is calculated directly from the conversion.

$$\zeta^{\beta} = C^{\beta} N_{Bu-Br}^0 \quad 4-22b$$

3. Kinetic model

This model is a time-dependent model for estimating the actual rate of reaction. The model is used for designing a reaction system for improving the rate of reaction. It requires one rate equation (4-22c) and the equation link between module 2 and 3 (4-22d). One parameter, the rate of organic phase reaction (k_{β}) is needed. In this model set, the extent of reaction is calculated from the differential equation, 4-22d, as a function of time.

$$R^{\beta} = k_{\beta} C_{Bu-Br} C_{QCl}^{\beta} \quad 4-22c$$

$$\frac{d\xi^\beta}{dt} = R^\beta V^\beta \quad 4-22d$$

From module 3, the batch reactor model (omitting inlet and outlet flow terms) is used. The amounts of bromide and chloride ions are initialised by equations 4-23 and 4-24.

$$N_{Br^-}^0 = N_{NaBr}^0 + N_{QBr}^{0,\alpha} \quad 4-23$$

$$N_{Cl^-}^0 = N_{NaCl}^0 + N_{QCl}^{0,\alpha} \quad 4-24$$

All reactive species change together, with equilibrium, conversion, or time depending on the type of the active set of species. Therefore, there are 8 balance equations (4-25 to 4-32) for each species type.

$$N_{Br^-}^\alpha = N_{Br^-}^0 + \xi^\alpha \quad 4-25$$

$$N_{Cl^-}^\alpha = N_{Cl^-}^0 - \xi^\alpha \quad 4-26$$

$$N_{Bu-Br}^\beta = N_{Bu-Br}^0 - \xi^\beta \quad 4-27$$

$$N_{Bu-Cl}^\beta = N_{Bu-Cl}^0 + \xi^\beta \quad 4-28$$

$$N_{QCl}^\beta = N_{QCl}^T - N_{QCl}^\alpha \quad 4-29$$

$$N_{QBr}^\beta = N_{QBr}^T - N_{QBr}^\alpha \quad 4-30$$

$$N_{QBr}^T = N_{QBr}^{\alpha,0} + N_{QBr}^{\beta,0} - \xi^\alpha + \xi^\beta \quad 4-31$$

$$N_{QCl}^T = N_{QCl}^{\alpha,0} + N_{QCl}^{\beta,0} + \xi^\alpha - \xi^\beta \quad 4-32$$

In total, there are 16 equations (17 in the case of the kinetic model). The equilibrium model does not require any extra parameter for reactor model, while conversion and kinetic models need one parameter. In section 5.2, the reactor models of the production of alkyl chloride in this section are coupled with the SAC and e-KT-UNIFAC thermodynamic models for estimations of the activity coefficients, to obtain a predictive capability and applicability toward design and analysis of the system with different design targets.

4.2.3 Epoxidation of Unsaturated Long Chain Fatty Acid

4.2.3.1 Process Introduction

An epoxide is a cyclic ether with a three-atom ring. It is mainly used as a substitute for phthalate plasticizer in PVC plastics and as a basis for surfactants and adhesives [35,58]. Epoxide compounds are produced from the reaction between unsaturated vegetable oil and hydrogen-

peroxide catalysed by short-chain carboxylic acids

As shown in Figure 4-8, the epoxidation process converts long-chain unsaturated fatty acids ($>C=C<$) to epoxide compounds (EPOX) by reaction with hydrogen peroxide (H_2O_2), catalysed by either formic ($HCOOH$) or acetic (CH_3COOH) acids. Initially, the reactor contains fatty acid solubilized in an organic phase composed of only the fatty acid (self-solvated) or an added organic solvent and water (H_2O) and hydrogen peroxide (H_2O_2) in an aqueous phase. The catalysing acid ($RCOOH$) is fed in, partitioning to the aqueous phase. The acid then reacts with hydrogen peroxide to form a peracid ($RCOOOH$) (3). The peracid transfers to the organic phase (4) and reacts with the unsaturated fatty acid to produce the epoxide product (EPOX) and reform the catalysing acid (1). The reformed acid transfers to the aqueous phase for additional reaction (5). While this scheme is the main reaction, water that may also partition into the organic phase (6) and react with the desired epoxide product and acid to create an unwanted epoxy cleavage side product (2).

The design targets are to increase the production rate of the epoxide compounds and to inhibit the formation of the cleavage.

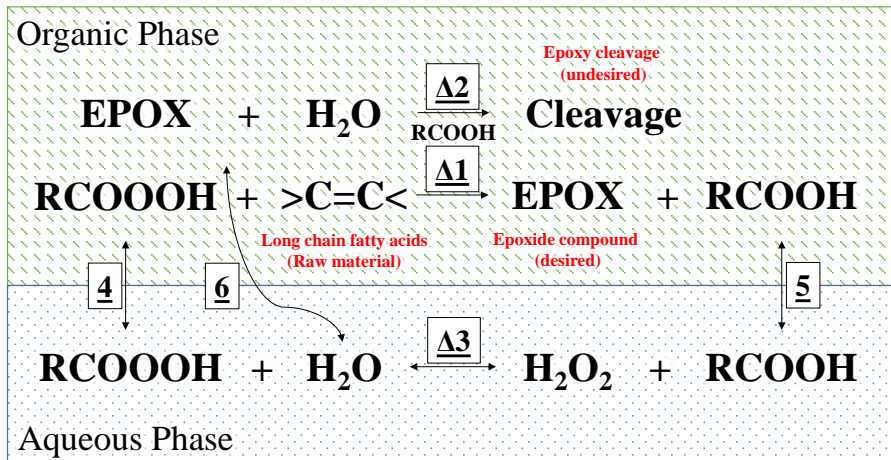


Figure 4-8: Epoxidation process reaction mechanism

4.2.3.2 Model Construction

In this work, the reactions of the unsaturated fatty acids in palm oil have been studied. Palm oil characterization data have been reported by Edem [119], as given in Table 4-9. For simplification, only the three largest acid species: saturated palmitic acid and unsaturated oleic and linoleic acids are being considered the model construction and calculations. Both single-phase aqueous systems with an organic phase of fatty acids and biphasic aqueous/organic systems with added solvent are studied. The classifications of the involved chemical species and the reaction types are shown in Tables 4-10 and 4-11 respectively. The essential physico-chemical properties are collected in Table 4-12. The reactor is a batch reactor, the concentration of water in the organic phase is assumed to be constant throughout the reaction period,

calculated from the solute-free solubility of water in the organic phase. And all reactions follow elementary rate law, with no mass transfer limit.

Table 4-9: Palm oil compositions and their respective molecular weight and reactive status

Fatty Acid	%	MW (g/mol)
Lauric	0.2	200.32
Myristic	1.1	228.38
Palmitic	44	256.43
Stearic	4.5	284.48
Oleic	39.2	282.47
Linoleic	10.1	280.45
Linolenic	0.4	278.44
Arachidic	0.1	312.54

Table 4-10: Classification of the involved chemical species in the epoxidation process

Chemical Species	Heterogeneous	Reactive	Solvent	Dissociation
Water	Y	Y	Y	N
Solvents	N (O)	N	Y	N
RCOOH	Y	Y	N	N
RCOOOH	Y	Y	N	N
H₂O₂	N (A)	Y	N	N
Palmitic	N (O)	N	Y	N
Oleic	N (O)	Y	Y	N
Linoleic	N (O)	Y	Y	N
Epoxide	N (O)	Y	N	N
Cleavage	N (O)	Y	N	N

*See bottom of 4-4 for the explanations

Table 4-11: Classification of the involved reactions in the epoxidation process

Reactions	Kinetic-Controlled	Equilibrium-Controlled	Mass Transfer
$\Delta 1$	O		
$\Delta 2$	O		
$\Delta 3$		A	
4			I
5			I
6			I

*Reaction numbers are as shown in 4-8

*See bottom of 4-5 for the explanations

Table 4-12: Physico-chemical properties of the involved species in the epoxidation process

Chemical Species	Molecular Weight (g·mol ⁻¹)	Density at 25 °C (kmol·m ⁻³)	Gibbs of Formation (kJ·mol ⁻¹)	Heat of Formation (kJ·mol ⁻¹)
Water	18.01	55.34	-237.21	-285.83
Formic	46.02	26.37	-362.40	-425.50
Performic	62.02	26.98*	-462.32*	-245.57*
Acetic	60.05	17.35	-389.00	-484.50
Peracetic	76.05	15.94	-262.00	-339.00
H ₂ O ₂	34.01	42.42	-120.30	-188.11
Palmitic	256.42	3.42	-311.70	-894.00
Oleic	282.46	3.13	-261.10	-802.49
Linoleic	280.44	3.21	-168.20	-674.04
Epoxide (I)**	298.46		-232.67*	-747.99*
Epoxide (II)**	296.44		-154.83*	-633.58*
Cleavage(I)**	316.47		-527.34*	-1084.37*
Cleavage(II)**	314.46		-448.15*	-970.64*

*Estimated from group contribution method by Marrero and Gani [114]

**Two of epoxide and cleavage compounds are generated from oleic and linoleic acids

In module 1, the physical equilibrium of the two heterogeneous species (acid and peracid) are expressed by the following equations 4-33 and 4-34.

$$P_{RCOOH} = \frac{\gamma_{RCOOH}^{\alpha}}{\gamma_{RCOOH}^{\beta}} \quad 4-33$$

$$P_{RCOOOH} = \frac{\gamma_{RCOOOH}^{\alpha}}{\gamma_{RCOOOH}^{\beta}} \quad 4-34$$

In the rate module, there are 2 kinetic driven reactions in the organic phase, an equilibrium-controlled reaction in the aqueous phase, and 2 instantaneous mass transfers across the co-exist phases. Rate equations are formulated as following equations

$$R_1^{\beta} = k_1^{\beta} (C_{CC} C_{RCOOH}^{\beta}) \quad 4-35$$

$$R_2^{\beta} = k_2^{\beta} (C_{EPOX} C_{RCOOH}^{\beta} C_W^{\beta}) \quad 4-36$$

$$0 = x_{RCOOH}^{\beta} - P_{RCOOH} x_{RCOOH}^{\alpha} \quad 4-37$$

$$0 = x_{RCOOOH}^{\beta} - P_{RCOOOH} x_{RCOOOH}^{\alpha} \quad 4-38$$

$$0 = x_{H_2O_2}^{\alpha} \gamma_{H_2O_2}^{\alpha} x_{RCOOH}^{\alpha} \gamma_{RCOOH}^{\alpha} - K_{Eq}^{\alpha} x_{RCOOOH}^{\alpha} \gamma_{RCOOOH}^{\alpha} \quad 4-39$$

where, the kinetic parameters (k_1^{β} and k_2^{β}) are expressed as the temperature dependent

parameters by Arrhenius' equation.

$$k_j = A_j e^{-\frac{E_{a,j}}{RT}} \quad 4-40$$

where, A_j is the pre-exponential factor of the reaction j , $E_{a,j}$ is the activation energy of the reaction j , R is the universal gas constant, and T is the operating temperature.

In the last module of balance equations, there are 2 differential equations (4-41 and 4-42) connecting the rate module to the balance module and 9 balance equations (4-43 to 4-51) for the 7 reactive species and 2 heterogeneous species. Though water is considered as reactive species, it is assumed that its concentration in the organic phase is constant throughout the reaction period, and there is no need for the balance equation of it.

$$\frac{d\xi_1^\beta}{dt} = R_1^\beta V^\beta \quad 4-41$$

$$\frac{d\xi_2^\beta}{dt} = R_2^\beta V^\beta \quad 4-42$$

$$N_{EPOX}^\beta = N_{EPOX}^0 + \xi_1^\beta - \xi_2^\beta \quad 4-43$$

$$N_{H_2O_2}^\beta = N_{H_2O_2}^0 - \xi_1^\beta \quad 4-44$$

$$N_{RCOOH}^\alpha = \xi_{RCOOH} - \xi^\alpha \quad 4-45$$

$$N_{RCOOH}^\alpha = \xi_{RCOOH} + \xi^\alpha \quad 4-46$$

$$N_{RCOOH}^\beta = N_{RCOOH}^{\beta,0} - \xi_{RCOOH} + \xi_1^\beta \quad 4-47$$

$$N_{RCOOH}^\beta = N_{RCOOH}^{\beta,0} - \xi_{RCOOH} - \xi_1^\beta \quad 4-48$$

$$N_{Ole}^\beta = N_{Ole}^0 - v_{Ole} \xi_1^\beta \quad 4-49$$

$$N_{Lino}^\beta = N_{Lino}^0 - v_{Lino} \xi_1^\beta \quad 4-50$$

$$N_{Cleav}^\beta = N_{Cleav}^0 + \xi_2^\beta \quad 4-51$$

Table 4-13 lists the equations and variables associated to the epoxidation reaction model. The mathematical model has 2 ordinary differential equations (ODEs) and 15 algebraic equations (AEs) containing 37 variables, out of which 2 are dependent differential variables, 15 are unknown algebraic variables, 7 are constitutive variables (that are calculated through the e-KT-UNIFAC model) and the remaining variables are specified - 4 reaction rate parameters; 2 system parameters for the composition of raw materials and 7 input specifications.

Table 4-13: Epoxidation model analysis

Equations	Eq. number
ODEs (2)	4-41 and 4-42
AEs (15)	4-33 to 4-40 and 4-43 to 4-51
Variables and Parameters	
Initial condition (2)	$\xi_1^{\beta,0} = 0$
Extents of reactions	$\xi_2^{\beta,0} = 0$
Input specification (7) Initial moles	$N_{EPOX}^0, N_{H_2O_2}^0, N_{Ole}^0, N_{RCOOH}^0, N_{RCOOH}^0,$ N_{Limo}^0, N_{Cleav}^0
System parameter (2) Raw materials compositions	V_{Ole}, V_{Limo}
Reaction rate parameters (4)	$A_1, A_2, E_{a,1}, E_{a,2}$
Constitutive model parameters (7) Activity coefficients	$\gamma_{RCOOH}^\alpha, \gamma_{RCOOH}^\beta, \gamma_{RCOOH}^\alpha, \gamma_{RCOOH}^\beta, \gamma_W^\beta,$ $\gamma_{CC}, \gamma_{EPOX}$
Unknown variables (15)	
- Partition coefficients (2)	P_{RCOOH}, P_{RCOOH}
- Reaction rates (2)	R_1^β, R_2^β
- Moles and concentrations (11)	$N_{EPOX}^\beta, N_{H_2O_2}^\alpha, N_{RCOOH}^T, N_{RCOOH}^T, N_{Ole}^\beta,$ $N_{Limo}^\beta, N_{Cleav}^\beta, x_{RCOOH}^\alpha, x_{RCOOH}^\beta, x_{RCOOH}^\alpha,$ x_{RCOOH}^β

4.2.4 Production of Furan Derivatives from Biomass

4.2.4.1 Process Introduction

Conversion of biomass resources to fuels and chemicals is becoming very important due to greenhouse gas emission and limited resources of fossil fuels. Furan derivatives, such as 5-hydroxymethylfurfural (HMF) and furfural, are platform chemicals for the production of diesel substitute fuels and a variety of useful acids, aldehydes, alcohols, and amides [49,120–122]. Furfural and HMF can be produced from the dehydration of the C₅ and C₆ sugars found in lignocellulosic wastes [46].

The literature reports the use of catalytic biphasic reacting systems to produce furan derivatives from biomass [49,50,52,120–122], since the reaction pathways and catalysts used to convert sugars to furan derivatives are similar to other such systems. Figure 4-9 shows a schematic of the reactions and phases. The dehydration reactions converting fructose to HMF and xylose to furfural occur in the aqueous phase (1, 2). Further, these products can also react in the aqueous phase to create unwanted side products (3). Upon formation, both desired and side products transfer to the organic phase (4, 5, 6). It has been found that the yield of desired furan derivatives can vary from 0 to 90%, depending on the organic solvent, catalyst, operating technique, and reaction conditions.

The design targets are to increase the production rates of HMF and furfural products, to increase the partitions of the products into the organic phase, to prevent the formation of the unwanted species, and to decrease the amount of impurity partitioned into the organic phase.

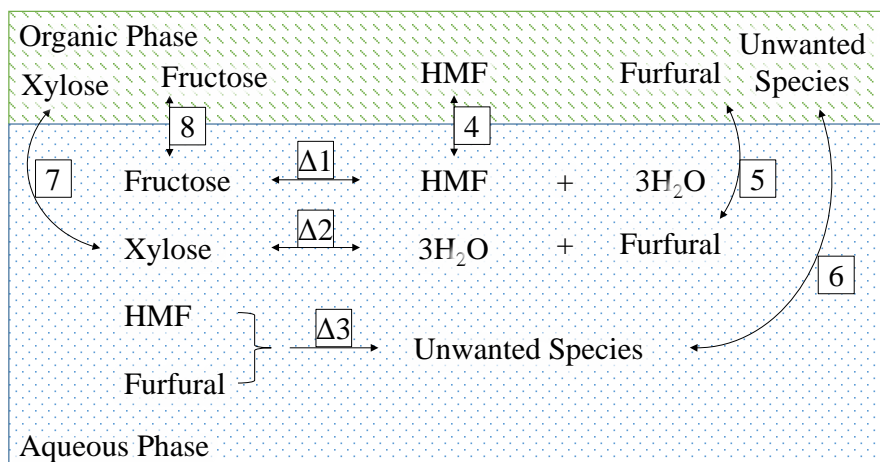


Figure 4-9: Production of furan derivatives reaction mechanism

4.2.4.2 Model Construction

A mathematical model has been constructed for the production of furan derivatives from rice straw in a biphasic reactor. The composition of rice straw has been reported by Amiri et al. [46]; it consists of 20% xylose, 35% fructose, and 45% chemically inert materials (dry weight %). The main reactions are apparently a combination of equilibrium- and kinetically-controlled reactions, while the side reactions are only kinetic-driven, and all reactions take place only in the aqueous phase. The reactants (fructose and xylose), products (HMF and furfural), and side products (Unwanted Species) are identified as heterogeneous species. There are five reactive species: fructose, xylose, HMF, furfural, and the lumped side products. For simplification, it is assumed that the reactions (1) and (2) have the same reaction rate coefficients and that the side reactions (3) from HMF and furfural to the unwanted species have a different reaction rate coefficient. Cyclopentanone is assumed to be the only side product. There is mass transfer limitation of HMF and furfural through the interface between the aqueous and organic phases; it is assumed that the mass transfer coefficients of these species are identical, while mass transfers of reactants and side product are instantaneous. The reactions classifications are shown in Table 4-14, all reactions are taking place in the aqueous phase only. The classifications of the chemical species and their physico-chemical properties are reported in Tables 4-15 and 4-16 respectively.

Table 4-14: Classification of the involved reactions in the furan derivatives production process

Reactions	Kinetic-Controlled	Equilibrium-Controlled	Mass Transfer
$\Delta 1$	A	A	
$\Delta 2$	A	A	
$\Delta 3$	A		
4			L
5			L
6			I
7			I
8			I

*Reaction numbers are as shown in Figure 4-9

*See bottom of 4-5 for the explanations

Table 4-15: Classification of the involved chemical species in the furan derivatives production process

Chemical Species	Heterogeneous	Reactive	Solvent	Dissociation
Water	N (A)	N	Y	N
Solvents	N (O)	N	Y	N
Fructose	Y	Y	N	N
Xylose	Y	Y	N	N
HMF	Y	Y	N	N
Furfural	Y	Y	N	N
Cyclopentanone	Y	Y	N	N

*See bottom of 4-4 for the explanations

Table 4-16: Physico-chemical properties of the involved species in the furan derivatives production process

Chemical Species	Molecular Weight ($\text{g}\cdot\text{mol}^{-1}$)	Density at 25 °C ($\text{kmol}\cdot\text{m}^{-3}$)	Gibbs of Formation ($\text{kJ}\cdot\text{mol}^{-1}$)	Heat of Formation ($\text{kJ}\cdot\text{mol}^{-1}$)
Water	18.01	55.34	-237.21	-285.83
Fructose	342.30		-1548.00	-2226.10
Xylose	150.13		-722.50	-1051.00
HMF	126.11	14.75	-286.43*	-533.50*
Furfural	96.08	12.01	-119.00	-201.60
Cyclopentanone	84.12	11.22	-103.20	-235.70

*Estimated from group contribution method by Marrero and Gani [114]

In module 1, physical equilibrium of the three heterogeneous species can be expressed by the following equations 4-52 to 4-56.

$$P_{HMF} = \frac{\gamma_{HMF}^{\alpha}}{\gamma_{HMF}^{\beta}} \quad 4-52$$

$$P_{FA} = \frac{\gamma_{FA}^{\alpha}}{\gamma_{FA}^{\beta}} \quad 4-53$$

$$P_{US} = \frac{\gamma_{US}^{\alpha}}{\gamma_{US}^{\beta}} \quad 4-54$$

$$P_{Fruc} = \frac{\gamma_{Fruc}^{\alpha}}{\gamma_{Fruc}^{\beta}} \quad 4-55$$

$$P_{Xyl} = \frac{\gamma_{Xyl}^{\alpha}}{\gamma_{Xyl}^{\beta}} \quad 4-56$$

where, *FA* denotes the furfural species, *HMF* denotes the 5-hydroxymethylfurfural, *US* denotes the unwanted species, *Fruc* and *Xyl* denote the fructose and xylose sugars respectively.

In the rate module, reaction 1 and 2 are the mixed kinetic-equilibrium-controlled reactions. Reaction 3 is the kinetic-driven reaction. There are 2 limited mass transfer rates across the phases and 3 instantaneous mass transfer equations. 9 equations of module 2 are formulated as shown below; equations 4-57 and 4-58 are the mixed kinetic-equilibrium-controlled equations, equations 4-59 and 4-60 are the kinetic-controlled equations, equations 4-61 and 4-62 are the limited mass transfer equations, and equations 4-63 to 4-65 are the instantaneous mass transfer equations.

$$R_1 = k_1 \left(C_{Fruc} \gamma_{Fruc} - \frac{C_{HMF} \gamma_{HMF}}{K_{Eq,1}} \right) \quad 4-57$$

$$R_2 = k_1 \left(C_{Xyl} \gamma_{Xyl} - \frac{C_{FA} \gamma_{FA}}{K_{Eq,2}} \right) \quad 4-58$$

$$R_{3-1} = k_2 C_{HMF} \quad 4-59$$

$$R_{3-2} = k_2 C_{FA} \quad 4-60$$

$$R_{HMF} = k_L S_A \left(X_{HMF}^{\alpha} - \frac{X_{HMF}^{\beta}}{P_{HMF}} \right) \quad 4-61$$

$$R_{FA} = k_L S_A \left(X_{FA}^{\alpha} - \frac{X_{FA}^{\beta}}{P_{FA}} \right) \quad 4-62$$

$$0 = x_{Fruc}^{\beta} - x_{Fruc}^{\alpha} P_{Fruc} \quad 4-63$$

$$0 = x_{Xyl}^{\beta} - x_{Xyl}^{\alpha} P_{Xyl} \quad 4-64$$

$$0 = x_{US}^{\beta} - x_{US}^{\alpha} P_{US} \quad 4-65$$

In the balance module, there are 6 equations (4-66 to 4-71) of the extent of reactions linking the rate and the balance modules and 10 balance (4-72 to 4-81) equations for 5 reactive species and 5 heterogeneous species.

$$\frac{d\xi_1}{dt} = R_1 V^{\alpha} \quad 4-66$$

$$\frac{d\xi_2}{dt} = R_2 V^{\alpha} \quad 4-67$$

$$\frac{d\xi_{3-1}}{dt} = R_{3-1} V^{\alpha} \quad 4-68$$

$$\frac{d\xi_{3-2}}{dt} = R_{3-2} V^{\alpha} \quad 4-69$$

$$\frac{d\xi_{HMF}}{dt} = R_{HMF} V^{\alpha} \quad 4-70$$

$$\frac{d\xi_{FA}}{dt} = R_{FA} V^{\alpha} \quad 4-71$$

$$N_{Fruc}^{\alpha} = N_{Fruc}^0 - \xi_1 - \xi_{Fruc} \quad 4-72$$

$$N_{Fruc}^{\beta} = \xi_{Fruc} \quad 4-73$$

$$N_{Xyl}^{\alpha} = N_{Xyl}^0 - \xi_2 - \xi_{Xyl} \quad 4-74$$

$$N_{Xyl}^{\beta} = \xi_{Xyl} \quad 4-75$$

$$N_{HMF}^{\alpha} = N_{HMF}^{0,\alpha} + \xi_1 - \xi_{3-1} - \xi_{HMF} \quad 4-76$$

$$N_{HMF}^{\beta} = N_{HMF}^{0,\beta} + \xi_{HMF} \quad 4-77$$

$$N_{FA}^{\alpha} = N_{FA}^{0,\alpha} + \xi_2 - \xi_{3-2} - \xi_{FA} \quad 4-78$$

$$N_{FA}^{\beta} = N_{FA}^{0,\beta} + \xi_{FA} \quad 4-79$$

$$N_{US}^{\alpha} = N_{US}^{0,\alpha} + \xi_{3-1} + \xi_{3-2} - \xi_{US} \quad 4-80$$

$$N_{US}^{\beta} = \xi_{US}$$

4-81

Table 4-17 lists the equations and variables associated to the furan derivatives production reaction model. The mathematical model has 6 ODEs and 24 AEs containing 50 variables, out of which 6 are dependent differential variables, 24 are unknown algebraic variables, and 10 are constitutive variables calculated through the e-KT-UNIFAC model. The remaining 10 variables are 7 input specification variables of the initial moles and 3 reaction rate parameters.

Table 4-17: Production of furan derivative model analysis

Equations	Eq. number
ODE (6)	4-66 to 4-71
AE (24)	4-52 to 4-65 and 4-72 to 4-81
Variables and Parameters	
Initial condition (6)	$\xi_1 = 0$
Extents of reactions	$\xi_2 = 0$
	$\xi_{3-1} = 0$
	$\xi_{3-2} = 0$
	$\xi_{HMF} = 0$
	$\xi_{FA} = 0$
Input specification (7) Initial moles	$N_{Fruc}^0, N_{Xyl}^0, N_{HMF}^{0,\alpha}, N_{HMF}^{0,\beta}, N_{FA}^{0,\alpha}, N_{FA}^{0,\beta}, N_{US}^{0,\alpha}$
Reaction rate parameters (3)	k_1, k_2, k_L
Constitutive model parameters (10) Activity coefficients	$\gamma_{HMF}^{\alpha}, \gamma_{HMF}^{\beta}, \gamma_{FA}^{\alpha}, \gamma_{FA}^{\beta}, \gamma_{US}^{\alpha}, \gamma_{US}^{\beta}, \gamma_{Fruc}^{\alpha}, \gamma_{Fruc}^{\beta}, \gamma_{Xyl}^{\alpha}, \gamma_{Xyl}^{\beta}$
Unknown variables (24)	
- Partition coefficients (5)	$P_{HMF}, P_{FA}, P_{US}, P_{Fruc}, P_{Xyl}$
- Reaction and mass transfer rates (6)	$R_1, R_2, R_{3-1}, R_{3-2}, R_{HMF}, R_{FA}$
- Moles and concentrations (10)	$x_{HMF}^{\alpha}, x_{HMF}^{\beta}, x_{FA}^{\alpha}, x_{FA}^{\beta}, x_{Fruc}^{\alpha}, x_{Fruc}^{\beta}, x_{Xyl}^{\alpha}, x_{Xyl}^{\beta}, x_{US}^{\alpha}, x_{US}^{\beta}$
- Extents of equilibrium reactions and instantaneous transfer (3)	$\xi_{Fruc}, \xi_{Xyl}, \xi_{US}$

4.2.5 Production of Alpha-Aminobutyric Acid

4.2.5.1 Process Introduction

α -aminobutyric acid (AABA) is an intermediate for Levetiracetam active pharmaceutical ingredient (API) [123,124]. The production of AABA in the biphasic system is shown in Figure 4-10. The reaction (1) between a 2-oxobutyric acid (2OA) and benzylamine (BA) takes place

in the aqueous phase using ω -aminotransferase as the catalyst, giving AABA as the main product and benzaldehyde (BD) as a by-product. The reaction is a mixed kinetic-equilibrium limited reaction with BD acts as product inhibitor of the enzyme and an organic solvent is added to extract the by-product and increase the reaction efficiency.

The objective of this example is to analyse the reaction and find a solvent which improves the performance of the reaction and intensifies the separation of the α -aminobutyric acid production process.

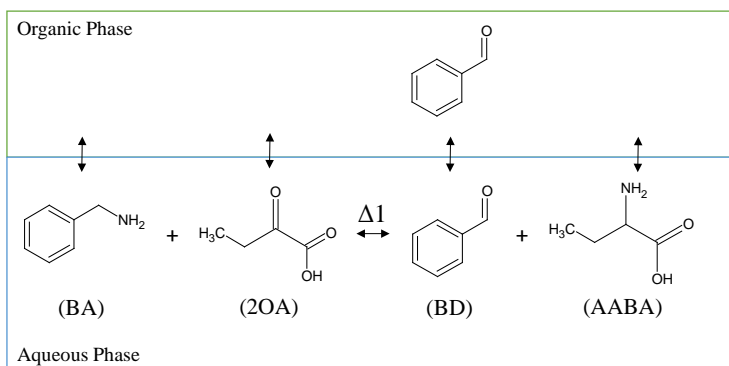


Figure 4-10: Production of α -aminobutyric acid in biphasic systems

4.2.5.2 Model construction

The model is developed for the production of AABA in the single and biphasic system as reported by Shin and Kim [55]. Aside from the aqueous and organic solvents, the involved species are heterogeneous and reactive species. There is only one mixed kinetic-equilibrium controlled reaction, which is assumed to follow the elementary reaction rate law. Mass transfer limited is neglected. The collected physico-chemical properties are displayed in Table 4-18.

Table 4-18: Physico-chemical properties of the involved species in the AABA production process

Chemical Species	Molecular Weight ($\text{g}\cdot\text{mol}^{-1}$)	Density at 25 °C ($\text{kmol}\cdot\text{m}^{-3}$)	Gibbs of Formation ($\text{kJ}\cdot\text{mol}^{-1}$)	Heat of Formation ($\text{kJ}\cdot\text{mol}^{-1}$)
Water	18.01	55.34	-237.21	-285.83
AABA	103.12		-296.08*	-441.10*
2OA	102.09	12.81	-521.40	-682.60
Benzylamine	107.15	9.13	180.10	34.20
Benzaldehyde	106.12	9.81	6.53	-86.82

*Estimated from group contribution method by Marrero and Gani [114]

In module 1, the physical equilibriums of four heterogeneous species are expressed as follow.

$$P_{AABA} = \frac{\gamma_{AABA}^{\alpha}}{\gamma_{AABA}^{\beta}} \quad 4-82$$

$$P_{2OA} = \frac{\gamma_{2OA}^{\alpha}}{\gamma_{2OA}^{\beta}} \quad 4-83$$

$$P_{BA} = \frac{\gamma_{BA}^{\alpha}}{\gamma_{BA}^{\beta}} \quad 4-84$$

$$P_{BD} = \frac{\gamma_{BD}^{\alpha}}{\gamma_{BD}^{\beta}} \quad 4-85$$

In module 2, there are 4 instantaneous mass transfers and one reaction equations.

$$0 = x_{AABA}^{\beta} - P_{AABA} x_{AABA}^{\alpha} \quad 4-86$$

$$0 = x_{2OA}^{\beta} - P_{2OA} x_{2OA}^{\alpha} \quad 4-87$$

$$0 = x_{BA}^{\beta} - P_{BA} x_{BA}^{\alpha} \quad 4-88$$

$$0 = x_{BD}^{\beta} - P_{BD} x_{BD}^{\alpha} \quad 4-89$$

$$R_1 = k_1 \left(C_{BA}^{\alpha} \gamma_{BA}^{\alpha} C_{2OA}^{\alpha} \gamma_{2OA}^{\alpha} - \frac{C_{BD}^{\alpha} \gamma_{BD}^{\alpha} C_{AABA}^{\alpha} \gamma_{AABA}^{\alpha}}{K_{Eq,1}} \right) \quad 4-90$$

In the last module, there is one extent of reaction equation and there are 8 balance equations for 4 heterogeneous species and 4 reactive species.

$$\frac{d\xi_1}{dt} = R_1 V^{\alpha} \quad 4-91$$

$$N_{AABA}^{\alpha} = N_{AABA}^{0,\alpha} + \xi_1 - \zeta_{AABA} \quad 4-92$$

$$N_{2OA}^{\alpha} = N_{2OA}^{0,\alpha} - \xi_1 - \zeta_{2OA} \quad 4-93$$

$$N_{BA}^{\alpha} = N_{BA}^{0,\alpha} - \xi_1 - \zeta_{BA} \quad 4-94$$

$$N_{BD}^{\alpha} = N_{BD}^{0,\alpha} + \xi_1 - \zeta_{BD} \quad 4-95$$

$$N_{AABA}^{\beta} = \zeta_{AABA} \quad 4-96$$

$$N_{2OA}^{\beta} = \zeta_{2OA} \quad 4-97$$

$$N_{BA}^{\beta} = \zeta_{BA} \quad 4-98$$

$$N_{BD}^{\beta} = \zeta_{BD}$$

4-99

Table 4-19 lists the equations and variables associated to the α -aminobutyric acid production reaction model. The mathematical model has 1 ODEs and 17 AEs containing 31 variables, out of which 1 are dependent differential variables, 17 are unknown algebraic variables, and 8 are constitutive variables calculated through the e-KT-UNIFAC model. The remaining 5 variables are 4 input specification variables of the initial moles and 1 reaction rate parameters.

 Table 4-19: Production of α -aminobutyric acid model analysis

Equations	Eq. number
ODE (1)	4-91
AE (17)	4-82 to 4-90 and 4-92 to 4-99
Variables and Parameters	
Initial condition (1)	$\zeta_1 = 0$
Extents of reactions	
Input specification (4)	$N_{AABA}^{0,\alpha}, N_{2OA}^{0,\alpha}, N_{BA}^{0,\alpha}, N_{BD}^{0,\alpha}$
Initial moles	
Reaction rate parameters (1)	k_1
Constitutive model parameters (8)	$\gamma_{AABA}^{\alpha}, \gamma_{AABA}^{\beta}, \gamma_{2OA}^{\alpha}, \gamma_{2OA}^{\beta},$
Activity coefficients	$\gamma_{BA}^{\alpha}, \gamma_{BA}^{\beta}, \gamma_{BD}^{\alpha}, \gamma_{BD}^{\beta}$
Unknown variables (17)	
- Partition coefficients (4)	$P_{AABA}, P_{2OA}, P_{BA}, P_{BD}$
- Reaction and mass transfer rates (1)	R_1
- Moles and concentrations (8)	$x_{AABA}^{\alpha}, x_{AABA}^{\beta}, x_{2OA}^{\alpha}, x_{2OA}^{\beta},$ $x_{BA}^{\alpha}, x_{BA}^{\beta}, x_{BD}^{\alpha}, x_{BD}^{\beta}$
- Extents of equilibrium reactions and instantaneous transfer (4)	$\zeta_{AABA}^{\alpha}, \zeta_{2OA}^{\alpha}, \zeta_{BA}^{\alpha}, \zeta_{BD}^{\alpha}$

4.3 COMPUTATIONAL ALGORITHM

ICAS-MoT (Integrated Computer Aided System – Modelling Testbed)[125,126] software has been used for constructing, analysing, and solving the mathematical model. The parameter regression was done by minimizing the objective function, as shown in equation 4-100.

$$Obj = \sum_i w_i \left(1 - \frac{Y_i}{Y_{i,exp}} \right)^2 \quad 4-100$$

where *Obj* is the objective function, w_i is the weight factor of the data point, Y_i and $Y_{i,exp}$ are the calculated and experimental values. Successive quadratic programming (SQP) method, available within ICAS-MoT, has been used for the parameters regression. The backward differential formula (BDF) method, also available in ICAS-MoT, has been used to solve the process model equation set comprising of ordinary differential and algebraic equations.

The constructed models combine the differential-algebraic equations contain the implicit algebraic equations within the differential equations. This section presents the algorithms required to solve the biphasic reaction system models. Figure 4-11 shows the computational algorithm for solving the differential algebraic equations of the biphasic reaction systems.

- Step 1: Specify known variables and parameters
- Step 2: Initialise dissociated species if presented
- Step 3: Initialise extent of reaction and time
- Step 4: Specify length of time needed to be calculated
 - Step 4.1: Solve equilibrium and balance equations implicitly
 - Step 4.2: Solve different equations,
 - Step 4.3: Adjust extent of reaction and time for the next time step
- Step 5: Check if the time is lower than the specified length of time
 - Yes: Redo step 4.1 to 4.3
 - No: Terminate the calculation

For example, the epoxidation process model (equations 4-33 to 4-51) is solved following the algorithm by:

1. Specifying the initial amount of the involved chemical species: epoxide, hydrogen-peroxide, catalysed acid, peracid, oleic, linoleic, and cleavage $\left(N_{EPOX}^0, N_{H_2O_2}^0, N_{RCOOH}^{\beta,0}, N_{RCOOH}^{\beta,0}, N_{Ole}^0, N_{Lino}^0, \text{ and } N_{Clev}^0 \right)$ and specifying the operating temperature (T).
2. There are no dissociated species, skip the step

3. Setting extents of reactions ($\xi_1^\beta, \xi_2^\beta, \xi^\alpha, \xi_{RCOOH},$ and ξ_{RCOOH}^α) are all 0 at the zeroth time step and initial time step is $t = 0$
4. Specifying t_{End} as the length of time needed
 - a. Solving equations 4-33 and 4-34 for partition coefficients, then solving equations 4-37 to 4-39 and 4-43 to 4-51 implicitly altogether for the pseudo-equilibrium of the time step.
 - b. Solving differential equations 4-41 and 4-42 for new extents of reaction (ξ_{Cal})
 - c. Adjusting time $t = t + \Delta t$ and $\xi = \xi_{Cal}$
5. Continuing step 4a to 4c until $t > t_{End}$

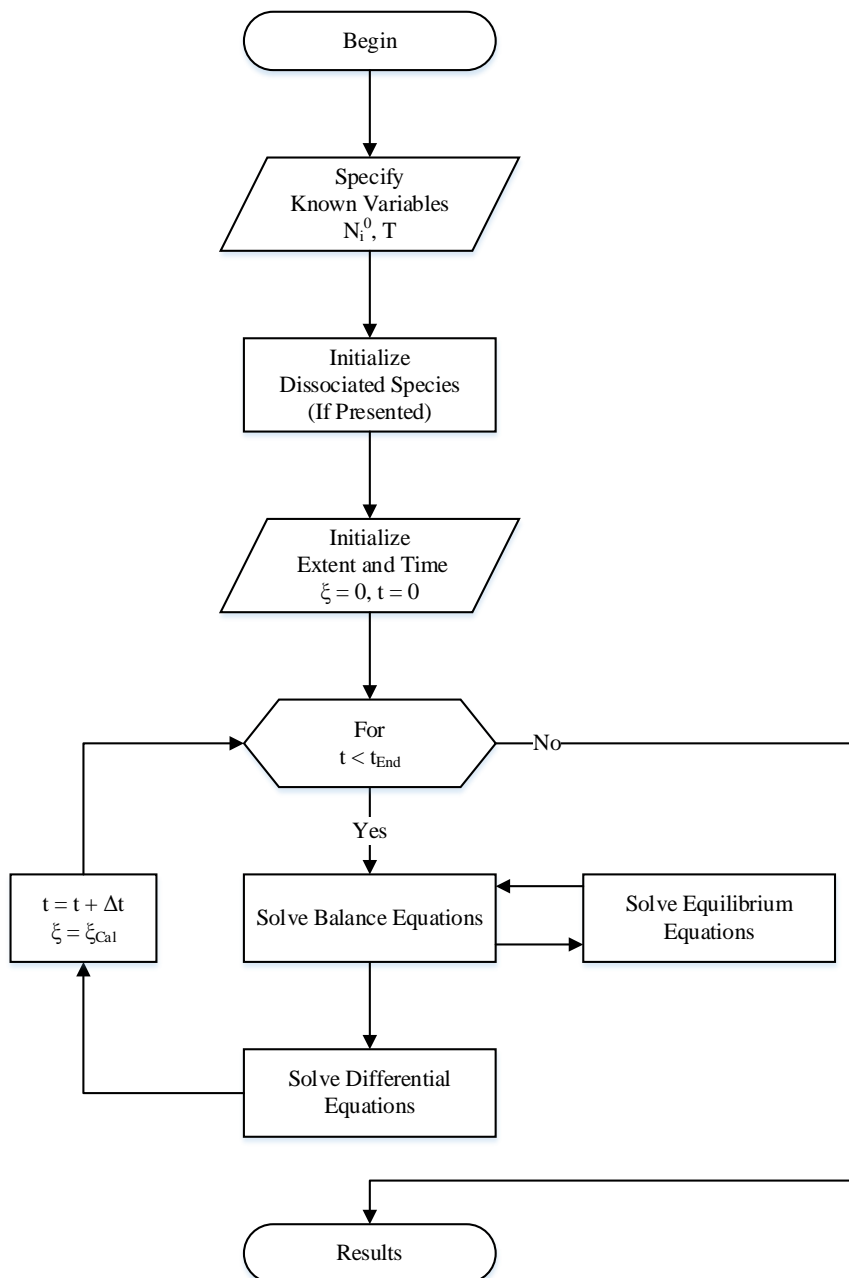


Figure 4-11: Algorithm for solving the models of the biphasic reaction systems

MODEL-AIDED DESIGN AND ANALYSIS

In the previous chapter, the models for distinct biphasic reaction systems have been formulated. The constructed models have to be validated. As well as, the rates related parameters have to be regressed for further design and analysis of the systems.

This chapter dedicates to the parameters regressions and the models validations. Depending on the design targets, the models are also employed for the analysis and/or design of the corresponding systems.

In sections 5.1 and 5.2, primarily, the reactor models are validated. Then, the applications of the pseudo-PTC and PTC systems models for the design and analysis based on the design targets are presented. Moreover, the benefits of the newly implemented and developed thermodynamic models are also demonstrated through these examples.

Sections 5.3 to 5.5 present the validation and application of the models for epoxide, furan derivatives, and α -aminobutyric acid productions processes. These processes contain different sets of chemical species, reaction pathways, and design targets. These sections justify the usefulness of the framework, which is developed diverse cases of biphasic reaction systems.

5.1 PTC I, BENZOIN CONDENSATION

In this section, the applications of the constructed models are described in detail. In section 5.1.1 the benzoin condensation model from section 4.2.1 is combined with the eNRTL models to follow the benzoin condensation process with various initial conditions.

5.1.1 PTC with Correlative Thermodynamic Models

In this case study, a pseudo-PTC reaction model is combined with NRTL/eNRTL the thermodynamic models for the prediction of benzoin condensation process behaviour. The objective is to check the applicability of the NRTL and eNRTL models.

For the benzoin condensation process case study, there are 12 sets of measured data with various initial conditions collected from literature [19]. One of the sets is selected for the parameter regression for the rate of reaction (k_4) from equation 4-10. The regressed value is $1.28 \times 10^4 \text{ cm}^3/\text{s} \cdot \text{mol}$, Figure 5-1 shows an acceptable fitting between the measured conversion of benzaldehyde and calculated value from the model.

The regressed parameter is used to determine the effect of the initial amounts of benzaldehyde, salt, and PTC needed for the known rate of reaction. As shown in Figure 5-2 over wide ranges of initial amounts of PTC, salt and reactant, the deviations of estimated conversion of benzaldehyde are less than 10% from measured data. The data used and calculated values of Figure 5-2 are given in Table S - I in the appendix.

Thus, the combination of NRTL and eNRTL are used to predict the PTC system behaviour with regression of a minimum of available experimental data for the specific rate of each reaction.

5.1.2 Summary

This case has been developed to verify the thermodynamic framework of Piccolo et al. [61]. The comparison in Figure 5-2 with various initial condition confirm the applicability of it.

However, the implemented thermodynamic (NRTL/ eNRTL) models for activity and partition coefficients calculation require measured data to regress the interaction parameters of active and inactive PTCs in both aqueous and organic phases. Therefore, 4 sets of data with minimum 2 data points per set are required for one computable system.

Although this model gives most accurate calculation, it is not possible of getting improved design without experimental work. Consequently, the partially predictive and predictive models are implemented in the following cases for improving the predictability range of the framework.

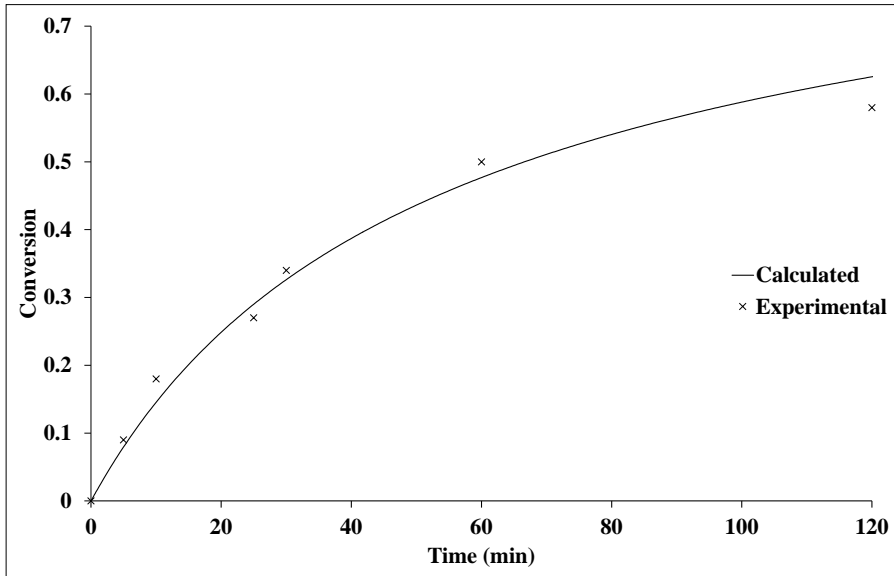


Figure 5-1: Conversion of benzaldehyde to benzoin, comparison between the measured data and the calculated value from the model

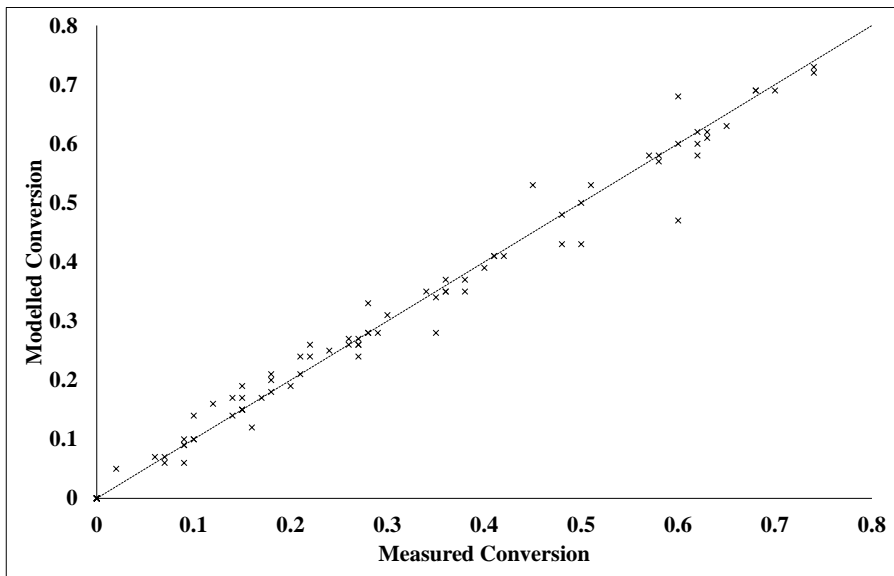


Figure 5-2: Conversion rate of benzaldehyde to benzoin at various initial conditions, comparison between the model prediction and the measured data

5.2 PTC II, CHLORINATION OF ORGANOBROMINE

There are 4 different design targets for the chlorination of butyl-bromide to butyl-chloride.

1. Maximising the organochloride production
2. Minimising the impurities
3. Accelerating the overall reaction rate
4. Optimising the fed-PTC amount

The reactor models are combined with SAC and e-KT-UNIFAC models to obtain a predictive capability and applicability toward design and analysis of the system.

5.2.1 PTC with SAC Models

First, this example is used to check the applicability of the SAC model. Different equation sets from chapter 4, section 4.2.2 are combined with the SAC models (NRTL-SAC and eNRTL-SAC) and employed for the design of the reaction system with different specified process design targets. All calculations use the same initial feed, operating condition, and reactor volume, which are given in Table 5-1.

Table 5-1: Initial condition of organobromine chlorination process

	Value
Temperature (K)	298.15
Initial mass of reactive species (m_i^0 – kg)	
<i>Butyl-Bromide</i>	50
<i>Na⁺Cl⁻</i>	100
<i>Na⁺Br⁻</i>	0
<i>QBr</i>	2
<i>QCl</i>	0
Initial mass of products, <i>Butyl-Chloride</i>	0
Solvents (Volume, dm³)	
Water	1000
Solvent	1000

In next sub-sections, the selections of the models for different design targets are demonstrated. The SAC models have a limitation in the predictability range, they can only be used with the parameterised chemical species. The SAC-segment parameters PTC the solvent are abundantly available in many open literatures [85,86,88]. On the other hand, the segment parameters of the PTC species are inadequately available. The parameters have been regressed from the measured data in chapter 4, section 4.1.1, and the tetraalkylammonium PTC systems with available parameters are reported in Table 5-2.

Table 5-2: The PTC systems with available parameters

PTC		Aqueous Phase	Organic Phase
Cation	Anion	(eNRTL-SAC)	(NRTL-SAC)
$(CH_3)_4N^+$	Br^-	Y	Y*
	Cl^-	Y	Y*
	I^-	Y*	Y
	OH^-	Y*	
	Ac^-	Y*	
$(C_2H_5)_4N^+$	Br^-	Y	Y*
	Cl^-	Y	Y*
	I^-	Y	Y
	OH^-	Y*	
	Ac^-	Y*	
$(C_3H_7)_4N^+$	Br^-	Y	Y*
	Cl^-	Y	
	I^-	Y*	Y
	OH^-	Y*	
	Ac^-	Y*	
$(C_4H_9)_4N^+$	Br^-	Y	Y
	Cl^-	Y	Y
	I^-		Y*
$C_{11}H_{17}NO^+$	Br^-	Y	
	Cl^-	Y	
$C_5H_{14}NO^+$	Br^-	Y	
	Cl^-	Y	
$C_6H_5(CH_3)_4N^+$	Br^-	Y	
	Cl^-	Y	
$C_8H_{21}NO_5^+$	Br^-	Y	

*Low-quality parameters fitted from inadequate numbers of data points

5.2.1.1 Maximising Product

To maximise the amount of the product (C_4H_9Cl) as the specified design target, equilibrium equations set (equations 4-17 to 4-21, 4-22a, and 4-23 to 4-32) is used to predict the maximum amount of the product in the reaction system.

The reactive systems with tetrabutylammonium ($(C_4H_9)_4NBr$) as PTC with 6 different solvents are studied. The results of calculations are shown in Figure 5-3. Among the 6 solvents studied, the reaction in toluene is found to give the highest conversion (73.4%) of the raw material, which is more than 2.5 times higher than the least conversion (27.5%) obtained for reaction with cyclohexane as solvent.

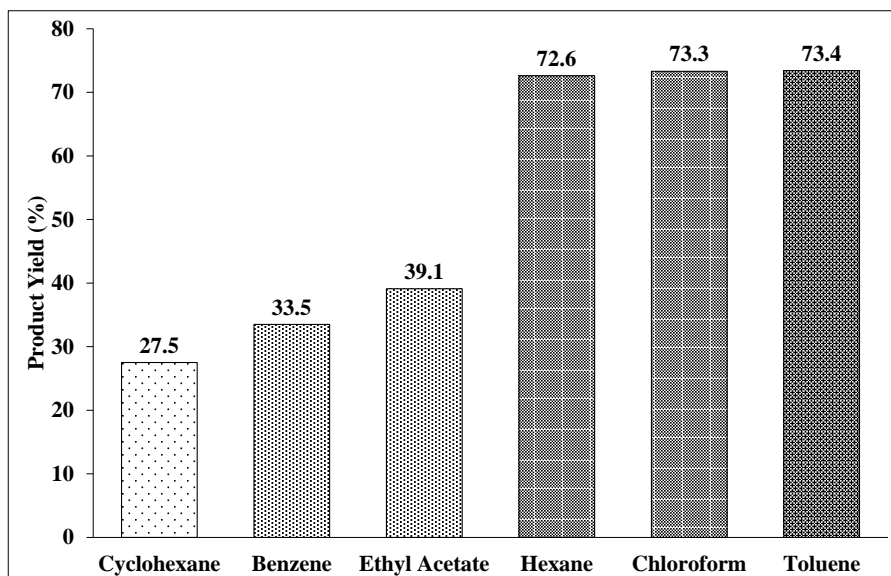


Figure 5-3: Maximum possible conversion of the reaction system with tetrabutylammonium PTC in different solvents

Reactions with hexane, chloroform, and toluene as organic solvents give almost similar conversions (around 70%), while reaction with benzene and ethyl acetate yield less than 40% conversion. However, before chloroform is also considered as an alternative, experimental validation of its side effect to the reaction mechanism is necessary because its structure is close to that of the product.

5.2.1.2 Minimising Impurities

The objective of this example is to minimise the impurity species that remains with the product. The conversion equations set (equations 4-17 to 4-21, 4-22b, and 4-23 to 4-32) is used to estimate the amount of the remaining impurities with the product in the organic phase at different stages of the reaction. This is not only easing the separation step but also preventing the loss of valuable PTC. The amount of the impurities that leave the reactor with the main product varies with the type of solvents and PTCs used. Based on the results in the previous section where reactions with hexane and toluene yielded similarly high conversions, 2 PTCs (tetraethylammonium, $(C_2H_5)_4N^+$ and tetrabutylammonium, $(C_4H_9)_4N^+$) and 2 solvents (hexane and toluene) are selected for this study.

Reactions with tetraethylammonium ($(C_2H_5)_4N^+$) PTC, in both toluene and hexane give smaller impurities than the reaction with tetrabutylammonium ($(C_4H_9)_4N^+$) PTC at almost every conversion value. Moreover, as the reaction progresses, the amount of the impurities decrease. Although at the initial state, the impurities in toluene are higher than in hexane, the drop in impurities concentration is sharper with the advancement of the reaction, and gets lower at conversions around 0.7 (see Figure 5-4).

On the other hand, with tetrabutylammonium PTC in toluene, the amount of the impurities is almost as high as with tetraethylammonium. Here, as the reaction progresses, the impurities

remain high and gradually increase as the reaction progresses. Therefore, for minimising impurities as a design target, pairs of tetraethylammonium PTC with toluene or hexane as solvents are recommended as better alternatives.

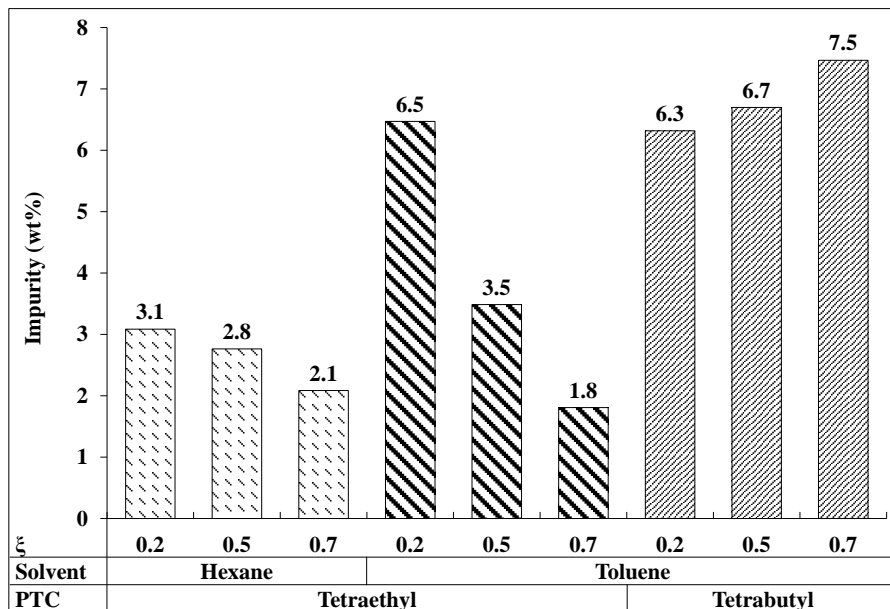


Figure 5-4: Impurities amount in organic phase at different conversion with two PTCs and two solvents

5.2.1.3 Accelerating the Overall Reaction Rate

The speed of the reaction is also a key design issue in reactive systems. In this context, the kinetic model equations set (equations 4-17 to 4-21, 4-22c-d, and 4-23 to 4-32) is used for the estimation of system half-life, equilibrium time, and actual apparent rate of the reactions in the reactive system.

With the same initial condition as in previous examples (see Table 5-1), 42 systems with pairs formed by 14 solvents and 3 PTCs are calculated. The detailed results of these calculations are given in the appendix (see Table S - II).

While the activity coefficients of active PTC in organic phase (γ_{QCl}^{β}) increases, half-lives of the system are also increasing. Similarly, the time that the system takes to reach equilibrium is also directly related to the activity coefficient of the active PTC in the organic phase. The equilibrium time is found to be around 2 orders of magnitude higher than half-life, meaning that it takes almost 2 hours for the reaction to move from half conversion to equilibrium stage (see Figure 5-5).

On the other hand, the apparent rate of reaction is inversely related to the activity coefficient of the active PTC in the organic phase - it decreases as the activity coefficient of the active PTC in the organic phase increases as shown in Figure 5-6.

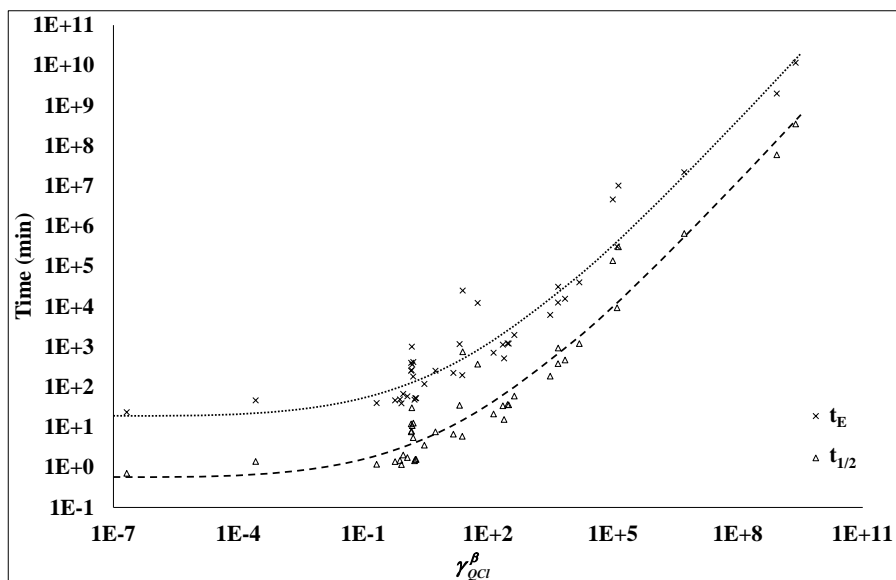


Figure 5-5: Relation between activity coefficient of active PTC organic phase (γ_{QCI}^{β}) and the reaction half-life ($t_{1/2}$) and equilibrium time (t_E) calculated from the kinetic model

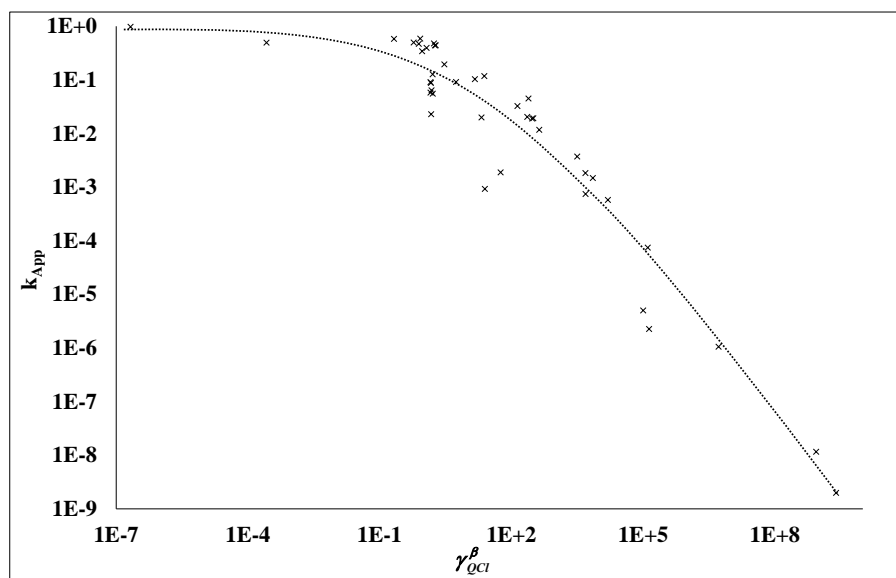


Figure 5-6: Relation between activity coefficient of active PTC organic phase (γ_{QCI}^{β}) and apparent rate of reaction (k_{App})

The simulated results show that the fastest reaction to reach equilibrium is the reaction with dichloromethane as a solvent and tetramethylammonium $((CH_3)_4N^+)$ as a PTC, while the slowest reaction is around 8 order of magnitude slower, is the reaction with the pair of hexane and tetramethylammonium as solvent and PTC, respectively. It is also worth mentioning that both systems use tetramethylammonium as the PTC and by changing only the solvent, it is possible to boost the rate of reaction by many orders of magnitude. Experimental verification is suggested to validate this significant result of pairing the PTC with an appropriate solvent.

5.2.1.4 Optimising the Fed-PTC Amount

In order to avoid loss or overuse of the valuable tetraalkylammonium PTC, optimisation of the fed amount of PTC is considered as one of the design targets. In the chlorination of organobromine system, it is preferable to have the active form of tetraalkylammonium chloride (QCl) in the organic phase.

To select the proper feed amount of the PTC, the kinetic model equation set is used. The rate is calculated by varying the concentration of the fed PTC in the inactive form (Q^+Br^-). The PTC then partitions into 4 species (see Figure 4-7) of (1) active species in the aqueous phase (x_{QCl}^α), (2) active species in the organic phase (x_{QCl}^β), (3) inactive species in the aqueous phase (x_{QBr}^α), and (4) inactive species in the organic phases (x_{QBr}^β). Mole fraction of each species of PTC are recorded, as shown in Figure 5-7.

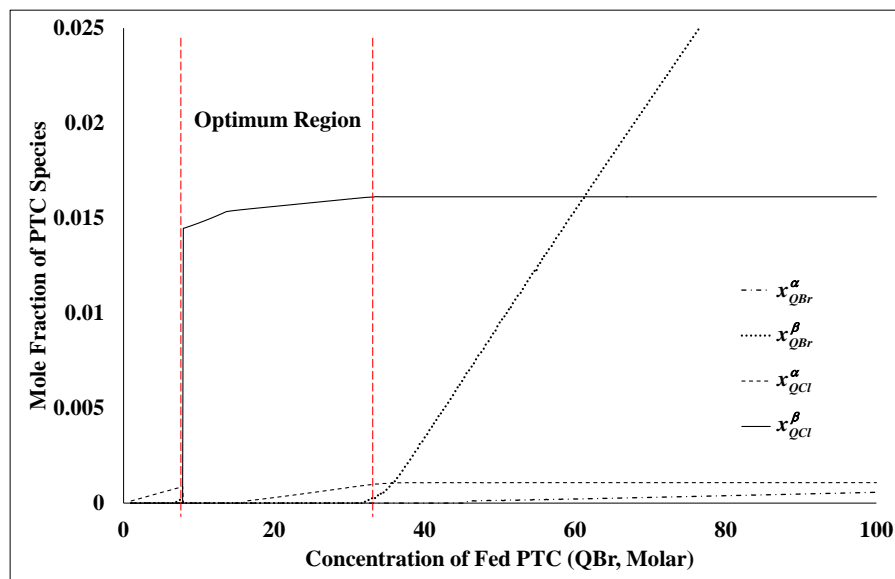


Figure 5-7: Relationship between amounts of PTC fed and the distribution of its into each form in both phases calculated by the kinetic model

Below the optimum feed region (less than 9 molar of PTC fed), though the PTC is converted to active species (QCl), it stays in the aqueous phase (x_{QCl}^α), causing slow organic phase

reaction. At the optimum feed region (between 9 and 32 molar of fed PTC) of the fed PTC concentration, the fed PTC is converted to the wanted active PTC species in the organic phase (x_{QCl}^{β}), thereby allowing and accelerating the reaction. On the contrary, above optimum region, the PTC accumulates as inactive species in the organic phase (x_{QBr}^{β}). The accumulation of the inactive PTC species leads to an unfavourable shift of equilibrium toward reactant side, slowing the rate of product creation, and losing of the valuable catalyst.

5.2.2 PTC with e-KT-UNIFAC

The combination of SAC thermodynamic model with different types of reactor models is studied in section 5.2.1. The SACs combination, however, has limited predictive capability in terms of selection of solvents. Although for systems with available data, accurate predictions are possible, they do not allow the creation of novel PTC or solvents. They are therefore good for verification purposes, while, the newly developed e-KT-UNIFAC, which is based on the group contribution method, is good for synthesis-design objectives.

With group contribution method, a new PTC-related group (N^+) is defined, structural parameters (R and Q) are calculated, and interaction parameters between old KT-UNIFAC groups, ions groups, and the newly defined group are regressed from the experimental data of PTCs that contain between 4 to 16 carbon atoms. Therefore, 98 distinct PTC cations with 4 to 16 carbon atoms attached are created, the detailed group configurations are given in the appendix (see Table S - III). The e-KT-UNIFAC model has the capability to predict the behaviour of the PTC in both aqueous and organic phases.

With the objective to maximise the product yield as the design target, the chlorination of organobromine process is re-designed with the aid of combined equilibrium reactive model and e-KT-UNIFAC thermodynamic model, to demonstrate the predictive capability of the model. 6 solvents, the same as the one used in section 5.2.1, are also studied here. In total, 588 pairs of solvent-PTC reactive systems have been considered.

The detailed results of the calculated conversions of the raw material in the different reaction systems are given in the appendix (Table S - IV). The calculated conversions range from 21% to 99%, the pair with 12 carbon atoms in the PTC and hexane as the solvent. The maximum, minimum and average conversions obtained with different atoms in PTC and hexane as the solvent are shown in Figure 5-8. The maximum, minimum and average conversions for different solvents and a fixed PTC are shown in Figure 5-9. The average conversions increase with the number of attached carbon atoms from 4 to 12 atoms and then decrease from 12 to 16 atoms.

The highest conversion of 98.87% is achieved with hexane as the solvent and the configuration number 4 of the 12 carbon atoms PTC. The PTC cation contains an ammonium (N^+), group, 6 CH_3 groups, 5 CH_2 groups, and 1 C group. The lowest conversion of 20.95% comes from the system that uses cyclohexane as the solvent and 16 carbon atoms PTC.

Also, comparing the calculated conversions with the e-KT-UNIFAC model with those reported with the SAC model (in section 5.2.1.1), it is seen that the two models give very similar results, indicating that both models cross verify each other (see Table 5-3).

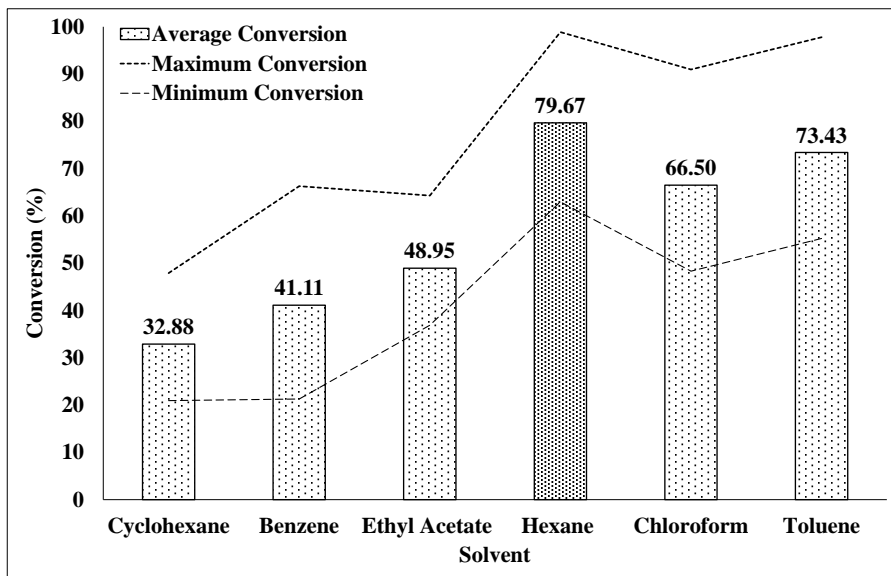


Figure 5-8: Maximum, minimum, and average conversion achieved from the reaction system by different configuration of tetraalkylammonium PTCs

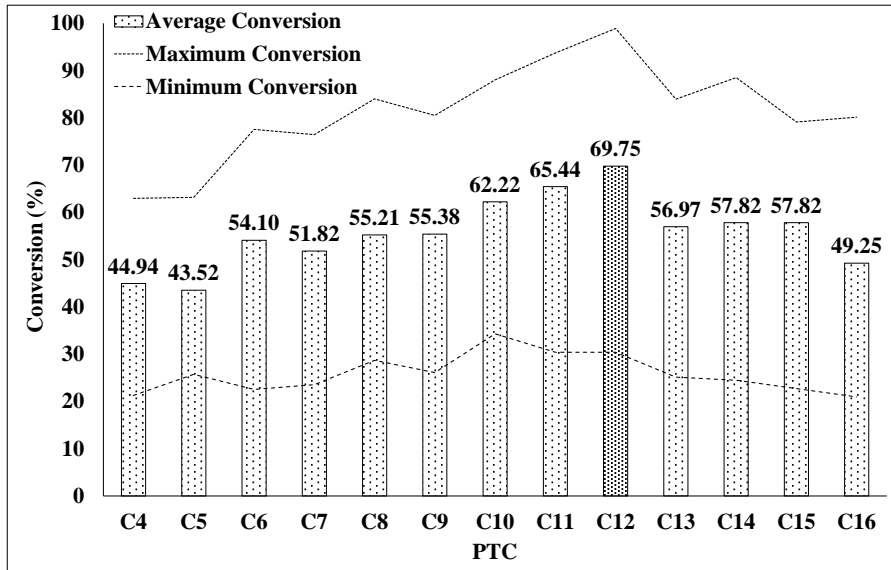


Figure 5-9: Maximum, minimum, and average conversion achieved from the reaction system using different solvents

Table 5-3: Comparison of conversions calculated with the SAC and e-KT-UNIFAC models

Solvent	Conversion calculated by	
	SAC models	e-KT-UNIFAC model
Cyclohexane	27.52	27.51
Benzene	33.47	32.23
Ethyl Acetate	39.10	40.66
Hexane	72.65	71.85
Chloroform	73.33	71.41
Toluene	73.41	74.56

5.2.3 Summary

The implementations of partially predictive SAC models and the predictive e-KT-UNIFAC model help broadening the range of applicability of the framework.

The SAC models implementation allow calculating of the overall reaction rate and the partitions of heterogeneous chemical species in the known solvents. Prior to the design and analysis, segment number parameters of involved PTCs need to be established. Then, the combined reaction-partition models have been applied to calculate the maximum conversion, the amount of impurities, the overall reaction rate, and the optimum fed-PTC amount of the reactions in any known solvents. Moreover, this case also demonstrates the flexibility of the framework for constructing different types of model to accommodate different design targets.

Nevertheless, this SAC implementation still lacks the potential to assemble a novel PTC ion. Subsequently, the implementation of the predictive e-KT-UNIFAC model eliminates this restriction. A better design of the system has been achieved through the combination of novel PTC ion and known solvent. Although only 4 to 16 carbon atom of tetraalkyl ammonium PTCs are feasible, the improvement of 20% conversion has been accomplished.

The improved and innovative designs have been obtained through different combination of reaction and partition models. Although the designs should be confirm experimentally, the extent of experiment is tremendously reduced.

5.3 EPOXIDATION OF UNSATURATED LONG CHAIN FATTY ACID

In this example, the epoxidation reaction model in section 4.2.3 is combined with e-KT-UNIFAC thermodynamic models for the prediction of the epoxidation process behaviour. The design targets of this example are to increase the rate of production of epoxide compounds and inhibiting the side reactions.

5.3.1 Model Validation

In a report by Gan et al. [58] there were available 176 measured data points of the time-dependent production of epoxide compounds from palm oil, using either formic or acetic acid catalyst in the batch reactor. The reaction data were measured at 25 °C, 40 °C, 60 °C, and 80 °C. In one case, the organic phase was the palm oil (self-solvated), in another, the oil was dissolved in added benzene. Thus, there are data for 16 reaction conditions in total. Though not necessary, all the data has been used for regression; the partition coefficients are calculated from the predicted activity coefficient from e-KT-UNIFAC model; the regressed kinetic parameters are shown in Table 5-4.

Table 5-4: Regressed reaction parameters from experimental data [58]

Parameter	Unit	Value
A_1	$\text{dm}^3 \cdot \text{mol}^{-1} \cdot \text{s}^{-1}$	108.157
A_2	$\text{dm}^3 \cdot \text{mol}^{-1} \cdot \text{s}^{-1}$	152.632
E_{a1}	$\text{kJ} \cdot \text{mol}^{-1}$	22.991
E_{a2}	$\text{kJ} \cdot \text{mol}^{-1}$	38.428

The graphical comparisons between collected experimental data and model calculations are shown in Figures 5-10 and 5-11. These parameters fitted all the data with average absolute deviation of 0.61% for the formic acid catalyst and 1.31% for the acetic acid catalyst. Given the uncertainties of the data, the comparisons in the figures show good agreement between model prediction and measurement.

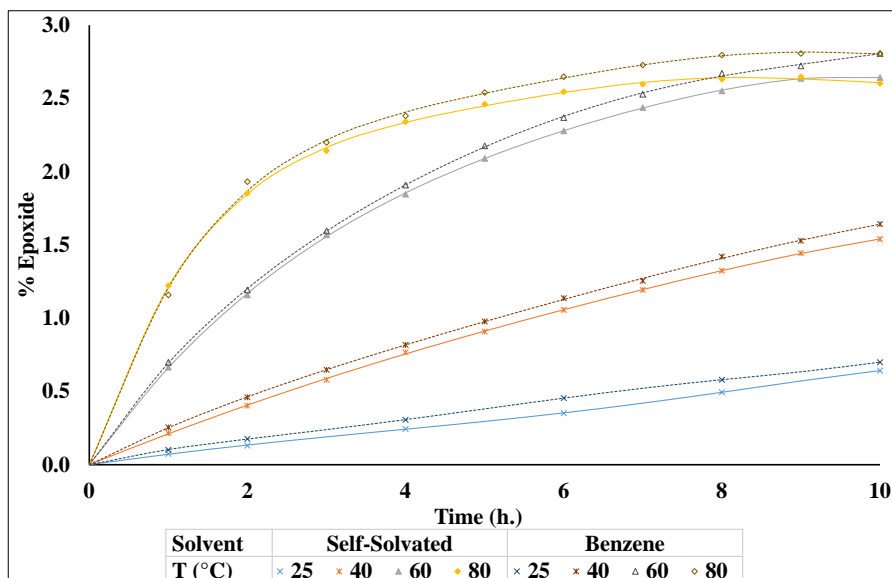


Figure 5-10: Production of epoxide compound, the comparison between measured data [58] and model prediction, a reaction catalysed by formic acid

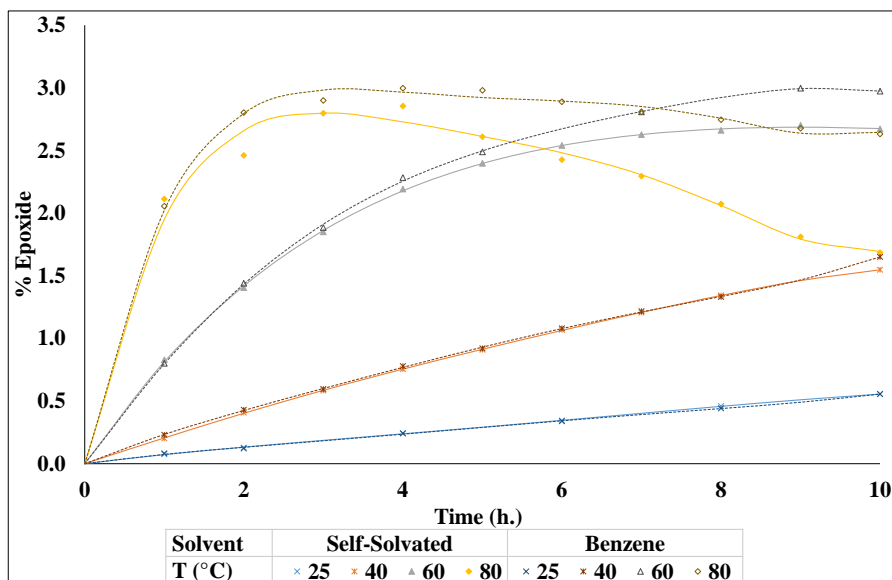


Figure 5-11: Production of epoxide compound, the comparison between measured data [58] and model prediction, a reaction catalysed by acetic acid

5.3.2 Model Applications

To obtain the better design of the process, the formation of side product is limited by inhibiting the partition of water or the catalysing acid into the organic phase. Whereas, the reaction rate is accelerated by increasing the partition of peracid into the organic phase. Multiple design targets can be achieved altogether by properly selecting or designing a novel solvent.

The mathematical model of section 4.2.3 with the regressed parameters of section 5.3.1 are used to obtain a better system design by estimating the effects of changing solvent, temperature, and initial concentration. In the present case, limitation of side-product formation can be accomplished by manipulating the partition coefficients (P_{RCOOH} and P_{RCOOOH}) and water concentration in the organic phase (C_w^β) for inhibiting the partitioning of water and catalysing acid into the organic phase. Also, the reaction rate can be increased with greater partitioning of peracid into the organic phase. These concepts suggest that careful organic solvent selection can significantly improve the effectiveness of this biphasic reacting system.

5.3.2.1 Solvents Selection

To examine the effect of changing the organic solvents, molecular structures of solvents with desirable properties are generated, screened, and selected by ICAS-ProCAMD [126,127] using group-contribution methods for the desired properties. The following solvent screening criteria are used: (1) raw material and product must be highly soluble in the organic solvent; (2) the solvent is effectively immiscible with water; (3) the solvent is liquid at the operating temperature; (4) the solvent structure is acyclic, cyclic, or aromatic, with functional groups of alkyl, aldehyde, ketone, ether, or ester. The screening results are given in Table 5-5. In total, 7167 solvents were generated from criterion (4). Of these, 3109 solvents passed the other screening criteria, with information about 104 solvents existing in the software database.

The solubilities of water into the organic phase are used for ranking and selecting the solvents for detailed calculation. The nine solvents with the lowest predicted solubility of water, as given in Table 5-6 were chosen for detailed calculations.

Table 5-5: Result of epoxide process solvent screening

	Acyclic	Aromatic	Cyclic	Total
Generate	3519	545	3103	7167
Screened Out By				
Boiling and Melting Point	697	98	458	1253
No Interaction Parameters	1438	101	1246	2785
Miscibility with Water	20	0	0	20
Results				
Screened Solvents	1364	346	1399	3109
In Database	75	18	11	104

Table 5-6: Selected solvent for detail calculation based on water solubility

Solvent	Boiling Temperature (K)	Melting Temperature (K)	Predicted Water Solubility
METHYLHEXANE	367.49	154.54	7.85E-04
n-HEPTANE	379.07	175.55	7.87E-04
TRIMETHYLPENTANE	374.73	124.96	8.48E-04
DIMETHYLHEXANE	385.92	152.14	8.50E-04
METHYLHEPTANE	396.54	173.6	8.52E-04
n-OCTANE	406.63	191.33	8.54E-04
ETHYLHEXANAL	447.31	228.13	0.0116
Octanal	447.15	246	0.0116
DI-sec-BUTYL-ETHER	394.2	173.15	0.0122
METHYLHEXANAL	415.15	230	0.0134

5.3.2.2 Detail Calculations

The biphasic reactor model is used to improve the design by analysing the solubility of water and the partitioning of the catalysing acid and peracid into the organic phase. Since water and the catalysing acid enhance the side reaction, their concentration should be minimized in the organic phase. Further, since the peracid enhances the rate of the epoxide production, so its concentration should be maximized in the organic phase.

Figure 5-12 shows the solubility of water (bars) and the partitioning of formic acid and performic acid (square symbols) and acetic acid and peracetic acid (round symbols) into the organic phases formed from various solvents. The predicted equilibrium mole fractions of water in the selected solvents are very small (not registered in the figure); while those found in the conventional solvent, benzene, is 0.0033 and in the palm oil, without additional solvent, is 0.012. Therefore, the side reaction should be lowered by choosing other solvents. On the other hand, the partitioning of acid and peracid are barely affected by solvent change, though it is worth noting that acetic acid and peracetic acid always have higher partitioning into the organic phase than does formic acid and performic acid.

Detailed reaction calculations at 80 °C with acetic and formic acid catalysts are shown in Figures 5-13 and 5-14 for all of the selected solvents together with benzene and the self-solvated palm oil organic phases. Results for only one alkyl solvent are given because all others appear to be identical.

The figures show that the apparent reaction rates are higher for the aldehyde solvents (octanal and 2-methylhexanal) compared with benzene and the palm oil (self-solvated) organic phase, but with alkyl solvents the rates are much slower. Further, rates with acetic acid catalyst are always higher than those with formic acid in the same solvent. Notably, no side reaction was found for the formic acid catalyst.

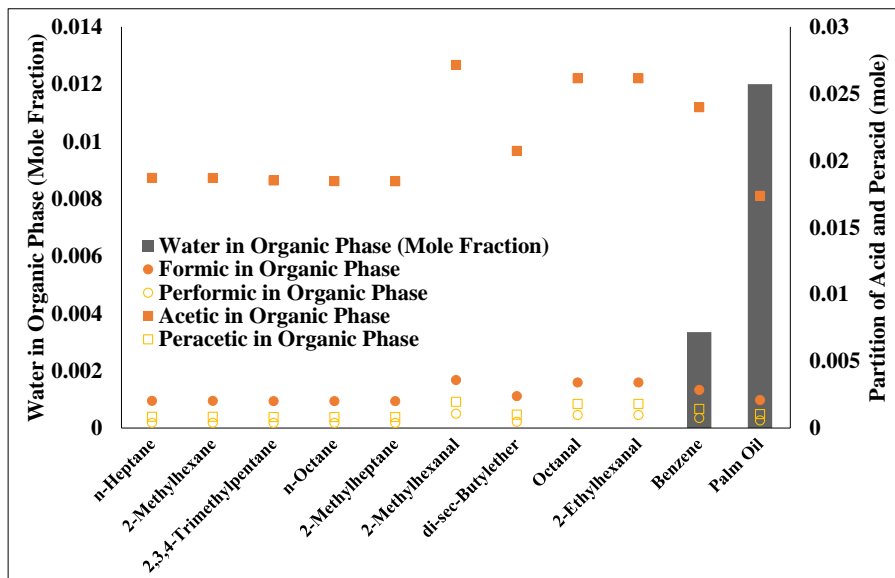


Figure 5-12: Solubility of water and partitions of acid and peracid into organic phase with different solvents

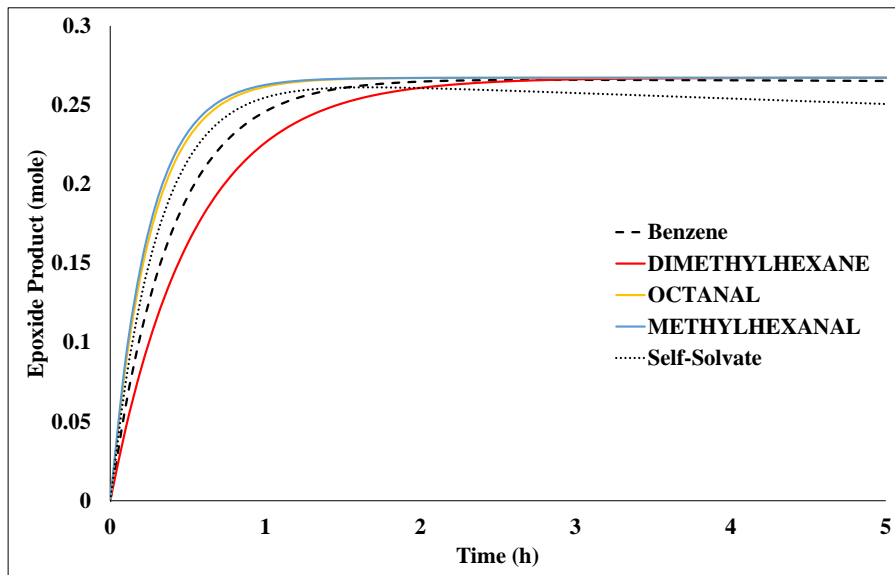


Figure 5-13: Production of epoxide at 80 °C catalysed by formic acid

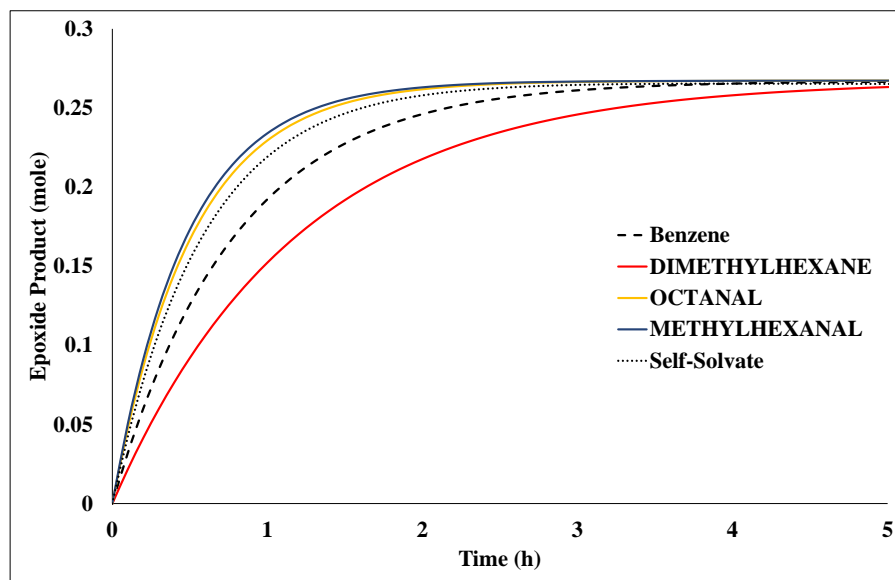


Figure 5-14: Production of epoxide at 80 °C catalysed by acetic acid

Figure 5-15 shows the rates of epoxide formation in the solvents of Figures 5-13 and 5-14. The aldehyde solvents (octanal and methylhexanal) have a higher rate of production with both formic and acetic acid catalysts. Thus, reaction with methylhexanal solvent and acetic acid catalyst goes 28% faster than with the conventional benzene solvent, and 10% faster than palm oil (self-solvated) with no added organic solvent. An added benefit is that no side reaction occurs.

From this study, it can be concluded that aldehyde solvents, together with acetic acid, should be considered as an outstanding operating choice for a maximum rate of epoxide production and minimum amount of unwanted epoxide cleavage. The next step would be experimental studies to determine the reliability of this modelling work

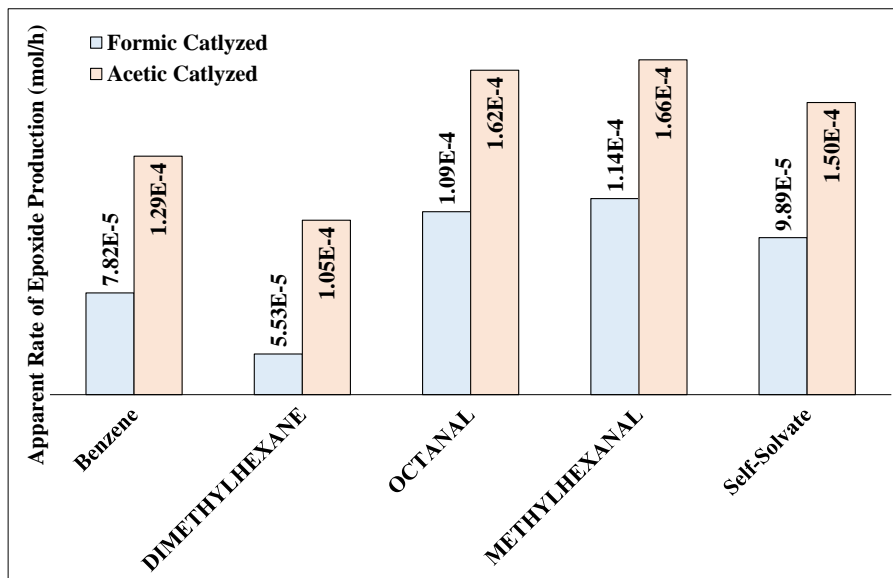


Figure 5-15: Apparent rate of reaction in different solvent

5.3.3 Summary

This case demonstrates a broad range of the framework applicability. The epoxidation process has reaction scheme similar to those of the PTC systems (see also Figure 4-6, 4-7, and 4-8), with a completely different set of chemical species. Moreover, effect of the temperature is also presented in the measured data.

The constructed model matches requires only 4 regressed temperature dependent parameters to match with the data measured with the reaction in 2 different organic solvents, 2 different heterogeneous species, and 16 reaction conditions.

The novel design, achieved through the model, reaches both design targets altogether. Not only is the reaction rate is accelerated, but the amount of impurities and unwanted side products are also minimised to trace amount.

5.4 PRODUCTION OF FURAN DERIVATIVES FROM BIOMASS

In this example, the furan derivatives reaction model in section 4.2.4 is combined with e-KT-UNIFAC thermodynamic models for the prediction of the process behaviour. The design targets of this example are

1. Increasing the rates of production of HMF and furfural
2. Increasing the partition of the products into the organic phase
3. Preventing the formation of the unwanted side product
4. Preventing the partition of the unwanted side product into the organic phase

5.4.1 Model Validation

There are 56 measured data of time-dependent production for eight different reaction scenarios in batch reactor reported by Ordonsky et al. [49]. These were measured at only a single temperature, 298.15 K. The systems were pure water and biphasic mixtures containing water and three different organic solvents: 2-Methyltetrahydrofuran (MTHF), cyclohexane, and n-butanol. Again, all the data has been used in the regression, though that would not be necessary. The parameters are given in Table 5-7. Graphical comparisons of data and model calculations for raw material conversion and furan derivative production are shown in Figures 5-16 and 5-17.

The average absolute deviation of the calculated values for raw material conversion is 4.36%; while the deviation for furan derivative production is 4.21%. Given the expected uncertainties of the data, these results suggest the validity of the model with its assumptions and regressed parameters. In particular, it seems that reaction rate constants and mass transfer coefficients can be assumed equal with different organic solvents so that changing the solvent only affects partitioning of heterogeneous species. This effect is taken into account by prediction, not regression. The next section examines the effect of varying the solvent to develop more effective processes

Table 5-7: Regressed reaction parameters for furan derivative production process from experimental data [49]

Parameter	Unit	Value
k_1	10^{-3} s^{-1}	3.23
k_2	10^{-3} s^{-1}	46.70
k_L	$\text{m} \cdot \text{s}^{-1}$	1.76

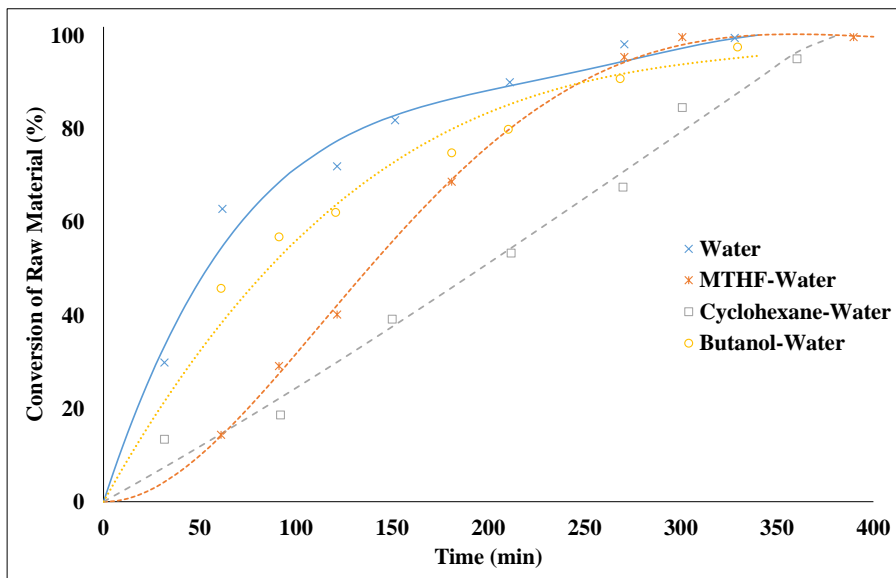


Figure 5-16: The rate of raw material conversion in 4 different reaction scenarios, the comparison between measured data [49] and model prediction

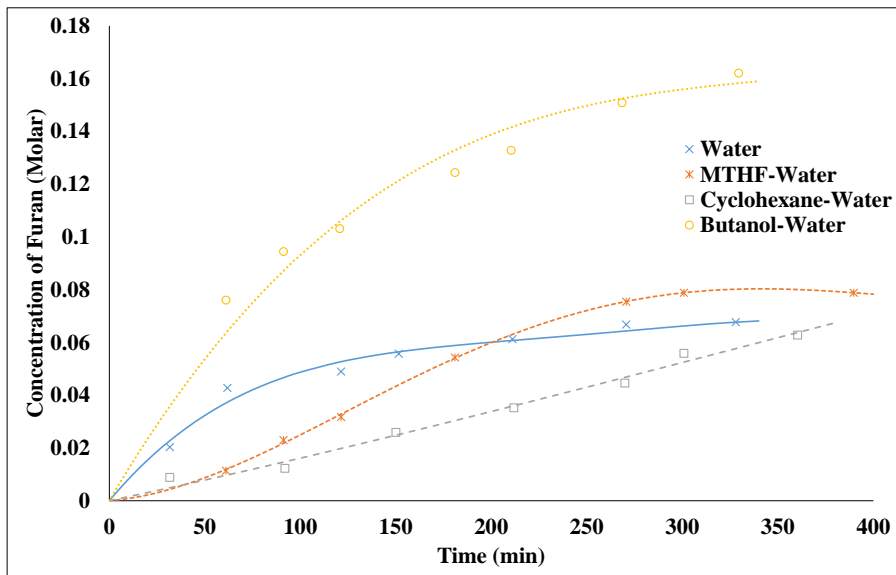


Figure 5-17: The rate of furan production in 4 different reaction scenarios, the comparison between measured data [49] and model prediction

5.4.2 Model Application

To obtain the better design of the process, the partitions of the main products (HMF and furfural) are essential. Not only they react and change into unwanted by-products, but they also inhibit the main reactions by themselves. Therefore, the desirable solvent should take as much HMF and furfural as possible, and at the same time, should not draw much by-products for the easier separation process. Multiple design targets can be achieved altogether by properly selecting or designing a novel solvent.

The model described in section 4.2.4 with the parameters established in section 5.4.1 is used to explore options for more effective reaction systems. Here, it is partitioning of HMF and furfural products that principally affects generation of unwanted species, as well as the ultimate production of desirable furan derivatives. Partitioning can be manipulated by changing the added solvent.

5.4.2.1 Solvent Selection

Prior to solvent selection, heterogeneous species and the best conventional solvent (n-butanol) are analysed for Hansen solubility parameters [128] using group contribution method based through the ICAS-ProPred software [126]. The predicted Hansen solubility parameters are shown in Table 5-8.

Table 5-8: Hansen solubility parameters of the analysed chemical species

Species	Hansen D	Hansen P	Hansen H
HMF	19.84	11.77	13.06
Furfural	18.29	11	6.7
Cyclopentanone	13.55	7.71	5.23

Two approaches for solvent selection are considered using the Hansen solubility parameters of Table 5-8. The sets of selection criteria are given in Table 5-9. One (I) finds solvents that have solubility parameter values close to those of the target products (HMF and furfural), while the other (II) finds solvents with values close to that of n-butanol. The first focuses on enhanced solubility of the products while the second recognizes from the measured data that reaction in n-butanol yields the highest amount of furan. Both criteria have the general stipulations of (1) the solvent is effectively immiscible with water, (2) the solvent is liquid at the operating temperature, (3) the solvent has acyclic or cyclic structure, and (4) the solvent contains alkyl, acid, alcohol, aldehyde, ketone, ether, or ester functional groups.

Table 5-9: Sets of criteria for solvents selection for production of furan derivative process

Criteria set (I)	Criteria set (II)
Common criteria	
<ul style="list-style-type: none"> - The solvents are immiscible with water - The solvents are liquid at the operating temperature - The solvents are acyclic or cyclic compounds - The solvents contain alkyls, acids, alcohols, aldehydes, ketones, ethers, or esters functional groups 	
Hansen solubility parameter related specific criteria	
- Hansen D: 17-21	- Hansen D: 13-16
- Hansen P: 10-13	- Hansen P: 5-8
- Hansen H: 6-14	- Hansen H: 12-15

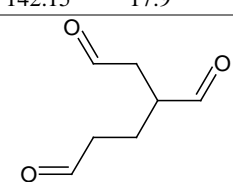
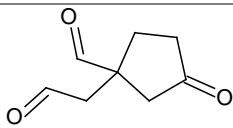
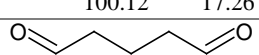
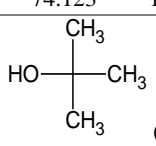
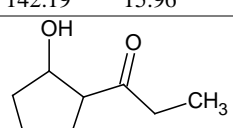
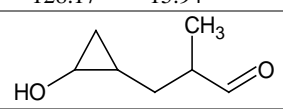
Table 5-10 lists the results from the screening step. A total of 8326 solvents met the general criteria, while 18 solvents passed criteria I and 191 solvents passed criteria II. Each set of criteria had a single known (available in the solvents database) solvent that passed the screening step, but all the rest are created by the molecular design method.

Three solvents (including that from experiment) from each criteria set are chosen, as shown in Table 5-11, for detailed calculation (the solvents found in the database are those that have the chemical name).

Table 5-10: Result of solvent screening for furan derivatives production process

Criteria Set	(I)			(II)		
	Acyclic	Cyclic	Total	Acyclic	Cyclic	Total
Generate	4497	3829	8326	4497	3829	8326
Screened Out By						
Hansen SolPar	4477	3817	8294	4393	3663	8056
Miscibility with Water	12	2	14	44	35	79
Results						
Screened Solvents	8	10	18	60	131	191

Table 5-11: Selected solvent for the furan derivatives production detailed calculation

Criteria Set	#	Chemical Formula	MW	Hansen D	Hansen P	Hansen H
		$C_7H_{10}O_3$	142.15	17.9	10.78	10.25
(I)	1					
		$C_8H_{10}O_3$	154.16	17.81	10.88	9.35
(I)	2					
		$C_5H_8O_2$	100.12	17.26	11.16	9.42
(I)	3	 (Pentanedial)				
		$C_4H_{10}O$	74.123	15.18	5.42	14.73
(II)	4	 (tert-Butanol)				
		$C_8H_{14}O_2$	142.19	15.96	6.78	12.75
(II)	5					
		$C_7H_{12}O_2$	128.17	15.94	8	14.41
(II)	6					

5.4.2.2 Miscibility Calculation

Since the selected solvents are mainly novel solvents, the phase splitting between the solvents and water are confirmed before applying for the detail calculation. ICAS simulation [126] has been applied for the miscibility calculations of all solvents.

Figures 5-18a and 5-18b display the predicted liquid-liquid equilibriums (LLE) between novel solvents 1-6 and water, the KT-UNIFAC thermodynamic model has been used for these calculations. Every selected solvents is immiscible with water at the operating temperature (298.15K) and above.

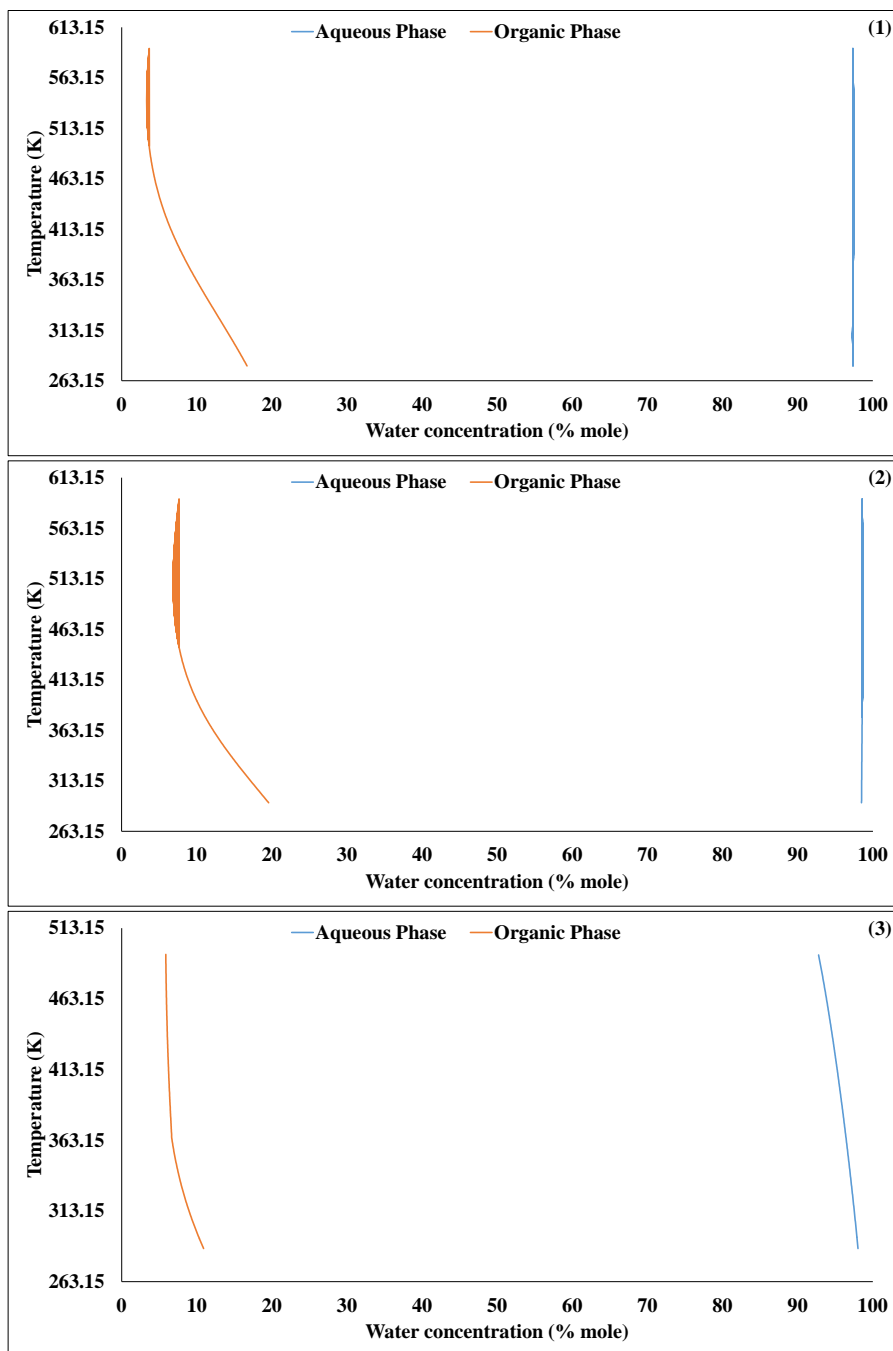


Figure 5-18a: LLE predictions between solvents (1), (2), (3) and water

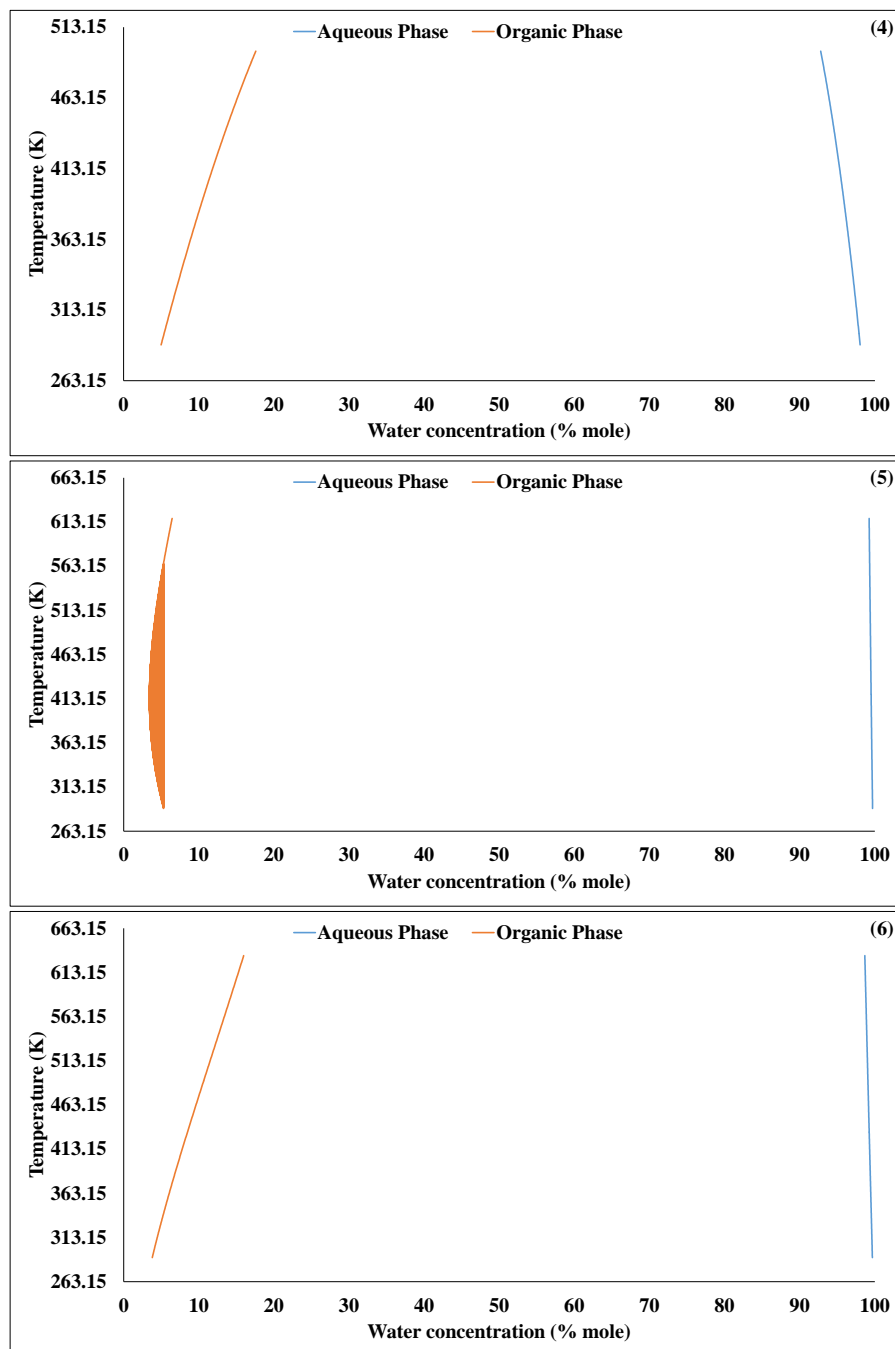


Figure 5-18b: LLE predictions between solvents (4), (5), (6) and water

5.4.2.3 Detail Calculation

The biphasic reactor model is used to improve the design by analysing the partitioning of the products (HMF and furfural) and waste into the organic phase. The favourable solvent should accumulate as much of the products (HMF and furfural) in the organic phase as possible. Further, waste (e.g., cyclopentanone) should be left in the aqueous phase for easiest separation.

Figure 5-19 displays the partitioning of products and waste (cyclopentanone) as calculated with the e-KT-UNIFAC model. Solvents 1-3, which are screened by criteria (I), have a higher partition of both products than the other solvents. On the other hand, solvents 4-6, screened by criteria (II), have lower or similar product partitioning to the conventional organic solvent (n-butanol), as expected. However, among all solvents, the partition of cyclopentanone is lowest in n-butanol.

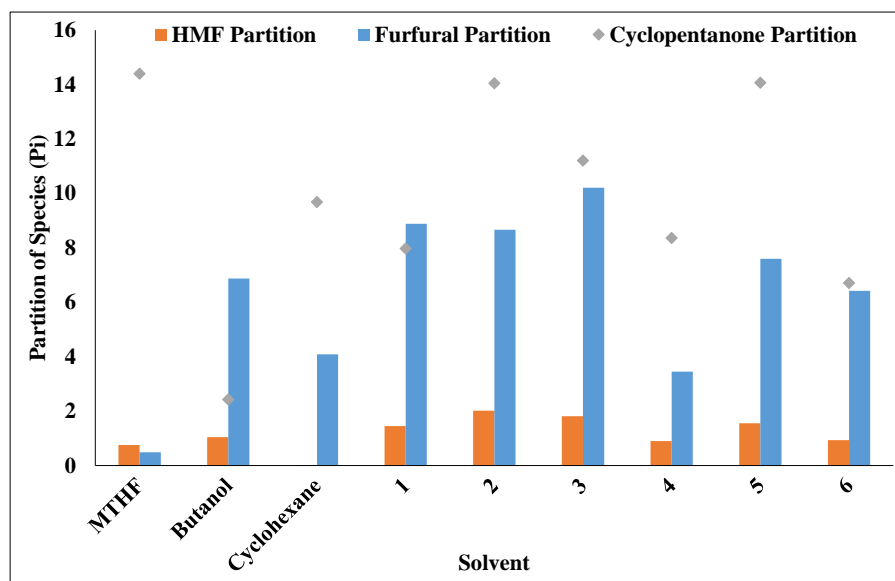


Figure 5-19: Partition of products (HMF and furfural) and waste (cyclopentanone) between the organic and aqueous phase in different solvents

The detailed calculations reveal the effect of different partitioning on the rate of production. Figures 5-20 and 5-21 show the time dependence of the total product amount and production amount in the organic phase. The production rate in n-butanol, used as the reference case, is the dashed line, while the coloured solid lines show calculations for selected solvents. The rates of production and amounts in the organic phase with solvents 1-3, screened by the criteria I, are higher than that of the reference. The solvents from screening criteria II have mixed results; reaction with solvent 5 has a higher rate, solvent 6 has the same rate, and solvent 4 has a lower rate than with n-butanol.

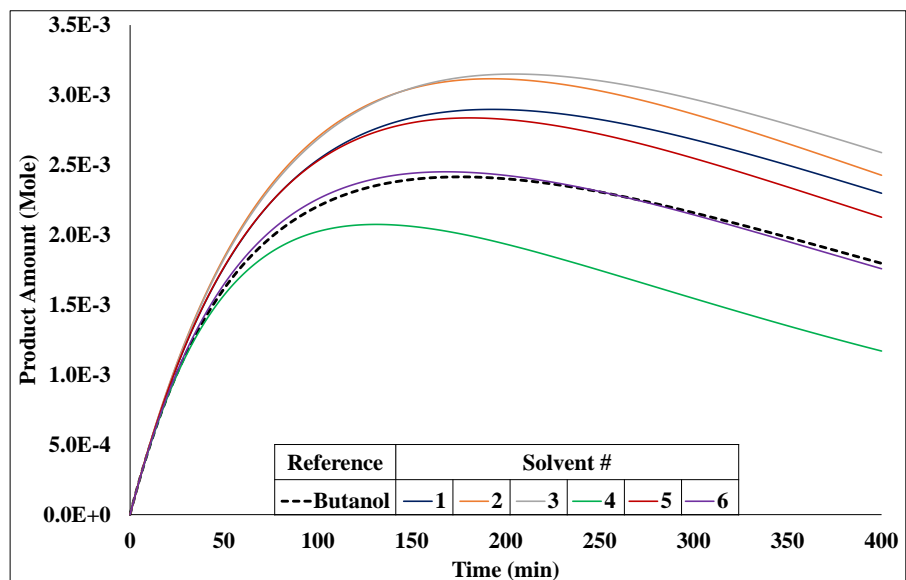


Figure 5-20: Rate of the overall products generation.

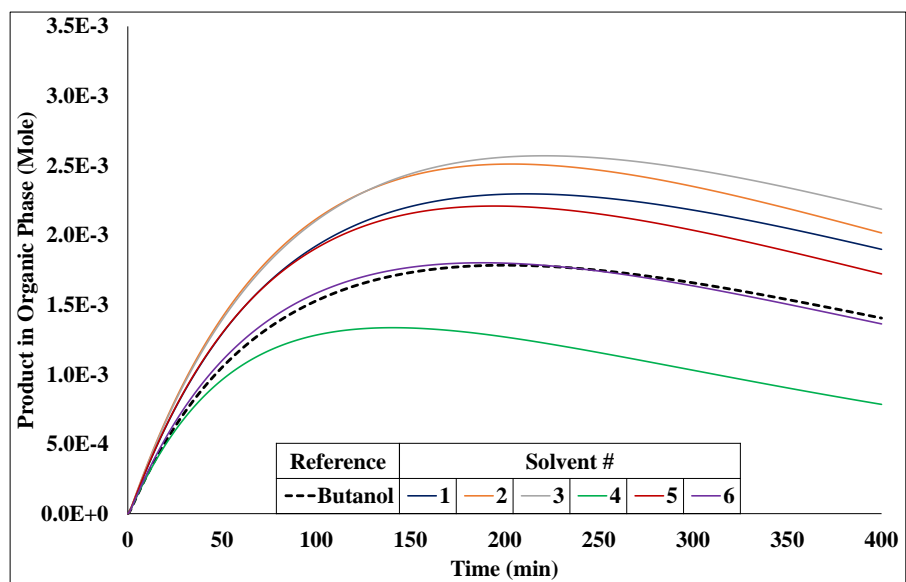


Figure 5-21: Rate of the products partitioned into the organic phase

Figure 5-22 displays the rates of production and waste generation together. The reactions with the three solvents from criteria I give higher rates of product generation and lower rates of waste creation when compared to reactions in the n-butanol reference case. Solvent 2 gives the highest rate of production, as well as the lowest rate of waste generation. Solvent 5 has less

enhancement of production rate and higher waste generation rate. In contrast, reactions with solvents 4 and 6 deliver poor results, with the rates of production and waste generation being similar to those with the reference solvent. Although the rate of waste generation can be lowered, it remains a problem. As shown in Figure 5-23, the minimum amount of waste in the organic phase over a period of 7 hours remains, at the minimum case with solvent 3, 3.5 times higher than the amount of the main product. Moreover, the amount of waste ends up in the organic phase could be as high as 7.1 times more than the amount of the main product with the reaction in solvent 4.

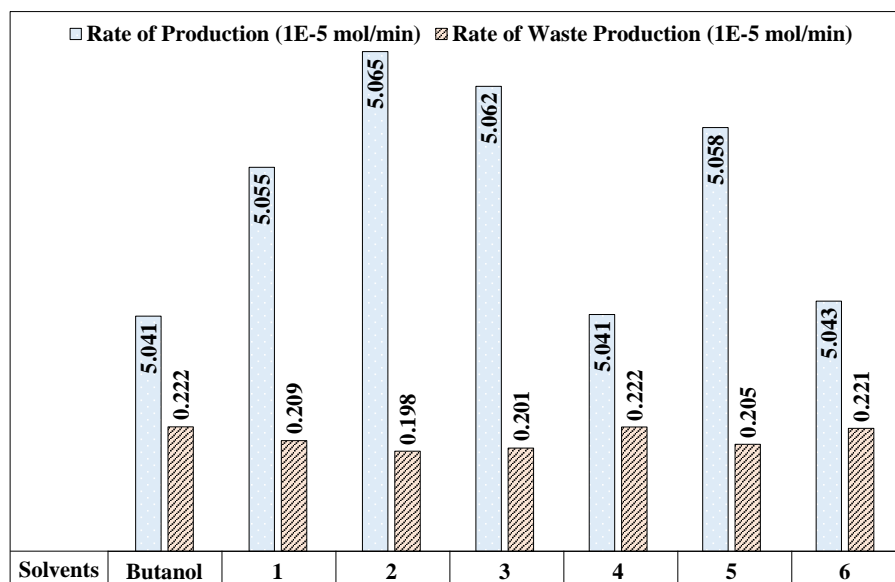


Figure 5-22: Rate of products and waste generation in different solvents

The detailed calculations indicate that product partitioning has slightly more impact on the overall rates of production and waste generation than does partitioning of waste species. However, because waste in the organic phase must be separated from the products after reaction, both partitionings should be carefully considered when designing a biphasic reactor system.

Although the calculation results show that there are improvements on the production rates of the main products (HMF and furfural) and the products also partition well into the organic phase, as well as, the formation of waste species is diminished; the results are still far from convincing, the effect of manipulation of the partition coefficients through solvents substitution is minimal, the partition of the unwanted side product is still higher than the products, and the rate of waste generation is still higher than the rate of product transfer to the organic phase.

A lot of work on both modelling and experimental sides is still required. Moreover, a methodology for solvents selection is still a challenge. However, this result confirms that the furan derivatives production process can be improved and all of the four design targets can be met through rationally selecting an optimal solvent and process condition.

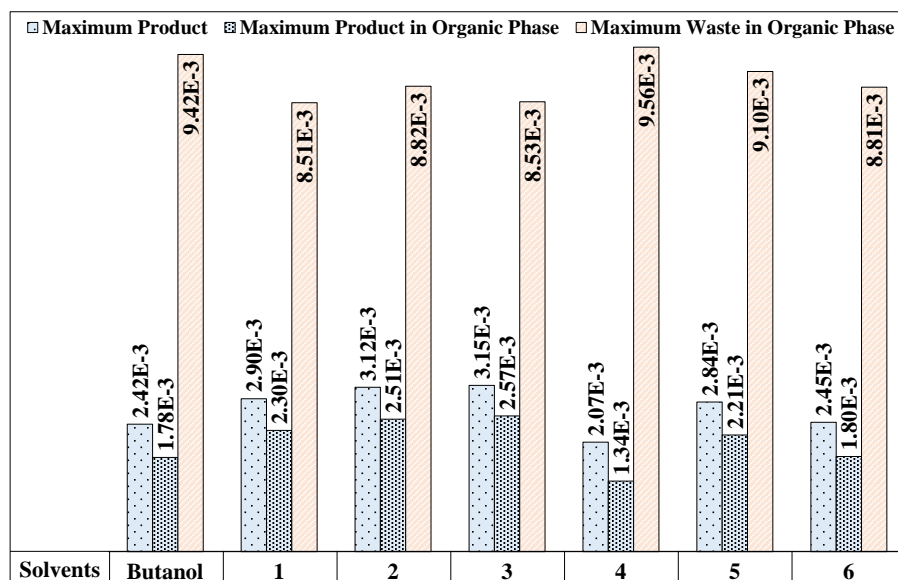


Figure 5-23: Maximum amount of products and waste generation during the reaction period

5.4.3 Summary

The application of biphasic reaction system to the production of furan is mainly for separation purpose. Therefore, the reaction scheme is completely different from the previous cases. Moreover, the mass transfer limit has an important role toward the production and separation.

This case involves with the reactions of bio-based compounds and enzyme in biphasic system. The framework is proven again to guide the construction of the model for this biochemical-biphasic reaction system that requires minimum experimental data for accurate prediction. Although the improvements are not immense; the proposed novel design has increased rate of production and product partition, as well as, inhibit the production of side product.

5.5 PRODUCTION OF ALPHA-AMINO BUTYRIC ACID

In this example, the α -aminobutyric acid production reaction model in section 4.2.5 is combined with e-KT-UNIFAC thermodynamic models for the prediction of the process behaviour. The design targets are to analyse the reaction and to improve the reactor performance through simple partitions analysis.

5.5.1 Model Validation

There are 16 measured data points in 2 data set of the time-dependent conversion rate of the 2-oxobutyric acid (2OA) to the α -aminobutyric acid in the single aqueous phase and the biphasic water-hexane systems, the data are reported by Shin and Kim [55].

The kinetic parameter (k_1) is regressed for both reaction scenarios, the value of the regressed parameter is $3.18 \cdot 10^3 \text{ cm}^3 \cdot \text{kmol}^{-1} \cdot \text{min}^{-1}$, the graphical comparison between the measured data and model prediction is shown in Figure 5-24, the absolute average deviation for the reaction in single phase is 1.49% and in the biphasic system is 2.22%.

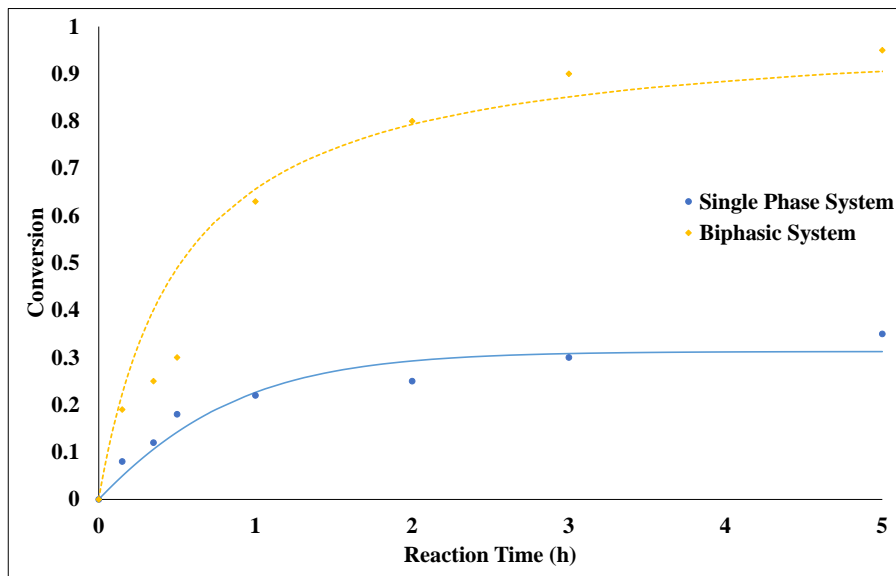


Figure 5-24: Comparison between model prediction biphasic and single phase production of α -aminobutyric acid and experimental data [55]

5.5.2 Model Application

To improve the rate of production, enhance the conversion, and reduce the separation steps, the partition coefficients of each species in the difference solvents are analysed as shown in Table 5-12 and Figure 5-25. The long chain hydrocarbon solvents (heptane, octane, and isooctane) are selected for the analysis since they share similar molecular structures and should not affect the reaction and/or the established separation process.

Table 5-12: Partition coefficient of the involved species in the long chain hydrocarbon solvents

Partition $\left(\frac{\gamma_i^\alpha}{\gamma_i^\beta}\right)$	Benzylamine	2OA	AABA	Benzaldehyde
Hexane	0.986	8.33E-06	4.50E-06	8.06E+03
Heptane	1.178	5.41E-06	3.56E-06	8.33E+03
Isooctane	3.096	8.33E-06	6.85E-06	1.59E+04
Octane	2.959	3.73E-04	1.19E-04	1.30E+04

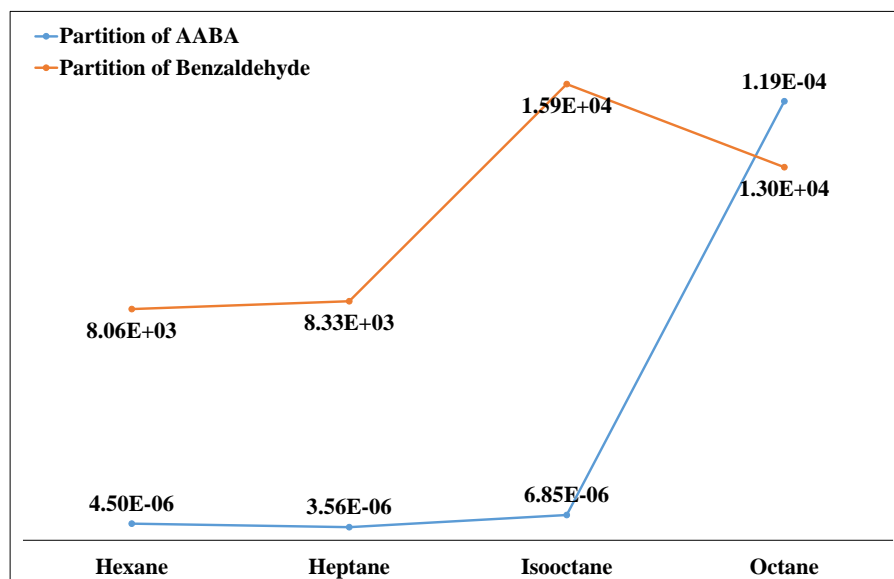


Figure 5-25: The partition coefficients of the involved species in hydrocarbon solvents

The desirable solvent should fetch the reaction inhibitor (benzaldehyde) in order to increase the overall reaction rate, as well as shift the equilibrium in favour to the product (AABA) creation. Whereas, the partition of AABA should be small in order to preserve it in the aqueous phase.

However, analysing the partition coefficients above, no concrete design decision can be made. The highest partition of benzaldehyde is acquired in isooctane, where the partition of AABA is also getting larger causing that loss of desirable product. On the other hand, the lowest partition of AABA is acquired in heptane, where the partition of benzaldehyde is also moderate.

Therefore, the detailed calculation is performed, the results are displayed in Table 5-13. Concerning the half-lives of the reaction and overall reaction rates, the reaction in isooctane offers highest reaction rate, following by the reaction in octane. Reactions in both octane and isooctane yield 97% conversion. However, the loss of the product is higher in octane, which resulting in lower amount of product at the end of the reaction. Nevertheless, it appears that branched-carbon group has a decent effect toward the partition coefficient of benzaldehyde. A shorter branched-hydrocarbon solvent should also be examined for a better solvent for the

production of the α -aminobutyric acid process further.

Table 5-13: Predicted reaction information carried out in different solvents

Solvents	Half-Life (hr.)	Overall Reaction Rate ($\mu\text{mol}\cdot\text{h}^{-1}$)	Maximum Conversion	Maximum Product (μmol)
Hexane	0.425	0.980	0.950	46.075
Heptane	0.475	0.977	0.947	45.930
Isooctane	0.302	1.380	0.970	46.075
Octane	0.311	1.340	0.970	33.950

The results of this example are used in an sustainable integrated systematic framework [129] which combines the reaction pathway identification, the reaction analysis (this work), and the process intensification together for the intensified design of the pharmaceutical process.

5.5.3 Summary

In this case, biphasic system is mainly implemented for its simultaneous reaction-separation scheme. It is proven that the framework can be used for modelling of the production of pharmaceutical compound in biphasic system. The constructed model are matched with the experimental data in single- and biphasic systems requiring only one reaction kinetic parameter.

The detailed calculations give the insight on the system. Since the conventional organic solvent (hexane) is already well performed, changing solvent gives only a slightly improvement over the reaction rate. However, it also indicates a possible improvement by applying branched-shorter chain hydrocarbon as organic solvent.

6

CONCLUSION

In short, the challenges in the modelling of biphasic reaction systems have been overcome with the developed framework together with the derived generic model. Following the framework, robust models of different processes have been developed and validated. The process models, together with their corresponding constitutive thermodynamic models, have been successfully employed for the improved and innovative design of the processes.

In this chapter, the summary of the achievements of this PhD project is presented in section 6.1 and the remaining challenges for future consideration are discussed in section 6.2.

6.1 ACHIEVEMENTS

The primary achievement of this work lies in the development of the modelling framework and the generic biphasic reaction process model. The modelling challenges listed in chapter 1 have been overcome.

1. Multiple modelling objectives can be achieved by assembling the model from different combinations of equations. Each combination can be applied for one or more modelling objectives depending on the scenario.
2. The list of required properties of the involved chemical species is given. All properties are either collected from available published data or estimated through group contribution method.
3. The equations for different reactor configurations (batch, fed-batch, and CSTR) are provided through the formation of different balance equations.
4. The formation of the reactions equations, depending on the location and the reaction-controlled mechanisms is provided. Including also the formation of mass transfer equations across the interface.
5. The distributions of chemical species between the phases can be correlated, partially-predicted, or predicted through different thermodynamic models and their combination.
6. The data requirement is reduced. Only kinetic-related parameters require experimental data. Novel solutions can be acquired through the proper use of the model.

The framework provides a broad range of application for chemical, biochemical, and pharmaceutical reactions systems. Five illustrative examples have been studied.

1. Correlated model has been developed for **pseudo-PTC system**. This early developed model can be used to correlate model with experimental data and estimate the effect of changing initial amount of involved compounds.
2. The partially predictive thermodynamic models have been implemented with the reactor models for **PTC system** with multiple design targets. The models can predict the effect of changing organic solvent toward the production, impurities amount, and reaction rate. As well as, the optimum fed amount of PTC can also be estimated. Moreover, the implementation of the predictive e-KT-UNIFAC allows designing of the novel PTC ions, which further improves the prediction range and enhances the result.
3. The temperature dependent is included into the formulation of the reaction model in **epoxidation** case. The process contains entirely different set of involved chemical species, with similar reaction scheme to the PTC cases. The model has been applied for finding a better design of the process. Ten substituted organic solvents have been analysed. The proposed solvent provides 28% faster reaction rate and eliminates the formation of the unwanted side product compare to the conventional practice.
4. The framework has been employed for modelling of the bio-based **furan production** process. The constructed model has been satisfactorily matched with the raw material conversion and production rates. Substituted solvents have been screened through two different criteria sets, six solvents have been selected for detail calculations. The possibility to improve rate of production and prevent side reaction is presented.

5. The **production of α -aminobutyric acid** has been analysed with the constructed biphasic reaction model. The model has been successfully applied for both reaction in single- and biphasic systems of this pharmaceutical compound production. A slight improvement of the reaction rate can be achieved through changing of the solvent. The result also presents a possibility for future study on the promising branched hydrocarbon solvents, which enhance the production rate of the amino acid.

Therefore, all of the three project objectives have been accomplished.

1. The modelling framework for biphasic reaction systems has been developed.
2. The framework allows the construction of problem-specific models for different scenarios, containing a diverse set of reactions, chemicals, and conditions.
3. The reactor models have been implemented with both correlative and predictive constitutive thermodynamic models. The assembled models provide a wide range of predictive capability for interpolation and extrapolation of systems with a minimum of rate-dependent measured data. These features make the framework particularly suitable for studies involving searches for solvents giving better product yields, faster reaction rates, and easier separations.

At this stage, the very useful results can be obtained for many biphasic reacting systems through this modelling framework. However, there are some challenges need to be further addressed in the future work. The remaining challenges are discussed in the next section.

6.2 REMAINING CHALLENGES

Although the modelling and the model application of biphasic reaction systems have progressed considerably with this work, there still are numbers of the area need further attention and development.

6.2.1 Interfacial Area

In this project, reactor structure is neglected, it is discreetly assumed that the reactor configuration remains unchanged. However, reactor configuration always changes from experimental scale to industrial scale; resulting in the change of size and shape of the interfacial area between the two liquids phases.

The simple correlation between the agitation speed and interfacial can be applied to overcome this problem. Nevertheless, most of those correlations are limited to one reactor configuration and are not much useful than what have already practised. On the other hand, the development of the multidimensional model that include formation and elimination of the interface should give a better insight of the system. However, this approach would inevitably increase the model complexity, sometimes without any apparent benefit. The AE steady-state model would transform into location-dependent ODE model. Likewise, the time-dependent ODE model would also propagate into multidimensional partial differential equations (PDE) model.

Therefore, prior to committing any effort on extending the model with simple correlation or multidimensional approach; the modeller should extensively estimate the magnitude of the interfacial effect toward the objective of the model.

6.2.2 Plug Flow Reactor

Three types of the reactor (batch, fed-batch, and CSTR) can be modelled by the framework. However, the model for the continuous plug flow reactor type cannot be formulated with this framework without the modified balance equations.

The plug flow reactor is omitted from this study for two reasons. First, there is no information on the formation of biphasic within this type of reactor. There is only one report by De Zani and co-workers [20], as discussed in chapter 2, which apply plug flow micro-reactor for alkylation process. Undoubtedly, the formation of biphasic in the industrial-scale plug flow reactor would be totally different from the formation of biphasic in a micro-reactor. Moreover, the balance equation of plug flow reactor is based on the length, or the resident time (τ), not the time (t). Therefore, the balance equation for batch reactor could be modified to match those of the plug flow reactor.

This issue could be solved together with the interfacial area issue, by employing detail multidimensional model that can accurately predict the formation of biphasic in different reactor configurations.

6.2.3 Complex Heat Transfer

Although the framework has been applied successfully with temperature dependent system (epoxidation case, sections 4.2.3 and 5.3), the implemented model only considers lumped and well-controlled temperature dependent system.

On the other hand, the highly endo- or exothermic systems are more complicated; the change in temperature in one phase, effect the partition and behaviour in the others. Moreover, it is also possible that the rates of heat generation or consumption and heat transfer across the interface are unequal; resulting in the formation of a temperature gradient across the reactor.

Although this issue should not concern most of the well-controlled industrial process, it is appealing academically.

6.2.4 Extension of e-KT-UNIFAC Model

Constitutive thermodynamic models play an important role for calculating the distribution of involved chemical species. In general, the e-KT-UNIFAC can handle a wide range of chemical compounds; however, it still lacks parameters for complex electrolyte system, for example, tetraalkylammonium PTC.

In this project, the prediction range of e-KT-UNIFAC has been extended to cover 4-16 carbon atoms PTC, which contain only hydrocarbon chains. Whereas, there are numerous useful PTCs that consist of other organic groups in their chains; as well as, PTC that contain potassium central atom instead of nitrogen.

The extension of e-KT-UNIFAC for multiple PTCs should be carried out together with the extension of the model for ionic liquid systems; since both IL and PTC systems share a similarity, the number of experimental data points and the validity of the model should increase.

6.2.5 Multiphase Systems

As examined in chapter 2, Nowothnick and co-worker [43] achieve an economically feasible process by applying surfactant-induced three phases system for hydroformylation process.

These multiple-phases systems could potentially open more reaction pathways for organic synthesis. However, the complexity of these systems also rises exponentially. The behaviours of involved chemical species need to be predictable in multiple phases, especially the behaviour of the additional surfactant that is hardly predictable.

The extension of e-KT-UNIFAC could also include the prediction of the non-ionic and ionic surfactants, as a fundamental step toward multiphase systems modelling.

**“A theory has only the alternative of being right or wrong.
A model has a third possibility: it may be right, but irrelevant.”
Manfred Eigen [130]**

REFERENCES

- [1] G.E.P. Box, Robustness in the Strategy of Scientific Model Building, in: *Robustness Stat.*, 1979: pp. 201–236. doi:10.1016/B978-0-12-438150-6.50018-2.
- [2] G.E.P. Box, Science and Statistics, *J. Am. Stat. Assoc.* 71 (1976) 791. doi:10.2307/2286841.
- [3] I.T. Cameron, R. Gani, *Product and Process Modelling A Case Study Approach*, Elsevier Science, Amsterdam, 2011. doi:10.1016/B978-0-444-53161-2.00013-3.
- [4] C.M. Starks, Phase-transfer catalysis. I. Heterogeneous reactions involving anion transfer by quaternary ammonium and phosphonium salts, *J. Am. Chem. Soc.* 93 (1971) 195–199. doi:10.1021/ja00730a033.
- [5] M. Halpern, M. Halpern, Phase-Transfer Catalysis, in: *Ullmann's Encycl. Ind. Chem.*, Wiley-VCH Verlag GmbH & Co. KGaA, Weinheim, Germany, 2000. doi:10.1002/14356007.a19_293.
- [6] W.H.C. Rueggeberg, A. Ginsbu'rg, R.K. Frantz, Benzyl Benzoate from Benzyl Chloride and Sodium Benzoate, *Ind. Eng. Chem.* 38 (1946) 207–211. doi:10.1021/ie50434a025.
- [7] A.K. Dillow, S.L.J. Yun, D. Suleiman, D.L. Boatright, C.L. Liotta, C.A. Eckert, Kinetics of a Phase-Transfer Catalysis Reaction in Supercritical Fluid Carbon Dioxide, *Ind. Eng. Chem. Res.* 35 (1996) 1801–1806. doi:10.1021/ie9600405.
- [8] D. Landini, A. Maia, F. Montanari, Mechanism of phase-transfer catalysis, *J. Chem. Soc. Chem. Commun.* (1977) 112. doi:10.1039/c39770000112.
- [9] D. Landini, A. Maia, F. Montanari, Phase-transfer catalysis. Nucleophilicity of anions in aqueous organic two-phase reactions catalyzed by onium salts. A comparison with homogeneous organic systems, *J. Am. Chem. Soc.* 100 (1978) 2796–2801. doi:10.1021/ja00477a036.
- [10] M. Vander Zwan, F. Hartner, Solid-liquid phase-transfer catalysis by a quaternary ammonium salt. A comparison with crown ethers and polyalkylamines, *J. Org. Chem.* (1978) 2655–2657.
- [11] J. Royer, H.P. Husson, Asymmetric synthesis. 2. Practical method for the asymmetric synthesis of indolizidine alkaloids: total synthesis of (-)-monomorphine I, *J. Org. Chem.* 50 (1985) 670–673. doi:10.1021/jo00205a023.
- [12] P.R. Schreiner, O. Lauenstein, E.D. Butova, P.A. Gunchenko, I. V Kolomitsin, A. Wittkopp, et al., Selective radical reactions in multiphase systems: phase-transfer halogenations of alkanes., *Chemistry*. 7 (2001) 4996–5003.
- [13] S. Yufit, S. Zinovyev, A comparative kinetic study of nucleophilic substitution under PTC conditions in liquid-liquid and solid-liquid systems, *Tetrahedron*. 55 (1999) 6319–6328.
- [14] F.F. Fleming, L. Yao, P.C. Ravikumar, L. Funk, B.C. Shook, Nitrile-containing pharmaceuticals: efficacious roles of the nitrile pharmacophore., *J. Med. Chem.* 53

- (2010) 7902–17. doi:10.1021/jm100762r.
- [15] C.M. Starks, R.M. Owens, Phase-transfer catalysis. II. Kinetic details of cyanide displacement on 1-halooctanes, *J. Am. Chem. Soc.* 95 (1973) 3613–3617. doi:10.1021/ja00792a025.
- [16] K. Chandler, C.W. Culp, D.R. Lamb, C.L. Liotta, C.A. Eckert, Phase-Transfer Catalysis in Supercritical Carbon Dioxide: Kinetic and Mechanistic Investigations of Cyanide Displacement on Benzyl Chloride, *Ind. Eng. Chem. Res.* 37 (1998) 3252–3259. doi:10.1021/ie970741h.
- [17] M. Małosza, M. Fedoryński, Phase Transfer Catalysis, *Catal. Rev.* 45 (2003) 321–367. doi:10.1081/CR-120025537.
- [18] S.K. Maity, N.C. Pradhan, A. V. Patwardhan, Reaction of benzyl chloride with ammonium sulfide under liquid–liquid phase transfer catalysis: Reaction mechanism and kinetics, *J. Mol. Catal. A Chem.* 250 (2006) 114–121. doi:10.1016/j.molcata.2006.01.045.
- [19] G.D. Yadav, A.A. Kadam, Atom-Efficient Benzoin Condensation in Liquid–Liquid System Using Quaternary Ammonium Salts: Pseudo-Phase Transfer Catalysis, *Org. Process Res. Dev.* 16 (2012) 755–763. doi:10.1021/op300027j.
- [20] D. de Zani, M. Colombo, Phase-Transfer Catalysis under Continuous Flow Conditions: An Alternative Approach to the Biphasic Liquid/Liquid O-Alkylation of Phenols, *J. Flow Chem.* (2012) 5–7. doi:10.1556/jfchem.2012.00020.
- [21] J.J. Vanden Eynde, I. Maillieux, QUATERNARY AMMONIUM SALT-ASSISTED ORGANIC REACTIONS IN WATER: ALKYLATION OF PHENOLS, *Synth. Commun.* 31 (2001) 1–7. doi:10.1081/SCC-100000172.
- [22] B. Lygo, B.I. Andrews, Asymmetric phase-transfer catalysis utilizing chiral quaternary ammonium salts: asymmetric alkylation of glycine imines., *Acc. Chem. Res.* 37 (2004) 518–25. doi:10.1021/ar030058t.
- [23] C. Cassani, L. Bernardi, F. Fini, A. Ricci, Catalytic Asymmetric Mannich Reactions of Sulfonylacetates, *Angew. Chemie Int. Ed.* 48 (2009) 5694–5697. doi:10.1002/anie.200900701.
- [24] M.-L. Wang, P. Vivekanand, M.-C. Yu, Hydrolysis of 4-methoxyphenylacetic acid butyl ester under liquid–liquid biphasic phase transfer condition and their kinetics, *J. Taiwan Inst. Chem. Eng.* 43 (2012) 207–214. doi:10.1016/j.jtice.2011.10.005.
- [25] I. Kaur, V. Kumari, P.K. Dhiman, Synthesis, characterization and use of polymer-supported phase transfer catalyst in organic reactions, *J. Appl. Polym. Sci.* 121 (2011) 3185–3191. doi:10.1002/app.33907.
- [26] E. Antonelli, R. D’Aloisio, M. Gambaro, T. Fiorani, C. Venturello, Efficient Oxidative Cleavage of Olefins to Carboxylic Acids with Hydrogen Peroxide Catalyzed by Methyltrioctylammonium Tetrakis(oxodiperoxotungsto)phosphate(3⁻) under Two-Phase Conditions. Synthetic Aspects and Investigation of the Reaction Course, *J. Org. Chem.* 63 (1998) 7190–7206. doi:10.1021/jo980481t.
- [27] T.B. Khlebnikova, Z.P. Pai, L.A. Fedoseeva, Y. V. Mattsat, Catalytic oxidation of fatty acids. II. Epoxidation and oxidative cleavage of unsaturated fatty acid esters containing additional functional groups, *React. Kinet. Catal. Lett.* 98 (2009) 9–17. doi:10.1007/s11144-009-0054-9.

- [28] Z.P. Pai, T.B. Khlebnikova, Y. V. Mattsat, V.N. Parmon, Catalytic oxidation of fatty acids. I. Epoxidation of unsaturated fatty acids, *React. Kinet. Catal. Lett.* 98 (2009) 1–8. doi:10.1007/s11144-009-0069-2.
- [29] E. Santacesaria, A. Sorrentino, F. Rainone, M. Di Serio, F. Speranza, Oxidative Cleavage of the Double Bond of Monoenic Fatty Chains in Two Steps: A New Promising Route to Azelaic Acid and Other Industrial Products, *Ind. Eng. Chem. Res.* 39 (2000) 2766–2771. doi:10.1021/ie990920u.
- [30] A. Köckritz, A. Martin, Oxidation of unsaturated fatty acid derivatives and vegetable oils, *Eur. J. Lipid Sci. Technol.* 110 (2008) 812–824. doi:10.1002/ejlt.200800042.
- [31] A. Campanella, M.A. Baltanás, Degradation of the oxirane ring of epoxidized vegetable oils in liquid–liquid heterogeneous reaction systems, *Chem. Eng. J.* 118 (2006) 141–152. doi:10.1016/j.cej.2006.01.010.
- [32] A. Campanella, C. Fontanini, M.A. Baltanás, High yield epoxidation of fatty acid methyl esters with performic acid generated in situ, *Chem. Eng. J.* 144 (2008) 466–475. doi:10.1016/j.cej.2008.07.016.
- [33] S. Dinda, A. V. Patwardhan, V. V. Goud, N.C. Pradhan, Epoxidation of cottonseed oil by aqueous hydrogen peroxide catalysed by liquid inorganic acids, *Bioresour. Technol.* 99 (2008) 3737–3744. doi:10.1016/j.biortech.2007.07.015.
- [34] E. Santacesaria, R. Tesser, M. Di Serio, R. Turco, V. Russo, D. Verde, A biphasic model describing soybean oil epoxidation with H₂O₂ in a fed-batch reactor, *Chem. Eng. J.* 173 (2011) 198–209. doi:10.1016/j.cej.2011.05.018.
- [35] E. Santacesaria, A. Renken, V. Russo, R. Turco, R. Tesser, M. Di Serio, Biphasic Model Describing Soybean Oil Epoxidation with H₂O₂ in Continuous Reactors, *Ind. Eng. Chem. Res.* 51 (2012) 8760–8767. doi:10.1021/ie2016174.
- [36] S. Sinadinović-Fišer, M. Janković, O. Borota, Epoxidation of castor oil with peracetic acid formed in situ in the presence of an ion exchange resin, *Chem. Eng. Process. Process Intensif.* 62 (2012) 106–113. doi:10.1016/j.cep.2012.08.005.
- [37] K. Sato, A “Green” Route to Adipic Acid: Direct Oxidation of Cyclohexenes with 30 Percent Hydrogen Peroxide, *Science* (80-.). 281 (1998) 1646–1647. doi:10.1126/science.281.5383.1646.
- [38] F.O. Ayorinde, G. Osman, R.L. Shepard, F.T. Powers, Synthesis of azelaic acid and suberic acid from *Vernonia galamensis* oil, *J. Am. Oil Chem. Soc.* 65 (1988) 1774–1777. doi:10.1007/BF02542380.
- [39] B. Nair, Final report on the safety assessment of Benzyl Alcohol, Benzoic Acid, and Sodium Benzoate., *Int. J. Toxicol.* 20 Suppl 3 (2001) 23–50.
- [40] Z.P. Pai, A.G. Tolstikov, P. V. Berdnikova, G.N. Kustova, T.B. Khlebnikova, N. V. Selivanova, et al., Catalytic oxidation of olefins and alcohols with hydrogen peroxide in a two-phase system giving mono- and dicarboxylic acids, *Russ. Chem. Bull.* 54 (2005) 1847–1854. doi:10.1007/s11172-006-0047-z.
- [41] I. Ojima, C.-Y. Tsai, M. Tzamarioudaki, D. Bonafoux, I. Ojima, C. Tsai, et al., The Hydroformylation Reaction, in: *Org. React.*, John Wiley & Sons, Inc., Hoboken, NJ, USA, 2000: pp. 1–354. doi:10.1002/0471264180.or056.01.
- [42] M.F. Sellin, P.B. Webb, D.J. Cole-Hamilton, Continuous flow homogeneous catalysis:

- hydroformylation of alkenes in supercritical fluid–ionic liquid biphasic mixtures, *Chem. Commun.* (2001) 781–782. doi:10.1039/b101046h.
- [43] H. Nowothnick, A. Rost, T. Hamerla, R. Schomäcker, C. Müller, D. Vogt, Comparison of phase transfer agents in the aqueous biphasic hydroformylation of higher alkenes, *Catal. Sci. Technol.* 3 (2013) 600–605. doi:10.1039/C2CY20629C.
- [44] L. Obrecht, P.C.J. Kamer, W. Laan, Alternative approaches for the aqueous–organic biphasic hydroformylation of higher alkenes, *Catal. Sci. Technol.* 3 (2013) 541. doi:10.1039/c2cy20538f.
- [45] Z. Xu, S. Wang, C. Chen, CO₂ absorption by biphasic solvents: Mixtures of 1, 4-Butanediamine and 2-(Diethylamino)-ethanol, *Int. J. Greenh. Gas Control.* 16 (2013) 107–115. doi:10.1016/j.ijggc.2013.03.013.
- [46] H. Amiri, K. Karimi, S. Roodpeyma, Production of furans from rice straw by single-phase and biphasic systems., *Carbohydr. Res.* 345 (2010) 2133–8. doi:10.1016/j.carres.2010.07.032.
- [47] J.M.R. Gallo, D.M. Alonso, M.A. Mellmer, J.A. Dumesic, Production and upgrading of 5-hydroxymethylfurfural using heterogeneous catalysts and biomass-derived solvents, *Green Chem.* 15 (2013) 85. doi:10.1039/c2gc36536g.
- [48] E. Gürbüz, S. Wettstein, J. Dumesic, Conversion of hemicellulose to furfural and levulinic acid using biphasic reactors with alkylphenol solvents, *ChemSusChem.* (2012) 383–387. doi:10.1002/cssc.201100608.
- [49] V.V. Ordonsky, J. van der Schaaf, T.A. Nijhuis, Biphasic single-reactor process for dehydration of xylose and hydrogenation of produced furfural, *Appl. Catal. A Gen.* 451 (2013) 6–13. doi:10.1016/j.apcata.2012.11.013.
- [50] V. Ordonsky, J. Schouten, J. van der Schaaf, T.A. Nijhuis, Multilevel rotating foam biphasic reactor for combination of processes in biomass transformation, *Chem. Eng. J.* 231 (2013) 12–17. doi:10.1016/j.cej.2013.06.110.
- [51] M.A. Dubé, A.Y. Tremblay, J. Liu, Biodiesel production using a membrane reactor., *Bioresour. Technol.* 98 (2007) 639–47. doi:10.1016/j.biortech.2006.02.019.
- [52] P. Lozano, J.M. Bernal, M. Vaultier, Towards continuous sustainable processes for enzymatic synthesis of biodiesel in hydrophobic ionic liquids/supercritical carbon dioxide biphasic systems, *Fuel.* 90 (2011) 3461–3467. doi:10.1016/j.fuel.2011.06.008.
- [53] C. Hongfa, P. Samunual, S. Sachdev, C. Lim, Thermomorphic Biphasic System—A Greener Alternative Route to the Synthesis of Biodiesel, *Energy & Fuels.* 27 (2013) 879–882. doi:10.1021/ef301456c.
- [54] S. Villarroya, J. Zhou, K.J. Thurecht, S.M. Howdle, Synthesis of Graft Copolymers by the Combination of ATRP and Enzymatic ROP in scCO₂, *Macromolecules.* 39 (2006) 9080–9086. doi:10.1021/ma061068n.
- [55] J.-S. Shin, B.-G. Kim, Transaminase-catalyzed asymmetric synthesis of 1-2-aminobutyric acid from achiral reactants, *Biotechnol. Lett.* 31 (2009) 1595–1599. doi:10.1007/s10529-009-0057-7.
- [56] B. Gutmann, D. Cantillo, C.O. Kappe, Continuous-Flow Technology-A Tool for the Safe Manufacturing of Active Pharmaceutical Ingredients, *Angew. Chemie Int. Ed.* 54 (2015) 6688–6728. doi:10.1002/anie.201409318.

- [57] K.D. Samant, D.J. Singh, K.M. Ng, Design of liquid-liquid phase transfer catalytic processes, *AIChE J.* 47 (2001) 1832–1848. doi:10.1002/aic.690470814.
- [58] L.H. Gan, S.H. Goh, K.S. Ooi, Kinetic studies of epoxidation and oxirane cleavage of palm olein methyl esters, *J. Am. Oil Chem. Soc.* 69 (1992) 347–351. doi:10.1007/BF02636065.
- [59] B. Rangarajan, A. Havey, E.A. Grulke, P.D. Culnan, Kinetic parameters of a two-phase model for in situ epoxidation of soybean oil, *J. Am. Oil Chem. Soc.* 72 (1995) 1161–1169. doi:10.1007/BF02540983.
- [60] R. Weingarten, J. Cho, W.C. Conner, Jr., G.W. Huber, Kinetics of furfural production by dehydration of xylose in a biphasic reactor with microwave heating, *Green Chem.* 12 (2010) 1423. doi:10.1039/c003459b.
- [61] C. Piccolo, A. Shaw, G. Hodges, P.M. Piccione, J.P. O’Connell, R. Gani, A framework for the design of reacting systems with phase transfer catalysis, *Comput. Aided Chem. Eng.* 30 (2012) 757–761. doi:10.1016/B978-0-444-59520-1.50010-5.
- [62] L.S. Belvèze, J.F. Brennecke, M.A. Stadtherr, Modeling of Activity Coefficients of Aqueous Solutions of Quaternary Ammonium Salts with the Electrolyte-NRTL Equation, *Ind. Eng. Chem. Res.* 43 (2004) 815–825. doi:10.1021/ie0340701.
- [63] A. Fukumoto, D. Dalmazzone, P. Paricaud, W. Fürst, Experimental Measurements and Modeling of the Dissociation Conditions of Tetrabutylammonium Chloride Semiclathrate Hydrates in the Presence of Hydrogen, (2014).
- [64] A. Galindo, A. Gil-Villegas, G. Jackson, A.N. Burgess, SAFT-VRE: Phase Behavior of Electrolyte Solutions with the Statistical Associating Fluid Theory for Potentials of Variable Range, *J. Phys. Chem. B.* 103 (1999) 10272–10281. doi:10.1021/jp991959f.
- [65] N. Papaiconomou, J. Simonin, O. Bernard, Solutions of Alkylammonium and Bulky Anions: Description of Osmotic Coefficients within the Binding Mean Spherical Approximation, *Ind. Eng. Chem. Res.* 51 (2012) 9661–9668. doi:10.1021/ie202954y.
- [66] J.-P. Simonin, O. Bernard, L. Blum, Real Ionic Solutions in the Mean Spherical Approximation. 3. Osmotic and Activity Coefficients for Associating Electrolytes in the Primitive Model, *J. Phys. Chem. B.* 102 (1998) 4411–4417. doi:10.1021/jp9732423.
- [67] Z. Lei, J. Zhang, Q. Li, B. Chen, UNIFAC Model for Ionic Liquids, *Ind. Eng. Chem. Res.* 48 (2009) 2697–2704. doi:10.1021/ie801496e.
- [68] R.S. Santiago, G.R. Santos, M. Aznar, Liquid–liquid equilibrium in ternary ionic liquid systems by UNIFAC: New volume, surface area and interaction parameters. Part I, *Fluid Phase Equilib.* 295 (2010) 93–97. doi:10.1016/j.fluid.2010.04.001.
- [69] L. Constantinou, R. Gani, New group contribution method for estimating properties of pure compounds, *AIChE J.* 40 (1994) 1697–1710. doi:10.1002/aic.690401011.
- [70] A. Kumar, S. Hartland, Correlations for Prediction of Mass Transfer Coefficients in Single Drop Systems and Liquid–Liquid Extraction Columns, *Chem. Eng. Res. Des.* 77 (1999) 372–384. doi:10.1205/026387699526359.
- [71] L. Coniglio, K. Knudsen, R. Gani, Model Prediction of Supercritical Fluid–Liquid Equilibria for Carbon Dioxide and Fish Oil Related Compounds, *Ind. Eng. Chem. Res.* 34 (1995) 2473–2484. doi:10.1021/ie00046a032.

- [72] G.K. Folas, G.M. Kontogeorgis, M.L. Michelsen, E.H. Stenby, Vapor–liquid, liquid–liquid and vapor–liquid–liquid equilibrium of binary and multicomponent systems with MEG, *Fluid Phase Equilib.* 249 (2006) 67–74. doi:10.1016/j.fluid.2006.08.021.
- [73] R. Gani, E.A. Brignole, Molecular design of solvents for liquid extraction based on UNIFAC, *Fluid Phase Equilib.* 13 (1983) 331–340. doi:10.1016/0378-3812(83)80104-6.
- [74] E.S. Pérez Cisneros, R. Gani, M.L. Michelsen, Reactive separation systems—I. Computation of physical and chemical equilibrium, *Chem. Eng. Sci.* 52 (1997) 527–543. doi:10.1016/S0009-2509(96)00424-1.
- [75] S.H. Kim, A. Anantpinijwatna, J.W. Kang, R. Gani, Analysis and modeling of alkali halide aqueous solutions, *Fluid Phase Equilib.* 412 (2016) 177–198. doi:10.1016/j.fluid.2015.12.008.
- [76] H. Renon, J.M. Prausnitz, Local compositions in thermodynamic excess functions for liquid mixtures, *AIChE J.* 14 (1968) 135–144. doi:10.1002/aic.690140124.
- [77] C. Chen, H. Britt, J. Boston, L. Evans, Local composition model for excess Gibbs energy of electrolyte systems. Part I: Single solvent, single completely dissociated electrolyte systems, *AIChE J.* 28 (1982) 588–596.
- [78] C.-C. Chen, Representation of solid-liquid equilibrium of aqueous electrolyte systems with the electrolyte NRTL model, *Fluid Phase Equilib.* 27 (1986) 457–474. doi:10.1016/0378-3812(86)87066-2.
- [79] C. Chen, L. Evans, A local composition model for the excess Gibbs energy of aqueous electrolyte systems, *AIChE J.* 28 (1986) 588–596.
- [80] B. Mock, L.B. Evans, C.-C. Chen, Thermodynamic representation of phase equilibria of mixed-solvent electrolyte systems, *AIChE J.* 32 (1986) 1655–1664. doi:10.1002/aic.690321009.
- [81] K.S. Pitzer, Electrolytes. From dilute solutions to fused salts, *J. Am. Chem. Soc.* 102 (1980) 2902–2906. doi:10.1021/ja00529a006.
- [82] C.-C. Chen, A segment-based local composition model for the gibbs energy of polymer solutions, *Fluid Phase Equilib.* 83 (1993) 301–312. doi:10.1016/0378-3812(93)87033-W.
- [83] P.J. Flory, Thermodynamics of High Polymer Solutions, *J. Chem. Phys.* 9 (1941) 660. doi:10.1063/1.1750971.
- [84] L. Simoni, Predictive Modeling of Fluid Phase Equilibria for Systems Containing Ionic Liquids, University of Notre Dame, 2009.
- [85] H.-H. Tung, J. Tabora, N. Variankaval, D. Bakken, C.-C. Chen, Prediction of pharmaceutical solubility Via NRTL-SAC and COSMO-SAC., *J. Pharm. Sci.* 97 (2008) 1813–20. doi:10.1002/jps.21032.
- [86] C. Chen, P. Crafts, Correlation and prediction of drug molecule solubility in mixed solvent systems with the nonrandom two-liquid segment activity coefficient (NRTL-SAC) model, *Ind. Eng. Chem. Res.* (2006) 4816–4824.
- [87] C.-C. Chen, Toward development of activity coefficient models for process and product design of complex chemical systems, *Fluid Phase Equilib.* 241 (2006) 103–112.

- doi:10.1016/j.fluid.2006.01.006.
- [88] V. Athès, P. Paricaud, M. Ellaite, I. Souchon, W. Fürst, Vapour–liquid equilibria of aroma compounds in hydroalcoholic solutions: Measurements with a recirculation method and modelling with the NRTL and COSMO-SAC approaches, *Fluid Phase Equilib.* 265 (2008) 139–154. doi:10.1016/j.fluid.2008.01.012.
- [89] C.-C. Chen, Y. Song, Extension of Nonrandom Two-Liquid Segment Activity Coefficient Model for Electrolytes, *Ind. Eng. Chem. Res.* 44 (2005) 8909–8921. doi:10.1021/ie0503592.
- [90] J.W. Kang, J. Abildskov, R. Gani, J. Cobas, Estimation of Mixture Properties from First- and Second-Order Group Contributions with the UNIFAC Model, *Ind. Eng. Chem. Res.* 41 (2002) 3260–3273. doi:10.1021/ie010861w.
- [91] A. Mohs, J. Gmehling, A revised LIQUAC and LIFAC model (LIQUAC*/LIFAC*) for the prediction of properties of electrolyte containing solutions, *Fluid Phase Equilib.* 337 (2013) 311–322. doi:10.1016/j.fluid.2012.09.023.
- [92] P. Debye, E. Hückel, On The Theory of Electrolytes. I. Freezing Point Depression and Related Phenomena., *Phys. Zeitschrift.* 24 (1923) 185–206.
- [93] C.-C. Chen, Y. Song, Solubility modeling with a nonrandom two-liquid segment activity coefficient model, *Ind. Eng. Chem. Res.* 43 (2004) 8354–8362. doi:10.1021/ie049463u.
- [94] Y. Song, C.-C.C. Chen, Symmetric nonrandom two-liquid segment activity coefficient model for electrolytes, *Ind. Eng. Chem. Res.* 48 (2009) 5522–5529. doi:10.1021/ie900006g.
- [95] S. Lindenbaum, G.E. Boyd, Osmotic and Activity Coefficients for the Symmetrical Tetraalkyl Ammonium Halides in Aqueous Solution at 25° 1, *J. Phys. Chem.* 68 (1964) 911–917. doi:10.1021/j100786a038.
- [96] S. Lindenbaum, L. Leifer, G.E. Boyd, J.W. Chase, Variation of osmotic coefficients of aqueous solutions of tetraalkylammonium halides with temperature. Thermal and solute effects on solvent hydrogen bonding, *J. Phys. Chem.* 74 (1970) 761–764. doi:10.1021/j100699a014.
- [97] G.E. Boyd, A. Schwarz, S. Lindenbaum, Structural Effects on the Osmotic and Activity Coefficients of the Quaternary Ammonium Halides in Aqueous Solutions at 25° 1, *J. Phys. Chem.* 70 (1966) 821–825. doi:10.1021/j100875a034.
- [98] W.-Y. Wen, S. Saito, C. Lee, Activity and Osmotic Coefficients of Four Symmetrical Tetraalkylammonium Fluorides in Aqueous Solutions at 25° 1, *J. Phys. Chem.* 70 (1966) 1244–1248. doi:10.1021/j100876a044.
- [99] Y. Wu, H. Friedman, Heats of solution of some tetraalkylammonium salts in water and in propylene carbonate and ionic enthalpies of transfer from water to propylene carbonate, *J. Phys. Chem.* 501 (1966) 2020–2024.
- [100] F. Franks, D.L. Clarke, Solubilities of alkylammonium iodides in water and aqueous urea, *J. Phys. Chem.* 71 (1967) 1155–1156. doi:10.1021/j100863a065.
- [101] M. Abraham, Solvent effects on the free energies of ion-pairs, and of transition states in an SN1 and an SN2 reaction, *Tetrahedron Lett.* 11 (1970) 5233–5236. doi:10.1016/S0040-4039(00)99982-9.

- [102] M.H. Abraham, Substitution at saturated carbon. Part VIII. Solvent effects on the free energy of trimethylamine, the nitrobenzyl chlorides, and the trimethylamine-nitrobenzyl chloride transition states, *J. Chem. Soc. B Phys. Org.* (1971) 299. doi:10.1039/j29710000299.
- [103] M.H. Abraham, Substitution at saturated carbon. Part XIV. Solvent effects on the free energies of ions, ion-pairs, non-electrolytes, and transition states in some S_N and S_E reactions, *J. Chem. Soc. Perkin Trans. 2.* (1972) 1343. doi:10.1039/p29720001343.
- [104] M.H. Abraham, Ionic entropies of transfer from water to nonaqueous solvents, *J. Chem. Soc. Faraday Trans. 1.* 69 (1973) 1375. doi:10.1039/f19736901375.
- [105] M.J. Kamlet, J.L.M. Abboud, M.H. Abraham, R.W. Taft, Linear solvation energy relationships. 23. A comprehensive collection of the solvatochromic parameters, π^* , α , and β , and some methods for simplifying the generalized solvatochromic equation, *J. Org. Chem.* 48 (1983) 2877–2887. doi:10.1021/jo00165a018.
- [106] W.E. Acree, Jr., M.H. Abraham, Solubility predictions for crystalline nonelectrolyte solutes dissolved in organic solvents based upon the Abraham general solvation model, *Can. J. Chem.* 79 (2001) 1466–1476. doi:10.1139/v01-165.
- [107] H. Talukdar, K.K. Kundu, Transfer energetics of tetraalkylammonium picrates in an aqueous ionic cosolvent system and the salt effect on hydrophobic hydration, *J. Phys. Chem.* 95 (1991) 3796–3800. doi:10.1021/j100162a065.
- [108] L. Lee, H. Huang, Solubility of tetrabutylammonium bromide in benzene between 298.15 K and 323.15 K, *J. Chem. Eng. Data.* (2002) 1135–1139.
- [109] Y. Marcus, Tetraalkylammonium Ions in Aqueous and Non-aqueous Solutions, *J. Solution Chem.* 37 (2008) 1071–1098. doi:10.1007/s10953-008-9291-1.
- [110] E.G. Amado, L.H. Blanco, Isopiestic Determination of the Osmotic and Activity Coefficients of Aqueous Solutions of Symmetrical and Unsymmetrical Quaternary Ammonium Bromides at T = (283.15 and 288.15) K †, *J. Chem. Eng. Data.* 54 (2009) 2696–2700. doi:10.1021/je900216m.
- [111] L.H. Blanco, E.G. Amado, J.C. Calvo, Osmotic and activity coefficients of dilute aqueous solutions of the series Me₄NI to MeBu₃NI at 298.15K, *Fluid Phase Equilib.* 268 (2008) 90–94. doi:10.1016/j.fluid.2008.04.008.
- [112] E.G. Amado, L.H. Blanco, Osmotic and activity coefficients of dilute aqueous solutions of symmetrical and unsymmetrical quaternary ammonium bromides at 293.15K, *Fluid Phase Equilib.* 243 (2006) 166–170. doi:10.1016/j.fluid.2006.03.001.
- [113] E.G. Amado, L.H. Blanco, Isopiestic determination of the osmotic and activity coefficients of dilute aqueous solutions of symmetrical and unsymmetrical quaternary ammonium bromides with a new isopiestic cell at 298.15K, *Fluid Phase Equilib.* 233 (2005) 230–233. doi:10.1016/j.fluid.2005.04.012.
- [114] J. Marrero, R. Gani, Group-contribution based estimation of pure component properties, *Fluid Phase Equilib.* 183-184 (2001) 183–208. doi:10.1016/S0378-3812(01)00431-9.
- [115] A.W. Herriott, D. Picker, Phase transfer catalysis. Evaluation of catalysis, *J. Am. Chem. Soc.* 97 (1975) 2345–2349. doi:10.1021/ja00842a006.
- [116] E. Kolvari, A. Ghorbani-Choghamarani, P. Salehi, F. Shirini, M.A. Zolfigol, Application of N-halo reagents in organic synthesis, *J. Iran. Chem. Soc.* 4 (2007) 126–

174. doi:10.1007/BF03245963.
- [117] S.D. Naik, L.K. Doraiswamy, Phase transfer catalysis: Chemistry and engineering, *AIChE J.* 44 (1998) 612–646. doi:10.1002/aic.690440312.
- [118] Z. Jie, X. Yan, L. Zhao, S.D. Worley, J. Liang, Eco-friendly synthesis of regenerable antimicrobial polymeric resin with N-halamine and quaternary ammonium salt groups, *RSC Adv.* 4 (2014) 6048. doi:10.1039/c3ra47147k.
- [119] D.O. Edem, Palm oil: Biochemical, physiological, nutritional, hematological and toxicological aspects: A review, *Plant Foods Hum. Nutr.* 57 (2002) 319–341. doi:10.1023/A:1021828132707.
- [120] Y. Román-Leshkov, C. Barrett, Z. Liu, J. Dumesic, Production of dimethylfuran for liquid fuels from biomass-derived carbohydrates, *Nature.* 447 (2007) 982–986. doi:10.1038/nature05923.
- [121] Y. Román-Leshkov, J. Dumesic, Solvent effects on fructose dehydration to 5-hydroxymethylfurfural in biphasic systems saturated with inorganic salts, *Top. Catal.* (2009) 297–303. doi:10.1007/s11244-008-9166-0.
- [122] X. Tong, Y. Ma, Y. Li, Biomass into chemicals: Conversion of sugars to furan derivatives by catalytic processes, *Appl. Catal. A Gen.* 385 (2010) 1–13. doi:10.1016/j.apcata.2010.06.049.
- [123] H.E. Schoemaker, Dispelling the Myths--Biocatalysis in Industrial Synthesis, *Science* (80-.). 299 (2003) 1694–1697. doi:10.1126/science.1079237.
- [124] A. Schmid, J.S. Dordick, B. Hauer, A. Kiener, M. Wubbolts, B. Witholt, Industrial biocatalysis today and tomorrow, *Nature.* 409 (2001) 258–268. doi:10.1038/35051736.
- [125] M. Sales-Cruz, R. Gani, A modelling tool for different stages of the process life, *Comput. Aided Chem. Eng.* 16 (2003) 209–249. doi:10.1016/S1570-7946(03)80076-7.
- [126] R. Gani, ICAS Documentations, Intern. Report, Tech. Univ. Denmark. (2015).
- [127] R. Gani, P.A. Gómez, M. Folić, C. Jiménez-González, D.J.C. Constable, Solvents in organic synthesis: Replacement and multi-step reaction systems, *Comput. Chem. Eng.* 32 (2008) 2420–2444. doi:10.1016/j.compchemeng.2008.01.006.
- [128] C.M. Hansen, *Hansen Solubility Parameters: A User's Handbook*, Second Edition, CRC Press, 2007.
- [129] E. Papadakis, A.K. Tula, A. Anantpinijwtana, D.K. Babi, R. Gani, Sustainable Chemical Process Development through an Integrated Framework, *Comput. Aided Chem. Eng.* 38 (2016) 841–846. doi:10.1016/B978-0-444-63428-3.50145-4.
- [130] M. Eigen, The Origin of Biological Information, in: *Phys. Concept. Nat.*, Springer Netherlands, Dordrecht, 1973: pp. 594–632. doi:10.1007/978-94-010-2602-4_30.

NOMENCLATURE

Superscripts

0	Initial value
$+, -$	Cation, anion
α	In α phase, usually aqueous
β	In β phase, usually organic
Cal	Calculated value from model
Exp	Experimental value

Subscripts

i, k	Species
j	Reaction
α_{ik}	Interaction parameter between group i and k
C_i	Concentration of species i
ε_{ij}	Order of reaction of species i in reaction j
ξ_j	Extent of reaction j
F_i	Molar flow of species i
K_{Eq}	Equilibrium of reaction
k_{App}	Apparent rate of reaction
k_j	Rate coefficient of reaction j
m_i	Mass of species i
M^+	Salt Cation
N_i	Molar amount of species i
σ	Mean absolute deviation
P_i	Partition coefficient of species i
Q	Surface area parameter of UNIFAC group
Q	Principal PTC Constituent
R	Volume parameter of UNIFAC group
r_{Ws}	Standard segment radius

R	Principal Reactant Constituent
R_j	Rate of reaction j
t	Time
$t_{1/2}$	Half-life of the reaction
t_E	Equilibrium time of the reaction
V	Reactor volume
ν_{ij}	Stoichiometric number of species i in reaction j
x_i	Mole fraction of species i
X, X^-	Reactive Constituent, PTC Anion
Y, Y^-	Product Constituent, PTC Anion
γ_i	Activity coefficient of species i
AABA	α -Amino butyric acid
CSTR	Continuous stirred tank reactor
IL	Ionic Liquid
NRTL	Non-random two-liquid activity coefficient model
eNRTL	Electrolyte NRTL activity coefficient model
PTC	Phase transfer catalyst
SAC	Segment activity coefficient model
SCCO ₂	Super critical carbon dioxide
TBA	Tetrabutylammonium
UNIFAC	UNIQUAC functional-group activity coefficient model
UNIQUAC	Universal quasichemical activity coefficient model

APPENDIX

Table S - I: Comparison between measured rate of conversion and model calculation of benzoin condensation process

Measured Set	Time	Measured Conversion	Modelled Conversion
1	0.00	0.00	0.00
	5.00	0.06	0.07
	15.00	0.15	0.19
	20.00	0.21	0.24
	25.00	0.28	0.28
	35.00	0.38	0.35
	60.00	0.60	0.47
	120.00	0.65	0.63
2	0.00	0.00	0.00
	5.00	0.07	0.06
	15.00	0.12	0.16
	20.00	0.18	0.21
	25.00	0.22	0.24
	35.00	0.30	0.31
	60.00	0.50	0.43
	120.00	0.62	0.58
3	0.00	0.00	0.00
	5.00	0.02	0.05
	15.00	0.10	0.14
	20.00	0.15	0.17
	25.00	0.18	0.20
	35.00	0.22	0.26
	60.00	0.38	0.37
	120.00	0.45	0.53
4	0.00	0.00	0.00
	5.00	0.09	0.09
	10.00	0.14	0.17
	25.00	0.28	0.33
	30.00	0.36	0.37
	60.00	0.51	0.53
	120.00	0.60	0.68
	5	0.00	0.00
5.00		0.09	0.06
10.00		0.16	0.12
25.00		0.27	0.24
30.00		0.35	0.28
60.00		0.48	0.43
120.00		0.58	0.58

Measured Set	Time	Measured Conversion	Modelled Conversion
6	0.00	0.00	0.00
	5.00	0.10	0.10
	10.00	0.15	0.15
	25.00	0.29	0.28
	30.00	0.36	0.35
	60.00	0.48	0.48
	120.00	0.60	0.60
7	0.00	0.00	0.00
	5.00	0.09	0.10
	10.00	0.18	0.18
	25.00	0.27	0.26
	30.00	0.34	0.35
	45	0.42	0.41
	60.00	0.50	0.50
	120.00	0.58	0.57
8	0.00	0.00	0.00
	5.00	0.15	0.15
	10.00	0.17	0.17
	25.00	0.26	0.27
	30.00	0.41	0.41
	60.00	0.62	0.60
	120.00	0.70	0.69
9	0.00	0.00	0.00
	5.00	0.10	0.10
	10.00	0.21	0.21
	25.00	0.27	0.27
	30.00	0.36	0.35
	60.00	0.63	0.62
	120.00	0.68	0.69
10	0.00	0.00	0.00
	5.00	0.07	0.07
	10.00	0.20	0.19
	25.00	0.27	0.26
	30.00	0.41	0.41
	60.00	0.62	0.62
	120.00	0.74	0.72
11	0.00	0.00	0.00
	5.00	0.14	0.14
	10.00	0.15	0.15
	25.00	0.28	0.28
	30.00	0.40	0.39
	60.00	0.57	0.58
	120.00	0.74	0.73

Measured Set	Time	Measured Conversion	Modelled Conversion
12	0.00	0.00	0.00
	5.00	0.09	0.09
	10.00	0.24	0.25
	25.00	0.26	0.26
	30.00	0.35	0.34
	60.00	0.63	0.61
	120.00	0.68	0.69

Table S - II: Apparent rate of reaction, reaction half-life, equilibrium time, and activity coefficients of PTC from kinetic model

Solvent	PTC	k_{App}	$t_{1/2}$ (min)	t_E (min)	γ_{QBr}^α	γ_{QBr}^β	γ_{QCl}^α	γ_{QCl}^β
Benzene	(C ₁) ₄ N	1.48E-3	4.68E+2	1.55E+4	5.51E+1	6.81E-1	5.38E+1	7.11E+3
	(C ₂) ₄ N	9.10E-2	7.62E+0	2.53E+2	5.18E+1	2.00E+2	5.53E+1	1.43E+0
	(C ₄) ₄ N	1.90E-2	3.65E+1	1.21E+3	5.52E+1	2.52E+0	5.18E+1	2.95E+2
Bromo- benzene	(C ₁) ₄ N	5.79E-4	1.20E+3	3.98E+4	5.47E+1	6.15E-1	5.35E+1	1.57E+4
	(C ₂) ₄ N	5.79E-2	1.20E+1	3.98E+2	5.14E+1	2.38E+2	5.50E+1	1.43E+0
	(C ₄) ₄ N	1.17E-2	5.92E+1	1.97E+3	9.23E+0	2.80E+0	5.15E+1	4.28E+2
Chloro- benzene	(C ₁) ₄ N	3.73E-3	1.86E+2	6.17E+3	5.50E+1	4.92E-1	5.35E+1	3.13E+3
	(C ₂) ₄ N	1.27E-1	5.47E+0	1.82E+2	5.17E+1	1.03E+2	5.51E+1	1.60E+0
	(C ₄) ₄ N	3.26E-2	2.13E+1	7.06E+2	5.47E+1	3.16E+0	5.17E+1	1.36E+2
Chlorofo- rm	(C ₁) ₄ N	1.18E-1	5.89E+0	1.96E+2	5.40E+1	9.37E-1	5.52E+1	2.40E+1
	(C ₂) ₄ N	3.42E-1	2.02E+0	6.72E+1	5.31E+1	3.69E+1	5.55E+1	9.19E-1
	(C ₄) ₄ N	1.88E-3	3.68E+2	1.22E+4	5.49E+1	4.41E-1	5.51E+1	5.64E+1
Cyclohe- xane	(C ₁) ₄ N	1.16E-8	5.97E+7	1.98E+9	4.72E+1	9.07E-1	5.35E+1	8.68E+8
	(C ₂) ₄ N	4.77E-1	1.45E+0	4.82E+1	5.30E+1	1.94E+4	5.48E+1	1.71E+0
	(C ₄) ₄ N	5.01E-6	1.38E+5	4.59E+6	5.25E+1	1.26E+1	5.38E+1	9.98E+4
1,1- Dichloro- -ethane	(C ₁) ₄ N	4.49E-2	1.54E+1	5.13E+2	5.50E+1	5.23E-1	5.42E+1	2.43E+2
	(C ₂) ₄ N	1.95E-1	3.56E+0	1.18E+2	5.26E+1	3.92E+1	5.55E+1	2.96E+0
	(C ₄) ₄ N	1.03E-1	6.71E+0	2.23E+2	5.40E+1	7.68E+0	5.37E+1	1.47E+1
1,2- Dichloro- -ethane	(C ₁) ₄ N	7.44E-5	9.31E+3	3.09E+5	5.48E+1	3.31E-1	5.42E+1	1.27E+5
	(C ₂) ₄ N	5.53E-2	1.25E+1	4.16E+2	5.17E+1	3.04E+2	5.55E+1	1.61E+0
	(C ₄) ₄ N	1.93E-2	3.59E+1	1.19E+3	5.54E+1	8.32E+0	5.19E+1	3.15E+2
Dichloro- - methane	(C ₁) ₄ N	9.77E-1	7.09E-1	2.36E+1	5.55E+1	6.43E-1	2.89E-3	2.10E-7
	(C ₂) ₄ N	2.29E-2	3.03E+1	1.01E+3	4.95E+1	1.64E-2	5.58E+1	1.48E+0
	(C ₄) ₄ N	4.96E-1	1.40E+0	4.64E+1	2.29E+6	3.43E-1	6.71E-1	2.63E-4
Ethyl ether	(C ₁) ₄ N	4.98E-1	1.39E+0	4.63E+1	5.37E+1	8.27E-1	5.58E+1	5.89E-1
	(C ₂) ₄ N	5.90E-1	1.17E+0	3.90E+1	5.42E+1	8.34E+0	5.49E+1	8.35E-1
	(C ₄) ₄ N	1.99E-2	3.48E+1	1.16E+3	5.46E+1	1.85E-1	5.40E+1	2.07E+1
Ethyl acetate	(C ₁) ₄ N	3.96E-1	1.75E+0	5.82E+1	5.39E+1	5.99E-1	5.52E+1	1.16E+0
	(C ₂) ₄ N	4.41E-1	1.57E+0	5.23E+1	5.39E+1	6.04E+0	5.50E+1	1.87E+0
	(C ₄) ₄ N	9.12E-2	7.60E+0	2.52E+2	5.43E+1	1.06E+0	5.40E+1	5.46E+0

Solvent	PTC	k_{App}	$t_{1/2}$ (min)	t_E (min)	γ_{QBr}^α	γ_{QBr}^β	γ_{QCl}^α	γ_{QCl}^β
Hexane	(C ₁) ₄ N	1.99E-9	3.49E+8	11.6E+9	5.31E+1	8.33E-1	5.35E+1	2.46E+9
	(C ₂) ₄ N	4.40E-1	1.58E+0	5.24E+1	5.26E+1	2.63E+4	5.43E+1	1.80E+0
	(C ₄) ₄ N	2.26E-6	3.06E+5	1.02E+7	5.18E+1	1.68E+1	5.35E+1	1.36E+5
Methyl cyclohex ane	(C ₁) ₄ N	1.05E-6	6.58E+5	2.18E+7	5.35E+1	5.58E-1	5.35E+1	5.21E+6
	(C ₂) ₄ N	6.38E-2	1.09E+1	3.61E+2	5.07E+1	1.93E+3	2.34E+1	1.51E+0
	(C ₄) ₄ N	7.46E-4	9.29E+2	3.09E+4	5.44E+1	7.65E+0	5.11E+1	4.85E+3
MTBE	(C ₁) ₄ N	5.81E-1	1.19E+0	3.96E+1	5.35E+1	6.66E-1	5.51E+1	2.11E-1
	(C ₂) ₄ N	4.71E-1	1.47E+0	4.89E+1	5.36E+1	3.57E+0	5.46E+1	7.70E-1
	(C ₄) ₄ N	9.26E-4	7.49E+2	2.49E+4	5.44E+1	9.63E-2	5.45E+1	2.47E+1
Toluene	(C ₁) ₄ N	1.83E-3	3.79E+2	1.26E+4	5.20E+1	6.66E-1	5.34E+1	4.81E+3
	(C ₂) ₄ N	8.78E-2	7.89E+0	2.62E+2	5.15E+1	1.69E+2	5.50E+1	1.46E+0
	(C ₄) ₄ N	2.04E-2	3.40E+1	1.13E+3	5.48E+1	2.55E+0	5.15E+1	2.28E+2

Table S - III: Configuration of PTC, between C4 to C16

Carbon Number of PTC	Configuration	Groups				
		N ⁺	CH ₃	CH ₂	CH	C
C4	1	1	4			
C5	1	1	4	1		
C6	1	1	4	2		
	2	1	5		1	
C7	1	1	4	3		
	2	1	5	1	1	
	3	1	6			1
C8	1	1	4	4		
	2	1	5	2	1	
	3	1	6		2	
	4	1	6	1		1
C9	1	1	4	5		
	2	1	5	3	1	
	3	1	6	1	2	
	4	1	6	2		1
	5	1	7		1	1
C10	1	1	4	6		
	2	1	5	4	1	
	3	1	6	2	2	
	4	1	6	3		1
	5	1	7		3	
	6	1	7	1	1	1

Carbon Number of PTC	Configuration	Groups				
		N ⁺	CH ₃	CH ₂	CH	C
C11	1	1	4	7		
	2	1	5	5	1	
	3	1	6	3	2	
	4	1	6	4		1
	5	1	7	1	3	
	6	1	7	2	1	1
	7	1	8		2	1
	8	1	8	1		2
C12	1	1	4	8		
	2	1	5	6	1	
	3	1	6	4	2	
	4	1	6	5		1
	5	1	7	2	3	
	6	1	7	3	1	1
	7	1	8		4	
	8	1	8	1	2	1
	9	1	8	2		2
	10	1	9		1	2
C13	1	1	4	9		
	2	1	5	7	1	
	3	1	6	5	2	
	4	1	6	6		1
	5	1	7	3	3	
	6	1	7	4	1	1
	7	1	8	1	4	
	9	1	8	2	2	1
	9	1	8	3		2
	10	1	9		3	1
	11	1	9	1	1	2
C14	1	1	4	10		
	2	1	5	8	1	
	3	1	6	6	2	
	4	1	6	7		1
	5	1	7	4	3	
	6	1	7	5	1	1
	7	1	8	2	4	
	8	1	8	3	2	1
	9	1	8	4		2
	10	1	9		5	
	11	1	9	1	3	1
	12	1	9	2	1	2
	13	1	10		2	2

Carbon Number of PTC	Configuration	Groups				
		N ⁺	CH ₃	CH ₂	CH	C
C15	14	1	10	1		3
	1	1	4	11		
	2	1	5	9	1	
	3	1	6	7	2	
	4	1	6	8		1
	5	1	7	5	3	
	6	1	7	6	1	1
	7	1	8	3	4	
	8	1	8	4	2	1
	9	1	8	5		2
	10	1	9	1	5	
	11	1	9	2	3	1
	12	1	9	3	1	2
	13	1	10	1	2	2
	14	1	10	2		3
15	1	11		1	3	
C16	1	1	4	12		
	2	1	5	10	1	
	3	1	6	8	2	
	4	1	6	9		1
	5	1	7	6	3	
	6	1	7	7	1	1
	7	1	8	4	4	
	8	1	8	5	2	1
	9	1	8	6		2
	10	1	9	2	5	
	11	1	9	3	3	1
	12	1	9	4	1	2
	13	1	10		6	
	14	1	10	1	4	1
	15	1	10	2	2	2
	16	1	10	3		3
	17	1	11		3	2
	18	1	11	1	1	3

Table S - IV: Conversion of organobromine with different PTC, in different solvents

PTC_Form	Conversion					
	Cyclohexane	Benzene	Ethyl Acetate	Hexane	Chloroform	Toluene
C4_1	27.52	21.27	36.89	62.97	58.95	62.03
C5_1	30.54	25.74	37.35	63.16	48.32	56.00
C6_1	27.13	43.53	48.96	77.54	66.37	73.08
C6_2	22.54	49.05	42.83	72.32	56.25	69.54

PTC_Form	Conversion					
	Cyclohexane	Benzene	Ethyl Acetate	Hexane	Chloroform	Toluene
C7_1	23.55	33.41	41.79	67.83	58.56	70.62
C7_2	26.25	42.76	48.69	76.41	72.48	66.82
C7_3	34.45	27.27	40.67	70.68	62.71	67.75
C8_1	29.44	42.97	49.66	76.80	54.83	67.32
C8_2	28.69	29.84	45.08	73.04	52.67	63.16
C8_3	36.42	50.68	47.83	82.22	63.06	79.92
C8_4	41.07	30.56	52.47	83.28	60.16	84.00
C9_1	32.57	29.37	51.77	79.47	77.86	78.54
C9_2	33.08	29.09	49.08	79.04	62.76	72.29
C9_3	35.27	48.63	46.26	74.60	64.29	67.85
C9_4	28.97	29.10	45.28	80.51	70.88	72.21
C9_5	26.11	31.78	52.88	80.47	61.66	69.74
C10_1	42.91	51.24	55.14	87.46	74.18	78.94
C10_2	37.21	48.41	53.32	88.00	72.06	75.34
C10_3	37.89	55.98	53.02	81.64	61.72	73.06
C10_4	34.31	47.66	55.48	83.07	77.79	84.50
C10_5	42.30	60.23	48.11	84.31	63.24	76.77
C10_6	34.48	50.31	48.25	78.50	64.32	78.95
C11_1	32.37	46.48	55.03	88.21	76.22	85.69
C11_2	37.84	35.61	53.88	89.68	74.44	93.69
C11_3	31.16	38.91	58.86	90.79	85.32	91.26
C11_4	47.15	31.52	55.04	93.09	83.50	92.72
C11_5	41.79	30.47	52.85	86.95	66.11	73.08
C11_6	41.64	37.21	58.00	92.08	83.75	80.99
C11_7	44.72	49.30	59.12	91.42	88.08	75.42
C11_8	46.86	53.02	61.35	93.32	82.63	82.56
C12_1	39.06	32.97	59.26	97.78	82.61	97.38
C12_2	39.43	60.74	59.61	96.71	82.51	96.44
C12_3	31.11	35.82	56.06	97.36	90.97	97.05
C12_4	45.25	39.18	57.77	98.87	74.60	85.77
C12_5	42.30	56.77	61.17	96.70	76.14	90.84
C12_6	44.87	57.93	59.48	97.04	79.64	87.43
C12_7	34.96	42.04	58.82	97.36	87.38	97.81
C12_8	37.33	66.28	58.38	95.35	88.99	94.17
C12_9	47.89	36.58	64.29	96.79	75.88	81.35
C12_10	30.42	63.15	62.45	95.09	71.99	95.91
C13_1	37.80	54.40	47.51	79.38	62.38	76.50
C13_2	34.88	25.59	51.37	81.57	69.91	83.93
C13_3	40.29	36.24	44.57	78.87	74.68	67.39
C13_4	35.47	28.53	49.07	83.64	61.75	70.72
C13_5	34.92	43.28	51.03	79.33	64.72	76.24
C13_6	28.34	28.39	50.85	79.56	63.91	78.10

PTC_Form	Conversion					
	Cyclohexane	Benzene	Ethyl Acetate	Hexane	Chloroform	Toluene
C13_7	28.96	52.17	44.46	78.79	73.39	67.70
C13_9	25.14	54.78	45.61	79.85	67.09	68.25
C13_9	26.97	45.99	50.28	80.24	71.22	67.80
C13_10	29.76	52.06	50.87	78.99	65.74	73.58
C13_11	31.97	33.03	48.62	78.86	62.65	69.90
C14_1	26.71	24.48	47.07	79.79	59.05	80.03
C14_2	36.30	46.51	49.43	83.31	62.27	73.77
C14_3	40.69	57.11	50.75	79.49	64.50	71.82
C14_4	24.50	51.07	45.04	78.71	69.23	72.74
C14_5	28.08	49.73	51.80	79.26	67.15	67.03
C14_6	34.33	37.13	52.08	78.41	72.73	69.33
C14_7	34.13	51.55	52.23	83.79	60.29	68.97
C14_8	24.69	42.92	44.80	81.03	63.57	72.35
C14_9	32.42	56.63	52.54	80.20	65.45	77.56
C14_10	27.24	42.32	52.43	88.50	66.61	71.23
C14_11	43.15	60.84	53.41	85.32	63.17	72.18
C14_12	37.67	56.51	48.49	78.97	63.04	67.97
C14_13	33.42	33.55	51.30	83.09	61.24	68.44
C14_14	31.51	45.64	47.87	82.67	59.63	72.56
C15_1	33.22	39.60	43.73	72.23	54.84	66.73
C15_2	25.73	27.55	46.32	71.74	62.54	72.30
C15_3	33.27	47.37	40.30	68.12	61.67	59.28
C15_4	28.87	41.26	39.39	69.27	57.15	66.55
C15_5	35.39	31.28	45.35	79.11	69.90	65.97
C15_6	28.06	38.32	40.59	70.06	57.03	65.33
C15_7	28.45	38.49	41.50	70.60	51.29	66.53
C15_8	30.95	30.75	40.26	70.19	57.89	59.23
C15_9	34.58	27.86	41.20	70.08	51.37	66.01
C15_10	36.06	34.34	44.10	76.92	71.18	67.92
C15_11	26.93	40.67	46.54	75.37	62.76	77.72
C15_12	32.14	37.83	39.46	69.97	60.36	70.45
C15_13	24.10	44.65	46.73	78.48	60.28	68.16
C15_14	22.71	41.61	45.00	73.92	54.84	70.32
C15_15	35.79	26.70	43.28	74.46	66.73	70.36
C16_1	27.51	32.23	40.66	71.85	71.41	74.56
C16_2	24.90	54.12	52.26	76.93	71.15	67.30
C16_3	29.39	33.43	50.63	76.15	63.74	68.97
C16_4	28.77	26.07	42.80	64.96	63.17	58.47
C16_5	27.34	38.63	45.98	72.95	62.66	64.55
C16_6	36.92	49.56	44.39	77.20	72.12	77.14
C16_7	29.05	35.54	43.28	69.72	51.79	64.41
C16_8	28.14	39.25	40.27	68.24	55.58	59.86

PTC_Form	Conversion					
	Cyclohexane	Benzene	Ethyl Acetate	Hexane	Chloroform	Toluene
C16_9	34.63	32.22	47.09	78.91	66.29	70.00
C16_10	36.45	56.40	52.86	80.13	76.84	67.38
C16_11	39.94	40.76	52.27	77.97	58.30	76.84
C16_12	33.75	27.14	46.71	72.95	69.71	69.72
C16_13	22.62	40.54	44.53	67.94	55.55	65.45
C16_14	20.95	26.37	40.65	66.22	57.45	65.13
C16_15	23.17	45.83	38.22	68.03	50.77	55.24
C16_16	28.35	29.41	41.38	65.30	55.12	65.58
C16_17	28.74	40.18	48.02	70.94	70.32	61.50
C16_18	31.47	32.49	44.07	71.70	63.92	71.83

Department of Chemical and Biochemical Engineering
Technical University of Denmark
Søltofts Plads, Building 229
2800 Kgs. Lyngby
Denmark

Phone: +45 45 25 28 00
Web: www.kt.dtu.dk/